TU DELFT FACULTY OF ARCHITECTURE

A parametric structural design tool for plate structures

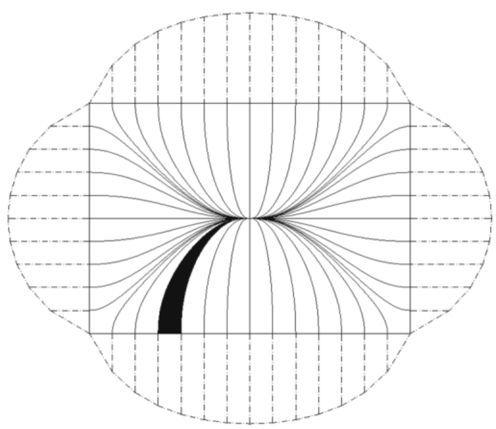

Michiel Oosterhuis

25-6-2010

Hereby, I would like to thank my mentors, Ir. Andrew Borgart, Dr.ir. Rudi Stouffs and Ir. Diederik Veenendaal for their guidance, support and ideas, during this thesis project.

TU Delft, Faculty of Architecture
Julianalaan 134
2628 BL Delft
Tel. (015) 278 9111
E-mail: informatie@bk.tudelft.nl

Michiel Oosterhuis *(author)*

+31(0)6-41582841
Balthasar van der Polweg 302
2628 AZ, Delft
michiel.oosterhuis@gmail.com

Members of the graduation committee:

Ir. A. Borgart *(first mentor)*

TU Delft, Faculty of Architecture
Department of Structural Mechanics
+31 (0)15-27-84157
Room number: 6.39 (Faculty of Civil Engineering and Geosciences)
a.borgart@tudelft.nl

Dr. Ir. R.M.F. Stouffs *(second mentor)*

TU Delft, Faculty of Architecture
Department of Design Informatics
+31 (0)15-27-81295
Room number: 01.WEST 0.30 ()Faculty of Architecture
r.m.f.stouffs @tudelft.nl

Ir. D. Veenendaal *(external mentor)*

ETH Zürich
+41 44-633-28-03
Room number 45.3 (Building HIL, Floor E)
Wolfgang-Pauli-Strasse 15 / CH-8093 Zürich
veenendaal@arch.ethz.ch

Witteveen+Bos
+31(0)570-69-75-11
Office building 'Stationsplein'
Leeuwenbrug 27
7411 TE Deventer

Contents

1 Introduction 6

1.1 Background & problem statements 6

1.2 Objectives & approach 8

1.3 Scope 9

1.4 Outline of this thesis 9

2 Theoretical framework 10

2.1 Introduction 10

2.2 Differential equations 11

2.3 Elastic membrane analogy 17

2.4 Force Density method 19

2.5 Rain flow analogy 24

2.6 Curvature ratio method 28

2.7 Finite difference method 31

2.8 Sand hill method 38

2.9 Application of the theoretical framework 40

3 Parametric structural design tool 43

3.1 Introduction 43

3.2 Functionality and usability 43

3.3 General outline and structure of the structural design tool 45

3.4 Implementation of the theoretical framework 47

3.5 Mesh Component 48

3.6 Force Density component ... 49

3.7 Derivative component ... 54

3.8 Curvature ratio component ... 56

3.9 Rain flow analogy component ... 57

3.10 Finite difference component ... 65

3.11 Sand hill & Voronoi component ... 73

3.12 Conceived structure and layout of the parametric structural design tool ... 78

4 Validation ... 79

4.1 Introduction ... 79

4.2 Shear forces ... 80

4.3 Bending- and torsional moments ... 82

5 Conclusions ... 85

5.1 Introduction ... 85

5.2 Theoretical framework ... 86

5.3 Parametric structural design tool ... 88

5.4 Validation ... 94

5.5 Final conclusion ... 95

Bibliography ... 96

List of symbols ... 98

Appendix I ... 99

1 Introduction

1.1 Background & problem statements

Partially as a result of the wide range of new technological possibilities, a trend towards the increased use of advanced geometry and computation can be observed within the fields of architectural and structural engineering (Coenders, 2006). Computation plays an important role in generating (complex) geometries and developing the (structural) design using design- and analysis software. Complex (structural) designs are often developed through an iterative process, consisting of design-, calculation- and production phases, driven by the possibility to exchange data (interfacing) between CAD programmes (Computer Aided Design) and FEM programmes (Finite Element Method) (Borgart, Hoogenboom, & De Leeuw, 2005). This sequence makes it possible to design, calculate and develop complex designs, resulting in for example free form architecture.

During the conceptual stage of the design process, many important design decisions are made with regard to structural considerations, laying the basis for the rest of the project. The first structural setup is usually conceived at this stage. Qualitative- and global quantitative insight in the mechanical behaviour of the structure is therefore very important. Qualitative insight in this respect refers to insight in the relation between parameters such as structural geometry, boundary conditions and materials properties and the resulting deformations and stress resultants (quantitative information). When such insight is obtained in the conceptual stage of the design process it could be employed for (structural) optimization purposes. Identifying the implications of specific design decisions with respect to esthetical appearance or constructability at an early stage, could lead to a reduction of risk and cost, and thus reduce problems during later stages.

FEM based structural analysis programs might not be the most appropriate computational structural analysis tools in the conceptual design stage. Even though FEM calculation results offer sufficient quantitative insight in the magnitude of the forces and deformations that might occur in a structure, they do not always give the engineer qualitative insight in the mechanical behaviour. Additionally, these analysis programs require a rather detailed structural model and the results produced are unnecessarily precise for the conceptual design stage. Most of the existing software tools for structural analysis are oriented towards advanced users and require a detailed understanding of the program and its underlying principles. Moreover, the calculation procedures within FEM programs in combination with the necessary interfacing between different CAD programs decreases the speed and flexibility of the design and analysis process.

In contrast to FEM programs, (classical) analytical methods offer, apart from quantitative insight, qualitative insight into the mechanical behaviour for a wide range of structural topologies. Graphic statics is a good example of such a method in which analytical relations between the structural geometry and the corresponding mechanical behaviour are used to generate a graphical representation of the flow and magnitude of forces.

A recent development in the field of computational design are parametric associative design tools which capture design information by defining logical relations between (geometrical) components, controlled by parameters. These techniques offer a very flexible approach to exploring complex geometries and are, currently, mainly used within the field of architectural design. Despite the wide range of possibilities for linking geometry to structural analysis they still find very little application within the field of structural engineering at the moment.

The main thought behind this thesis is that the application of (simple) analytical methods into parametric software applications could help both the engineer and the designer. Both qualitative and quantitative insight in the relation between structural topology and the flow of forces could be assessed in a flexible manner during the conceptual design stage. Especially when implementing these relations in a computational model they offer a quick and precise insight in the (relations between) the above mentioned quantities. The obtained knowledge could be used to make thoughtful considerations with respect to the interwoven aspects of aesthetics and structure. In that way it might even be helpful to bridge the gap between the often separated fields of architecture and structural engineering.

Some (academic) approaches towards the implementation of mechanical analysis methods into a parametric model are worth mentioning. One example is the Structural Components approach which was first described by J.L. Coenders. This approach is aimed at the assembly of a toolbox filled with structural components which can be used to compose a mechanical model. The model can subsequently be analysed with the implemented rules of the thumb and FEM methods. Although this method is very flexible with regard to assembly and analysis of a structural topology, it does not give much qualitative insight in the flow of forces of plate structures as the structural analysis is not based on analytical methods. Another example is the recently developed application of the Thrust Network Analysis into a parametric model by Professor Block. This graphical method forms a very inspiring example of how analytical mechanics can give a designer both qualitative and quantitative mechanical insight in the flow and magnitude of forces in structures. Nevertheless, this graphical method is mainly confined to designing and analyzing masonry vaults.

This thesis aims at developing a structural design tool by implementing simple structural analysis methods within a parametric environment, in a manner that differs from the above mentioned approaches. The intention is to introduce structural evaluation into the conceptual design process in an intuitive and flexible manner.

Two problem statements, forming the incentive for writing this thesis, are deduced from this background:

1) *There is a deficiency of simple structural analysis tools, based on analytical relations, which give both the architect and engineer besides quantitative insight also qualitative insight in the (flow of) forces of structures during a conceptual design stage.*
2) *Parametric design applications are not used to their full potential within the field of structural engineering.*

1.2 Objectives & approach

In this thesis, it will be assessed whether the premise holds that statement 2 contains the solution for statement 1.. This will be done by developing a computational structural design tool, based on analytical structural analysis methods, by using the parametric associative design approach. Consequently, the main objective is defined as:

"Develop a structural design tool for architects and engineers, based on simple analytical structural analysis methods, which gives both quantitative and qualitative (real time) insight in the flow and magnitude of forces within a specific structure during a conceptual design stage."

To guide the development of this parametric structural design tool a series of secondary objectives is defined:

1a Define a theoretical framework, by stating which- and how- analytical and numerical structural analysis techniques can be used to provide both quantitative and qualitative insight in the relation between structural geometry and the flow- and magnitude of forces and deformations within structures and have the potential to be implemented into a (parametric) computational tool.

The presumption with respect to *1a* is that simple analytical structural analysis methods, which have the potential to be developed further by combining, extending and applying them within a computational application, can contribute to insight into the mechanical behaviour of structures.

1b Define which demands, concerning functionality- and usability, have to be fulfilled by the parametric structural design tool.

With respect to *1b*, the design tool is presumed to be used by both architects and structural engineers during a conceptual design stage. To be able to achieve objective *1b*, a concise enquiry is held amongst experts from practice (Witteveen+Bos).

1c Define an appropriate general outline and structure for the parametric structural design tool with respect to the demands concerning functionality and usability (see 1b).

1d Implement the theoretical framework (see 1a) into the defined general setup (see 1c).

1e Validate the produced calculation results in a qualitative- and a quantitative manner.

In case these objectives are reached and have resulted in a parametric structural design tool, the main objective within the scope of this thesis is considered to be reached.

1.3 Scope

Although there is a broad range of structural topologies, the scope of this thesis is confined to thin isotropic plates simply supported along their edges. Plates are considered as a logical starting point because:

- Their mechanical behaviour is extensively described by (analytical) calculation methods which can be used to validate the calculation results provided by the envisioned structural design tool.
- They form a very common structural component, which increases the practical relevance of this research.
- Since the introduction of FEM calculation methods many students and even some engineers only have a superficial insight in their mechanical behaviour. This forms a great opportunity to regain insight and understanding on how plates transmit their loads by providing them with a useful design tool.

The development of the envisioned structural design tool for thin plate structures is considered as a logical first step in the development of a parametric structural analysis tool which is applicable to a wider range of structural topologies.

1.4 Outline of this thesis

This thesis is structured in correspondence with the presented objectives. They will be the basis on which the design tool will be developed chronologically:

Chapter 2 A description of the theoretical framework (referring to objective 1a) will be given by means of a concise explanation of the theory behind the different structural analysis methods. It will also be explained how the methods are used within this thesis.

Chapter 3 First, the demands concerning functionality and usability will be defined (referring to 1b). Second, the conceived general setup of the parametric structural design tool will be described (referring to 1c). Third, it will be explained how the different components of the design tool function by implementing the structural analysis methods from the theoretical framework (referring to 1d).

Chapter 4 The achieved calculation results, provided by the different components of the structural design tool, will be validated in a qualitative and a quantitative manner by comparing them to corresponding results produced by respectively FEM based software applications and analytical results (referring to 1e).

Chapter 5 Conclusions will be drawn for this thesis project, defining whether and to what extend the main- and secondary objectives have been reached. Additionally, recommendations and suggestions are made for future development and improvement of the structural design tool.

2 Theoretical framework

2.1 Introduction

This chapter will elaborate on the theoretical framework, referring to objective 1a:

"Define a theoretical framework, by defining which- and how- analytical and numerical structural analysis techniques can be used to provide both quantitative and qualitative insight in the relation between structural geometry and the flow- and magnitude of forces and deformations within thin plate structures and have the potential to be implemented into a (parametric) computational tool."

The theoretical framework forms the basis for the development of the structural design tool. In accordance with the approach as defined in chapter 1, it consists mainly of (classic) analytical structural analysis method(s) for plate structures. Analytical methods provide the exact relation between the structural geometry, boundary conditions and materials properties as parameters and the resulting deformations and stress resultants in an unequivocal way by exact algebraic equations. As a result, they provide an engineer with both qualitative and quantitative information on the mechanical behaviour of a structure.

The emphasis within this thesis lies on the computational application of (classic) analytical theories preferably those that were not implemented into a (parametric) computational model before. It was presumed that implementation of these methods into the envisioned parametric structural design tool induces a faster and more flexible structural process than a FEM based calculation sequence, which is more appropriate for the conceptual design process. The methods which were selected on basis of this approach are:

1) Differential equations for thin plates
2) Elastic membrane analogy
3) Force Density method
4) Rain flow analogy
5) Curvature ratio method
6) Finite difference method
7) Sand hill analogy

As mentioned before in the introduction, the scope of this thesis is (mainly) confined to thin isotropic plates simply supported along their edges, loaded perpendicular to their plane. Although the mentioned structural analysis methods are only used within this thesis for plate structures, some of them can be used for other structural topologies as well (e.g. wall or thin shell structures).

In the upcoming paragraphs, a description of the theoretical framework will be given by means of a concise explanation of the theory behind the different structural analysis methods 1-7. In addition, it will be explained how the different methods are combined into several (novel) structural analysis sequences to obtain insight in the mechanical behaviour of thin plate structures.

2.2 Differential equations

2.2.1 Introduction

The classic analytical differential equations give an exact mathematical description of the mechanical behaviour of simply supported thin plate structures subjected to loads perpendicular to their plane. The equations are based on mathematical relations between the deformations, strains, stress resultants and loads by respectively kinematic-, constitutive-, and equilibrium-equations.

The relations between the deformations and the degrees of freedom strains are expressed by kinematic equations. The relations between the deformations and the stress resultants represent the material behaviour and are expressed by constitutive equations. The relations between the stress resultant and the loads are expressed by equilibrium equations. For (thick and thin) plates, the relations between these quantities are presented in the diagram below (figure 1).

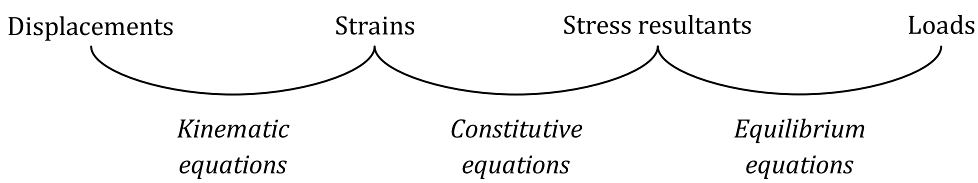

Fig.1. Diagram illustrating the relations between the quantities

The scope of this thesis is confined to homogeneous isotropic (rectangular) plates which are able to carry the applied loads in two directions to their supports (in contradiction to beams). The considered plates are simply supported along their edges loaded by a distributed load p perpendicular to its plane that is assumed to be positive in the positive z-direction. Since the ratio between the thickness of the plate and the span is assumed to be smaller than 1:5 (which is valid in many practical applications of plate structures) the plates can be indicated as thin. As a result, the shear deformations will be negligibly small compared to the bending deformations allowing the set of differential equations to be reduced and simplified in comparison with the corresponding equations for thick plates.

The compressed procedure for deriving the differential equations for thin plates is mainly deduced from the Reader Plate Analysis written by J. Blaauwendraad, professor at the Technical University Delft (Faculty of Civil Engineering and Geosciences) (Blauwendraad, Plate Analysis, Theory and Application Volume 1, Theory, 2006).

2.2.2 Deriving the differential equations

Before the corresponding differential equations will be presented, several assumptions are made with respect to the mechanical behaviour of the plate.

- No extensional forces (membrane forces) will occur due to the support constraints.
- A straight line perpendicular to the mid plane of the plate in an unloaded state will remain straight after application of the load.
- Stresses in the z-direction are negligibly small and therefore assumed to be zero
- Possible small differences in the displacement over the thickness of the slab are neglected.

For deriving the basic equations, an elementary block is considered with infinitesimal small dimensions d_x and d_y with the height t of the plate (figure 2).

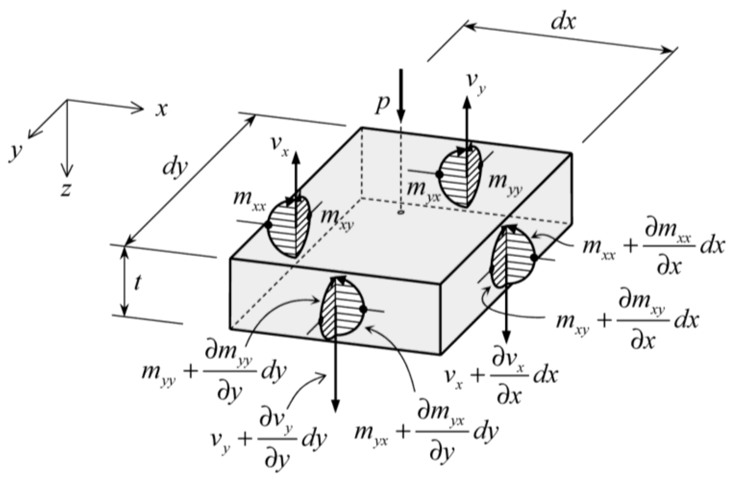

Fig.2. Loads and stress resultants acting on the elementary plate part

First, the kinematic equations will be given, followed by the constitutive equations and then the equilibrium equations. When these basis equations are derived they can be combined into the well known governing fourth order differential equation which expresses the relation between the displacements and the load.

The kinematic relations between the displacement (degrees of freedom) and the deformations are given by the equations:

$$\kappa_{xx} = \frac{\partial \varphi_x}{\partial x} = \frac{\partial^2 w}{\partial x^2}$$
$$\kappa_{yy} = \frac{\partial \varphi_y}{\partial y} = \frac{\partial^2 w}{\partial y^2} \qquad (2.1)$$
$$\kappa_{xy} = \frac{1}{2} \cdot \left(\frac{\partial \varphi_x}{\partial x} + \frac{\partial \varphi_y}{\partial y} \right) = \frac{\partial^2 w}{\partial x \partial y}$$

The constitutive equations, representing the relation between the deformations and the stress resultants, are:

$$
\begin{aligned}
m_{xx} &= D\cdot(\kappa_{xx}+\upsilon\cdot\kappa_{yy}) \\
m_{yy} &= D\cdot(\kappa_{yy}+\upsilon\cdot\kappa_{xx}) \\
m_{xy} &= D\cdot(1-\upsilon)\cdot\kappa_{xy}
\end{aligned}
\tag{2.2}
$$

Within these equations (2.2) the constant D represents the plate stiffness which is defined as:

$$
D=\frac{E\cdot t^3}{12\cdot(1-\upsilon^2)}
\tag{2.2}
$$

The shear forces v_x and $v_y$on the elementary plate part can be expressed by:

$$
\begin{aligned}
v_x &= \frac{\partial m_{xx}}{\partial x}+\frac{\partial m_{xy}}{\partial y} \\
v_y &= \frac{\partial m_{yy}}{\partial y}+\frac{\partial m_{yx}}{\partial x}
\end{aligned}
\tag{2.3}
$$

Substitution of these equations (2.3) for the shear forces into the equilibrium equations (2.4), which describe the relation between the shear forces and the load, yields:

$$
\begin{aligned}
&\frac{v_x}{\partial x}+\frac{v_y}{\partial y}=p \\
&\left(\frac{\partial^2 m_{xx}}{\partial x^2}+2\cdot\frac{\partial^2 m_{xy}}{\partial x\partial y}+\frac{\partial^2 m_{yy}}{\partial y^2}\right)=p
\end{aligned}
\tag{2.4}
$$

Substitution of the kinematic equations (2.2) into the constitutive equations yields:

$$
\begin{aligned}
m_{xx} &= -D\cdot\left(\frac{\partial^2 w}{\partial x^2}+\upsilon\cdot\frac{\partial^2 w}{\partial y^2}\right) \\
m_{yy} &= -D\cdot\left(\frac{\partial^2 w}{\partial y^2}+\upsilon\cdot\frac{\partial^2 w}{\partial x^2}\right) \\
m_{xy} &= -(1-\upsilon)\cdot D\cdot\frac{\partial^2 w}{\partial x\partial y}
\end{aligned}
\tag{2.5}
$$

Substitution of these equations into the equilibrium equations (2.4) yields:

$$
-D\cdot\left(\frac{\partial^4 w}{\partial x^4}+2\cdot\frac{\partial^4 w}{\partial x^2\partial y^2}+\frac{\partial^4 w}{\partial y^4}\right)=p
\tag{2.6}
$$

This fourth order differential equation (2.6) must be solved with respect to the governing boundary conditions. For a rectangular simply supported plate two boundary conditions per edge can be specified.

$$w = 0 \rightarrow m_{xx} = \frac{\partial^2 w}{\partial x^2} = 0 \qquad \textit{along edges parallel to the x axis}$$
$$w = 0 \rightarrow m_{yy} = \frac{\partial^2 w}{\partial y^2} = 0 \qquad \textit{along edges parallel to the y axis} \tag{2.7}$$

As shown in (2.7), the displacements are zero on the edge and thereby the bending moments perpendicular to the edges are also zero.

The support reactions along the edge consist of a combination of a shear force and a concentrated shear force. The concentrated shear force is a result of the torsional stresses induced by the varying slope perpendicular to the edge along the edge. As the torsional stresses vary linearly over the thickness of the plate they cannot act on the free edge and therefore they have to go round at the ends, resulting in a concentrated shear force. This happens within a distance from the edge which equals approximately half the thickness of the plate. From vertical equilibrium for an elementary plate part it can be deduced that the magnitude of the concentrated shear force equals the increase of the torsional moment over an elementary distance. The support reactions at the edges of the plate, as external distributed line load acting on the plate, can be expressed by:

$$f_{w_x} = v_x + V_x = v_x + \frac{\partial m_{xy}}{\partial y}$$
$$f_{w_y} = v_y + V_y = v_y + \frac{\partial m_{yx}}{\partial x} \tag{2.8}$$

It can be concluded that the torsional moment turns out to be resisted in the form of additional support reactions. In the corner of the plate, two simple supports come together and from equilibrium for an elementary plate part it can be deduced that the contribution of the distributed line load and p vanishes and thereby a concentrated support reaction in the corner occurs of which the magnitude equals the summation of both torsional moments. For isotropic plates it yields that $m_{xy} = m_{yx}$ and therefore the corner reaction $R = 2 \cdot m_{xy}$. Depending on the sign convention this reaction force can be either compressive or tensile.

Once a solution for the displacements (displacement field) is found, the bending and torsional moments can be calculated by the equations (2.5) which describe the relations between the displacements and the stress resultants. Subsequently the shear forces can be calculated by using equations (2.3), describing the relations between the moments and the shear forces.

As can be observed in equation (2.3), the shear forces are directly related to the moments. Therefore the shear forces can (similar to the moments in (2.5)) also be expressed in the displacements w as shown in (2.9) and (2.10) below:

$$v_x = \frac{\partial m_{xx}}{\partial x} + \frac{\partial m_{xy}}{\partial y} = -D \cdot \left(\frac{\partial^3 w}{\partial x^3} + \upsilon \cdot \frac{\partial^3 w}{\partial x \partial y^2} \right) - (1-\upsilon) \cdot D \cdot \frac{\partial^3 w}{\partial x \partial y^2} \rightarrow$$
$$v_x = -D \cdot \left(\frac{\partial^3 w}{\partial x^3} + \frac{\partial^3 w}{\partial x \partial y^2} \right) \quad (2.9)$$

$$v_y = \frac{\partial m_{yy}}{\partial y} + \frac{\partial m_{yx}}{\partial x} = -D \cdot \left(\frac{\partial^3 w}{\partial y^3} + \upsilon \cdot \frac{\partial^3 w}{\partial y \partial x^2} \right) - (1-\upsilon) \cdot D \cdot \frac{\partial^3 w}{\partial y \partial x^2} \rightarrow$$
$$v_y = -D \cdot \left(\frac{\partial^3 w}{\partial y^3} + \frac{\partial^3 w}{\partial y \partial x^2} \right) \quad (2.10)$$

From the principle of the corrected sum of bending moments as defined in (2.11), it can be derived that the shear forces are also related to the bending moments in the following manner:

$$\bar{M} = \frac{m_{xx} + m_{yy}}{(1+\upsilon)} \quad (2.11)$$

$$v_n = \frac{\partial}{\partial n} \cdot \bar{M} \quad (2.12)$$

$$v_x = \frac{\partial}{\partial x} \cdot \bar{M} \quad (2.13)$$

$$v_y = \frac{\partial}{\partial y} \cdot \bar{M} \quad (2.14)$$

When we consider an elementary triangular plate part as is shown in figure 3 with the shear forces acting on its edges we can determine the relation between the principle shear forces v_n and their components v_x and v_y in the x- and y-direction. We can see the top of the arrow (a point) or the back (a cross). An arrow coming towards the reader (the point is seen) indicates shear forces on faces with a negative normal vector; an arrow moving away (the cross is seen) indicates shear forces on faces with a positive normal vector.

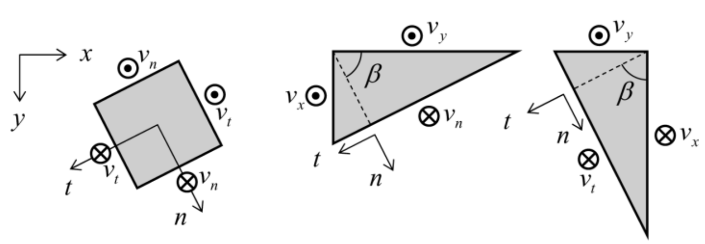

Fig.3. Vertical equilibrium of an elementary plate part

From the equilibrium of this plate part it follows:

$$v_n = v_x \cos\alpha + v_y \sin\alpha \quad (2.15)$$

$$v_t = -v_x \sin\alpha + v_y \cos\alpha \quad (2.16)$$

The magnitude of the principle shear force in an arbitrary point on the plate can be calculated by:

$$v_{n,\max} = \frac{v_x^{\ 2} + v_y^{\ 2}}{\sqrt{v_x^{\ 2} + v_y^{\ 2}}} = \sqrt{v_x^{\ 2} + v_y^{\ 2}} \qquad (2.17)$$

The principle direction of this principle shear force equals:

$$\tan\beta = \frac{v_y}{v_x} \qquad (2.18)$$

A graphical method for determining the shear forces in a specific point on the plate is the so called shear force circle. Such a circle gives a direct insight in the magnitude of a shear force in all directions. The plane perpendicular to the shear force represents the considered section on the surface.

The first order differential equations of (2.12 – 2.14) can be used to construct a direction field which represents the direction of the principle shear forces in a plate for a series of grid of points with a proper density (Weisstein, Vector Field). Such a direction field is in fact a graphical representation of the solution of the differential equations and gives the engineer a qualitative insight on how the shear forces flow to the supports. The direction of the shear forces can be calculated by:

$$\tan\beta = \frac{v_y}{v_x} = \frac{\partial^2 y}{\partial^2 x} \qquad (2.19)$$

A small line segment is drawn from each point. The direction of these lines is equal to the solution of the equation in the associated grid point.

When the correct values for m_{xx}, m_{yy} and m_{xy} are obtained, the principle moments m_1 and m_2 can be calculated with Mohr's equations:

$$m_1 = \frac{m_{xx} + m_{yy}}{2} + \sqrt{\left(\frac{m_{xx} - m_{yy}}{2}\right)^2 + m_{xy}^{\ 2}} \qquad (2.20)$$

$$m_2 = \frac{m_{xx} + m_{yy}}{2} - \sqrt{\left(\frac{m_{xx} - m_{yy}}{2}\right)^2 + m_{xy}^{\ 2}} \qquad (2.21)$$

2.3 *Elastic membrane analogy*

2.3.1 Introduction

The 'elastic membrane analogy', also known as the 'soap-film analogy', is based on the fact that the second order differential equation for the deflection surface of a homogeneous membrane, subjected to uniform lateral pressure and a uniform surface tension, is similar to the equation for the sum of curvatures surface belonging to thin plate structures (Prandtl, 1903).

2.3.2 Deriving the elastic membrane analogy

As we have seen in the previous chapter, the corrected (with respect to Poison's ratio: $\upsilon = 0$) sum of bending moments $\bar{M}$ can be represented by:

$$\bar{M} = \frac{m_{xx} + m_{yy}}{1+\upsilon} = -D \cdot \Delta w \tag{2.22}$$

This corrected sum of bending moments is invariant with respect to the rotation of the x-y coordinate system about its origin. The plate stiffness D is again defined as:

$$D = \frac{E \cdot t^3}{12 \cdot (1-\upsilon^2)} \tag{2.23}$$

From the kinematic equations (2.1) and the constitutive equations (2.2) follows:

$$\bar{M} = D \cdot \left(\frac{\partial \varphi_x}{\partial x} + \frac{\partial \varphi_y}{\partial y} \right) = D \cdot \left(\frac{\partial^2 w}{\partial x^2} + \frac{\partial^2 w}{\partial y^2} \right) \tag{2.24}$$

The fourth order differential equation (2.6) for plates was defined as:

$$\frac{p}{D} = \left(\frac{\partial^2}{\partial x^2} + \frac{\partial^2}{\partial y^2} \right) \cdot \left(\frac{\partial^2 w}{\partial x^2} + \frac{\partial^2 w}{\partial y^2} \right) = \frac{\partial^4 w}{\partial x^4} + 2 \frac{\partial^4 w}{\partial x^2 \partial y^2} + \frac{\partial^4 w}{\partial y^4} \tag{2.25}$$

By making use of the sum of bending moments (2.22) this equation can be parsed into two second order differential equations:

$$-\frac{\bar{M}}{D} = \frac{\partial^2 w}{\partial x^2} + \frac{\partial^2 w}{\partial y^2} \tag{2.26a}$$

$$-p = \frac{\partial^2 \bar{M}}{\partial x^2} + \frac{\partial^2 \bar{M}}{\partial y^2} \tag{2.26b}$$

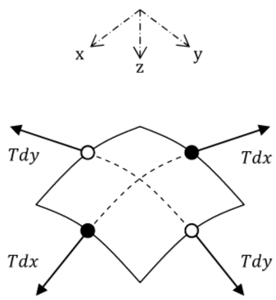

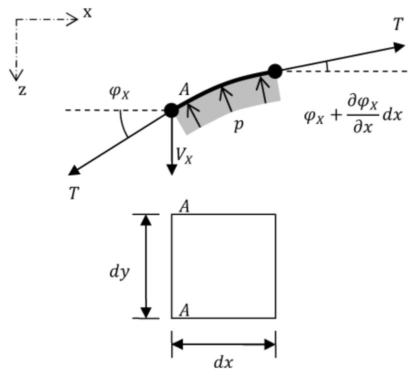

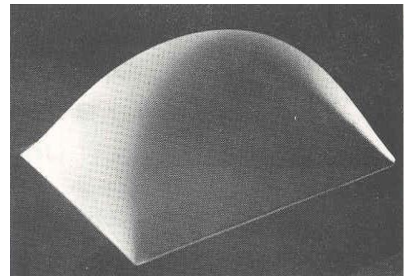

Fig.4. Elementary membrane part *Fig.5. Vertical equilibrium along section A-A* *Fig.6. Physical membrane shape*

For an elementary part (figure 4,5) of an air inflated membrane (figure 6), which is equally tensioned in all directions, the vertical equilibrium situation can be represented as follows:

$$-T \cdot \varphi_x \cdot dy + T \cdot \left(\varphi_x + \frac{\partial \varphi_x}{\partial x} \cdot dx \right) \cdot dy - T \cdot \varphi_y \cdot dx + T \cdot \varphi_y + \frac{\partial \varphi_y}{\partial y} \cdot dy \cdot dx + p \cdot dxdy = 0 \qquad (2.27)$$

This formula can be rewritten as:

$$\frac{\partial \varphi_x}{\partial x} + \frac{\partial \varphi_y}{\partial y} = -\frac{p}{T} \qquad (2.28)$$

By expressing the rotations φ_x and φ_y in the displacement w_m, the equation can be rewritten as:

$$\frac{\partial^2 w_m}{\partial x^2} + \frac{\partial^2 w_m}{\partial y^2} = -\frac{p}{T} \qquad (2.29)$$

It is clear that this equation (2.29) has exactly the same structure as the earlier presented second order differential equations (2.26a/b). Therefore, as an analogy, the sum of bending moments surface also represents an air inflated membrane. It must be noted that this analogy is only true for small curvatures, whereas $sin\varphi \simeq \varphi$ and $cos\varphi \simeq 1$.

2.3.3 Membrane analogy and the sum of bending moments surface

In both equations (2.26 & 2.29) the plate stiffness D and the membrane force T take the same position. In case the plate stiffness D is set to one, the curvatures are equal to the bending moments and the sum of curvatures is thereby equal to the sum of bending moments. When the same is done for the membrane equation (2.28), by setting the membrane force T to 1, the membrane surface is equal to the sum of bending moments surface, as shown in the equation (2.30). The vertical deflection of the surface in an arbitrary point is equal to value $\bar{M}$.

$$\bar{M} = \Delta w = \frac{\partial^2 w_m}{\partial x^2} + \frac{\partial^2 w_m}{\partial y^2} = p \quad ; \quad (D = 1) \qquad (2.30)$$

2.4 Force Density method

2.4.1 Introduction to form finding

Membrane structures have a very distinguishing esthetical appearance, which is a direct expression of their (efficient) structural behaviour. Due to the small structural dimensions, with an infinitesimal small bending stiffness, the structure can only react to external forces and loads by extensional forces (often referred to as membrane forces). An equilibrium of these membrane forces results geometrically in the characteristic double curved surfaces. Finding the equilibrium shape of these pure tension or compression structures is geometrically a non-linear problem and consists of determining the membrane geometry which is compatible with a set of given pre-stress conditions and boundary conditions starting from an initial geometry. The process of determining the equilibrium shape is known as form finding.

The first form finding methods relied on building physical models based on for example chain models, soap bubbles, hanging fabric and air inflated elastic membranes. These experimental methods helped greatly in visualizing and understanding the structural behaviour of tensile structures. A disadvantage was however, that the creation, measuring and structural analysis of these models took a considerable amount of time restraining the number of design variants that could be explored in the design process.

Computational techniques, which were developed several years later, provided a more flexible approach to form finding. Several computational form finding techniques were developed through the years relying on different mathematical techniques leading to the equilibrium geometry of a pre stressed membrane subjected to a certain load case and a set of predefined boundary conditions. The main methods which are used in practice are the force density method (Schek, 1973) and the dynamic relaxation method. The application of these methods seems to be geographically determined (Veenendaal, 2008). Other methods like the update reference strategy, spring particle system are until this moment only used within academic circles. It must be noted that although these computational techniques offer great advantages with respect to flexibility, precision and interfacing possibilities with other CAD programs they do not directly contribute to a more intuitive understanding of the structural behaviour of membrane structures, which is induced to a greater extend by working with physical methods. Moreover, at this moment, the aspect of manufacturability is often not implemented within these form finding applications (Veenendaal, 2008).

For the purposes of this thesis, the choice was made to use the Force Density form finding method based on various arguments. First, a set of comprehensive sources was found explaining the principles of Force Density method which simplified the process of apprehension and subsequently the computational computation. Second, the Force Density method is assumed to be faster than Dynamic Relaxation method within the scope of this thesis. This assumption is based on the facts that the linear Force Density calculation for a relative simple square mesh within the concerned rectangular boundary shapes will lead to an advantage with respect to computational efficiency and CPU usage, determined by the number of computation steps resulting in the total calculation time. Finally, there is no need for a series of intermediate solutions provided by iterative calculation methods which suggest a dynamic structural behaviour of the structure until it approaches its equilibrium shape.

The following paragraphs will start with a condensed description of the mathematical theory of the Force Density method, largely based on the paper written by H. Scheck in 1975 (Schek, 1973). Schek and Linkewitz together proposed the method in 1972 when it was used for determining the membrane shape of the Olympic stadium in Munich.

2.4.2 *Force Density method for form finding*

The force density method calculates the equilibrium state of a predefined initial net structure by transforming a system of non-linear equilibrium equations into a system of linear equilibrium equations by prescribing a constant force- density value. In order to do this, the membrane surface is transformed into a discrete cable nest system where the cable elements represent parts of the membrane. The force density method is based on the mathematical assumption that the ratio between the length and tension within each cable element is a constant value (Lewis 2003). The mathematical sequence of deriving the equilibrium equations is not presented within this paragraph since it is not of direct significance within the context of this thesis. Only the necessary steps in assembling and solving the equilibrium equations will be described as this is of direct significance for implementing the method into the envisioned computational model. For more information regarding the mathematical background of the Force Density method refer to the paper of H. Scheck.

As input for the force density method an initial mesh (net structure) is formed which consists of a series of points (nodes), connected by lines (branches). This mesh topology is mathematically described by using a branch node matrix by setting the connectivity between the points and braches. For this reason all points n_s are numbered from 1 to n and the braches from 1 to m. For later application it is advisable that first the free points n are declared and afterwards the fixed points n_f, so that $n_s = n + n_f$. The usual branch-node matrix C is defined by:

$$c(i,j) = \begin{matrix} +1 & \text{for } i(j)=1 \\ -1 & \text{for } k(j)=1 \\ 0 & \text{in other cases} \end{matrix} \tag{2.31}$$

The branch node matrix C_s has m rows and n_s columns. According to the classification of the points into free and fixed points the matrix can be divided into respectively two sub matrixes C and C_s:

$$\mathbf{C_s} = \mathbf{C} + \mathbf{C_f} = \begin{array}{c} \begin{array}{cc} \mathbf{C} & \mathbf{C_f} \end{array} \\ \left[\begin{array}{ccc|ccc} c_{f\,11} & \cdots & c_{f\,1n} & c_{f\,1n+1} & \cdots & c_{f\,1n_s} \\ \vdots & \ddots & \vdots & \vdots & \ddots & \vdots \\ c_{f\,m1} & \cdots & c_{f\,mp} & c_{f\,m1} & \cdots & c_{f\,mp} \end{array}\right] \end{array} \tag{2.32}$$

An example of the assembly of a branch node matrix (figure 8) for a arbitrary mesh topology (figure 7) is shown on the next page. The free points are indicated as dashed molecules and the fixed points as molecules with a continous line.

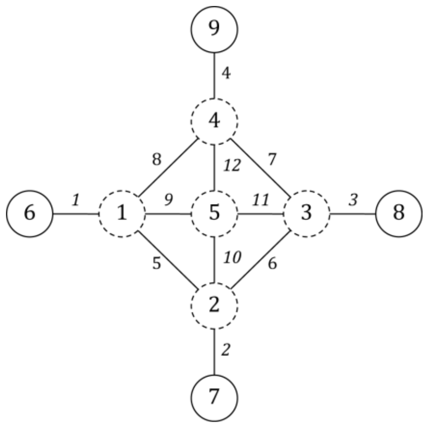

$$
\boldsymbol{C_s} = \begin{array}{c|ccccc|cccc}
 & \mathbf{1} & \mathbf{2} & \mathbf{3} & \mathbf{4} & \mathbf{5} & \mathbf{6} & \mathbf{7} & \mathbf{8} & \mathbf{9} \\
\mathbf{1} & 1 & \cdot & \cdot & \cdot & \cdot & -1 & \cdot & \cdot & \cdot \\
\mathbf{2} & \cdot & 1 & \cdot & \cdot & \cdot & \cdot & -1 & \cdot & \cdot \\
\mathbf{3} & \cdot & \cdot & 1 & \cdot & \cdot & \cdot & \cdot & -1 & \cdot \\
\mathbf{4} & \cdot & \cdot & \cdot & 1 & \cdot & \cdot & \cdot & \cdot & -1 \\
\mathbf{5} & 1 & \cdot & \cdot & -1 & \cdot & \cdot & \cdot & \cdot & \cdot \\
\mathbf{6} & 1 & -1 & \cdot & \cdot & \cdot & \cdot & \cdot & \cdot & \cdot \\
\mathbf{7} & \cdot & 1 & -1 & \cdot & \cdot & \cdot & \cdot & \cdot & \cdot \\
\mathbf{8} & \cdot & \cdot & 1 & -1 & \cdot & \cdot & \cdot & \cdot & \cdot \\
\mathbf{9} & \cdot & \cdot & \cdot & 1 & -1 & \cdot & \cdot & \cdot & \cdot \\
\mathbf{10} & 1 & \cdot & \cdot & \cdot & -1 & \cdot & \cdot & \cdot & \cdot \\
\mathbf{11} & \cdot & 1 & \cdot & \cdot & -1 & \cdot & \cdot & \cdot & \cdot \\
\mathbf{12} & \cdot & \cdot & 1 & \cdot & -1 & \cdot & \cdot & \cdot & \cdot \\
 & & & \boldsymbol{C} & & & & \boldsymbol{C_f} & &
\end{array}
$$

Fig.7. Mesh topology

Fig.8. Branch node matrix

The next step is to form several matrixes containing force-density values, point coordinates and loads, which are necessary for the assembly of the system of equilibrium equations. Firstly, three n_f dimensional coordinate matrixes, $\mathbf{x_f}$, $\mathbf{y_f}$ and $\mathbf{z_f}$ are formed by specifying the x-, y- and z-coordinates of the fixed points:

$$
\mathbf{x_f} = \begin{bmatrix} x_{f_1} \\ \vdots \\ x_{f_n} \end{bmatrix} \qquad \mathbf{y_f} = \begin{bmatrix} y_{f_1} \\ \vdots \\ y_{f_n} \end{bmatrix} \qquad \mathbf{z_f} = \begin{bmatrix} z_{f_1} \\ \vdots \\ z_{f_n} \end{bmatrix} \tag{2.33}
$$

Secondly, three n dimensional matrixes are formed by specifying the loads in respectively the x-, y- and z-direction for the free points n.

$$
\mathbf{p_x} = \begin{bmatrix} p_{x_1} \\ \vdots \\ p_{x_n} \end{bmatrix} \qquad \mathbf{p_y} = \begin{bmatrix} p_{y_1} \\ \vdots \\ p_{y_n} \end{bmatrix} \qquad \mathbf{p_z} = \begin{bmatrix} p_{z_1} \\ \vdots \\ p_{z_n} \end{bmatrix} \tag{2.34}
$$

Thirdly, a diagonal $m \times m$ dimensional force density matrix $\mathbf{Q}$ is formed by specifying the constant force density values:

$$
\mathbf{q} = \mathbf{L}^{-1} \times \mathbf{s}
$$

$$
\mathbf{Q} = \begin{bmatrix} q_{11} & 0 & 0 \\ 0 & \ddots & 0 \\ 0 & 0 & q_{mm} \end{bmatrix} \tag{2.35}
$$

Now all the necessary matrixes are determined, the three systems of linear equilibrium equations can be assembled for the x, y– and z–direction which are defined as:

$$
\begin{aligned}
\mathbf{C^tQCx} + \mathbf{C^tQC_f x_f} &= \mathbf{p_x} \\
\mathbf{C^tQCy} + \mathbf{C^tQC_f y_f} &= \mathbf{p_y} \\
\mathbf{C^tQCz} + \mathbf{C^tQC_f z_f} &= \mathbf{p_z}
\end{aligned}
\tag{2.36}
$$

We can simplify these equations by:

$$
\begin{aligned}
\mathbf{D} &= \mathbf{C^tQC} \\
\mathbf{D_f} &= \mathbf{C^tQC_f} \\
\\
\mathbf{Dx} + \mathbf{D_f x_f} &= \mathbf{p_x} \\
\mathbf{Dy} + \mathbf{D_f y_f} &= \mathbf{p_y} \\
\mathbf{Dz} + \mathbf{D_f z_f} &= \mathbf{p_z}
\end{aligned}
\tag{2.37}
$$

Since we want to calculate the new coordinates of the points as part of the equilibrium mesh we can rewrite the equilibrium equations as:

$$
\begin{aligned}
\mathbf{x} &= \mathbf{D^{-1}}(\mathbf{p_x} - \mathbf{D_f x_f}) \\
\mathbf{y} &= \mathbf{D^{-1}}(\mathbf{p_y} - \mathbf{D_f y_f}) \\
\mathbf{z} &= \mathbf{D^{-1}}(\mathbf{p_z} - \mathbf{D_f z_f})
\end{aligned}
\tag{2.38}
$$

By solving the three systems of linear equilibrium equations, the 'new' coordinates of the free points are obtained. By using the branch node matrix the points the corresponding mesh can be constructed making the membrane shape clearly visible. Two examples are shown which were produced by H. Scheck (Schek, 1973).

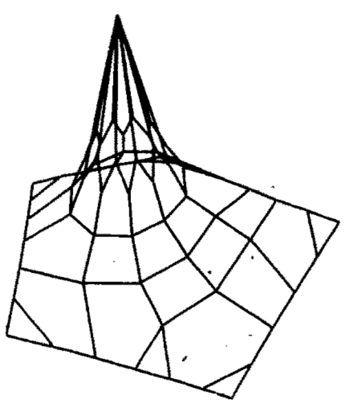

Fig.9. *Membrane shape*

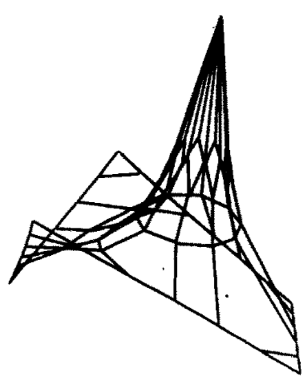

Fig.10. *Membrane shape*

2.4.3 *Additional boundary conditions*

Up to this point, the initial mesh points are classified based on of their freedom of movement in free points and fixed points. It could also be interesting to see what happens if (some) points are only allowed to move in a certain direction or plane as it introduces more possibilities to manipulate the form finding process.

As shown before, the branch node matrix describes the connectivity between the points and branches within the mesh topology. This branch node matrix $\mathbf{C_s}$ was divided into two sub matrixes; a matrix $\mathbf{C}$ for the free points and a matrix $\mathbf{C_f}$ for the fixed points. Since the movement of the points was either totally fixed or totally free in all directions this branch node matrix could be used for all equilibrium equations. But in case some points are only free to move in certain directions, the branch node matrixes for the corresponding directions are different too. Therefore, in these cases it is necessary to assemble multiple branch node matrixes:

$$\begin{aligned} \mathbf{C}_{x_s} &= \mathbf{C}_x + \mathbf{C}_{x_f} \\ \mathbf{C}_{y_s} &= \mathbf{C}_y + \mathbf{C}_{y_f} \\ \mathbf{C}_{z_s} &= \mathbf{C}_z + \mathbf{C}_{z_f} \end{aligned} \tag{2.39}$$

As a result, three sub matrixes for $\mathbf{D}$ and $\mathbf{D_f}$ matrixes are needed as well:

$$\begin{aligned} &\mathbf{D}_x = \mathbf{C}_x{}^t\mathbf{Q}\mathbf{C}_x && \mathbf{D}_y = \mathbf{C}_y{}^t\mathbf{Q}\mathbf{C}_y && \mathbf{D}_z = \mathbf{C}_z{}^t\mathbf{Q}\mathbf{C}_z \\ &\mathbf{D}_{x_f} = \mathbf{C}_x{}^t\mathbf{Q}\mathbf{C}_{x_f} && \mathbf{D}_{y_f} = \mathbf{C}_y{}^t\mathbf{Q}\mathbf{C}_{y_f} && \mathbf{D}_{z_f} = \mathbf{C}_z{}^t\mathbf{Q}\mathbf{C}_{z_f} \end{aligned} \tag{2.40}$$

This transforms the equations into:

$$\begin{aligned} \mathbf{D}_x\mathbf{x} + \mathbf{D}_{x_f}\mathbf{x_f} &= \mathbf{p}_x \\ \mathbf{D}_y\mathbf{y} + \mathbf{D}_{y_f}\mathbf{y_f} &= \mathbf{p}_y \\ \mathbf{D}_z\mathbf{z} + \mathbf{D}_{z_f}\mathbf{z_f} &= \mathbf{p}_z \end{aligned} \tag{2.41}$$

The equilibrium equations eventually have the same structure as the ones for a collection of totally free points and fixed points and can be solved in the same way to obtain the coordinates of the moved points.

2.5 Rain flow analogy

2.5.1 Introduction

The rain flow analogy (Beranek, 1976) can be used in combination with the sum of curvatures surface to determine continuous principle shear force trajectories along which the shear forces will flow to the supports. W.J. Beranek, emeritus professor of structural mechanics in the architectural department of Delft University of Technology, introduced the shower analogy to illustrate the phenomenon of the direction of the load discharge.

2.5.2 Principle shear force trajectories

Within the rain flow analogy, one imagines the (distributed) load p as a rain shower of constant intensity falling down on a surface which represents the sum of curvatures (or the sum of bending moments, in case $D = 1$) surface of the plate. The stream lines which a single drop of water describes from the moment it hits the surface towards a support, by flowing down in the direction of the steepest descent, is the same trajectory as the flow of the principle shear force v_n. The amount of water passing through a section is directly related to the angle of surface (which determines the flow speed) and thereby gives an indication of the magnitude of the principle shear force. All shower water between two trajectories flows parallel to the trajectories and does not pass trajectories (stream lines). It is important to notice that the analogy only works if the influence of the speed accumulation along the trajectory and the change of direction due to collisions between drops are neglected.

2.5.3 Magnitude of principle shear forces

The magnitude of the principle shear force v_n in a certain section in the plate can be determined graphically by integrating the associated load which flows between two trajectories, corresponding to the start and end points of the section, towards the section. Both rain flow trajectories end up in a (local) maximum which is the highest point on the sum of bending moment surface. By dividing this integral value through the length of the section, the concentrated principle shear force in the section can be calculated. There is a direct relation between the length of the section and the accuracy of the determined principle shear force: the smaller the length of the section, the more accurate the results will be. As is shown in figure 11 and 12 (Beranek, 1976), the magnitude of the support reactions, excluded the concentrated shear forces, can be determined by defining a series of sections along the plate edges.

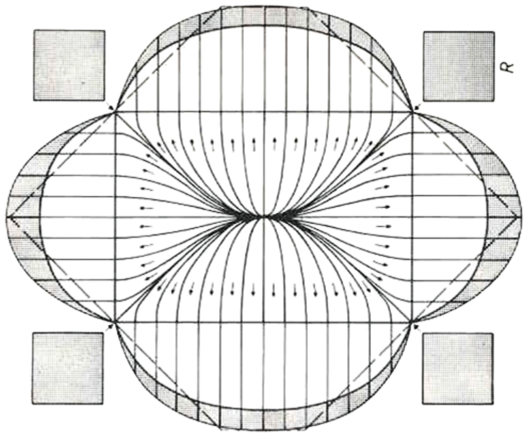

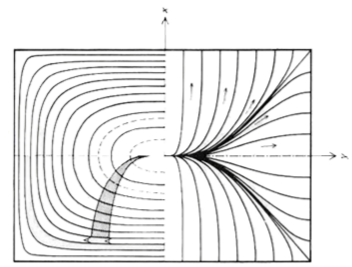

Fig.11. Shear force trajectories and support reactions

Fig.12. Integration of the load between two trajectories

In the examples presented above, the considered sections are part of the contour lines of the sum of curvatures or sum of bending moments surface and thereby we know that the direction of the principle shear force vector is perpendicular to this section. In case a particular section is chosen which is not (part of) a contour line, the direction of the principle shear force vector is not perpendicular to the section. In these cases the direction of the shear forces can be determined by using equation (2.11) which is derived in paragraph 2.2.

2.5.4 Rain flow analysis for shell structures

Shell structures are known for their structural efficiency, resulting in slender and elegant structures with a large span to thickness ratio. The structural performance of a shell relies on the curvature of the surface, which means that the loads are transferred to the supports mainly by extension forces and only small (corrective) bending moments will occur. This principle is called shell behaviour (figure 14).

Fig.13. Shell structure (Heinz Isler)

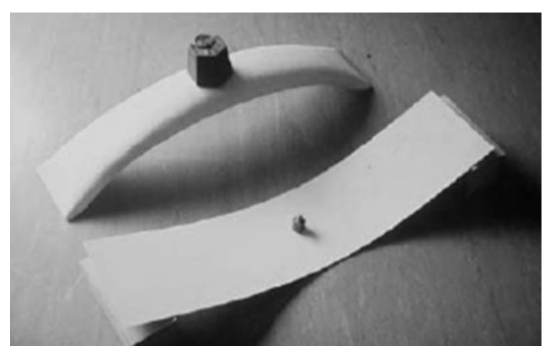

Fig.14. Shell behaviour

Geometrically regular curved surfaces can be described by analytical mathematical functions which can be used subsequently to derive a set of (differential) equations for describing their mechanical behaviour. For irregular curved surfaces there are very little analytical equations available, thereby it is more difficult to derive (differential) equations which describe the relation between their mechanical behaviour. Computational structural analysis programs, based on FEM, can be used for calculating the stress resultants and deformations within shell structures to obtain a quantitative insight in their mechanical behaviour. Nevertheless, due to the calculation techniques based on solving large matrixes, no qualitative insight is obtained about the relation between for example the structural geometry and mechanical behaviour (Borgart, Hoogenboom, & De Leeuw, 2005).

A recent theory is an extension of the previously described rain flow analysis for plates to shell structures, first introduced by A. Borgart. The hypothesis of this theory states that the sum of curvatures surface can be replaced by the shell surface itself. The rain flow trajectories then visualize again how the load flows to the supports by following the steepest descent.

2.5.5 Computational application of the rain flow analogy

A computational application of the rain flow analysis was developed by M. Haasnoot as part of his master thesis at the Faculty of Architecture at the TU Delft. This application generates the rain flow trajectories by using the dynamics-engine provided by the three dimensional animation software package Maya. The rain flow trajectories are generated by tracking the paths of a series of particles which are released above- and subsequently flow down on an arbitrary surface within a simulation involving physical effects as gravitation and friction.

2.5.6 Case study

This computational application is used to test the rain flow hypothesis for shell structures by using it within a case study to generate the rain flow trajectories for a free form shell structure for an indoor ski-slope which was designed by H. Hanselaar (student of the TU Delft Faculty of Architecture) (Hanselaar, 2003). Two pictures (figure 15 and 16) of the achieved results are shown below.

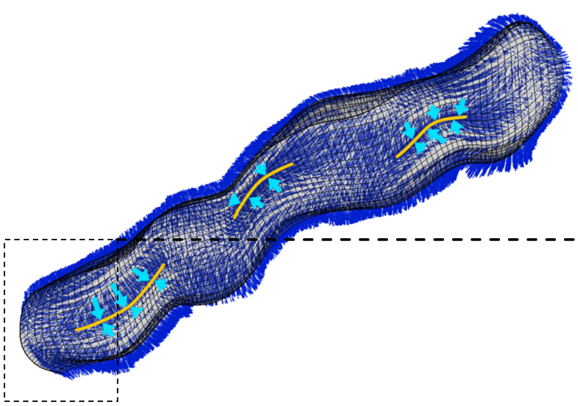

Fig.15. Rain flow trajectories on the free form shell structure

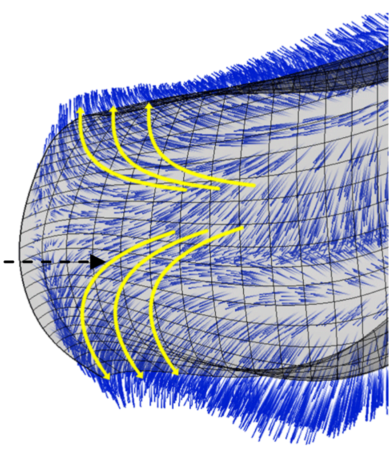

Fig.16. Rain flow trajectories directed to support by edge shape

The results of the case study showed that the generated rain flow trajectories can provide a designer or engineer with important information on the relation between the shell geometry and the structural performance of free form shell structures. The surface shape influences how the loads flow to the supports and thereby what type of stress resultants and deformations will occur. In case of a well designed shell structure (from a structural point of view) these forces will be mainly extensional (membrane forces) forces and little corrective bending moments or hoop forces which have to ensure that the pressure surface converges with the system surface. Within the case study several undesirable and desirable situations with respect to the structural performance are distinguished.

Desirable situations are surface parts with a steep slope which induce a quick flow of extensional forces towards the supports. Another beneficial effect was noticed at raised edges with an anticlastic curvature (figure 16), where the shape of the edge directs the forces towards the supports. Along the lines of the rain flow analogy one can compare this with a natural gutter by which the rain water is transferred towards the supports. In these cases the load is carried by membrane forces, which is more desirable than a situation where the load is carried by concentrated shear forces, which will contribute to the development of bending moments along the edges.

Three types of undesirable situations were distinguished within the aforementioned case study. The first situation occurred at free edges where the rain water flows over the edges as a result of the edge shape. This indicates that the loads could not be transferred to the supports by compression forces and hoop forces or corrective bending moments have to carry the loads of which the latter is an undesirable situation as this might result in increased structural dimensions. The second situation occurred at ditches where multiple trajectories merge into one drain curve. It was noted that such drain curves can transfer loads by membrane forces under certain conditions depending on to what extend the drain shape is anticlastic or the surface slope (see figure 15). The last situation are surface parts which are nearly horizontal inducing a slow flow of forces and

2.6 *Curvature ratio method*

2.6.1 Introduction

During this research it was found that the ratio between the curvatures of the membrane surface (so that $sin\varphi \simeq \varphi$ and $cos\varphi \simeq 1$) itself and the sum of bending moment values (same as the displacements of the membrane surface in case $D = 1$ and $\upsilon = 0$) can be used for determining the bending moments m_{xx} and m_{yy}.

2.6.2 Definition of curvature

The concept of extrinsic curvature, for objects embedded in another space (Euclidean space) relating to the radius of curvature of oscillating circles that touch the object, is used within this thesis to determine the curvature of the membrane surface in the x-, y- and principle directions. The curvature of a curve is by definition the reciprocal of the radius of the osculating circle. The curvature is taken to be positive if the curve turns in the same direction as the surface's chosen normal and otherwise negative. The directions of the normal plane where the curvature takes its maximum and minimum values are always perpendicular (Euler, 1767), and are called principal directions (Weisstein, Principal Curvatures).

The planar (sectional) curvatures k_{xx} and k_{yy} of a on the surface that lies in a single plane in the x- and y-direction in a particular point on a surface can be determined by using the radius of the associated oscillating circles R in these directions as follows:

$$\kappa_{xx} = \frac{1}{R_{xx}} \quad ; \quad \kappa_{yy} = \frac{1}{R_{yy}} \tag{2.42}$$

These planar curvatures can also be determined by using the tangential angle ϕ and the arc length s:

$$\kappa_{xx} = \frac{d\phi_x}{ds_x} \quad ; \quad \kappa_{yy} = \frac{d\phi_y}{ds_y} \tag{2.43}$$

The principle curvatures k_1 and k_2 in a point on the surface can be determined by:

$$\kappa_1 = \frac{1}{R_1} \quad ; \quad \kappa_2 = \frac{1}{R_2} \tag{2.44}$$

These principle curvatures can also be determined again by using the tangential angle ϕ and the arc length s:

$$\kappa_1 = \frac{d\phi_1}{ds_1} \quad ; \quad \kappa_2 = \frac{d\phi_1}{ds_2} \tag{2.45}$$

The aforementioned oscillating circles are graphically displayed for an elementary surface part in the figures 17 and 18.

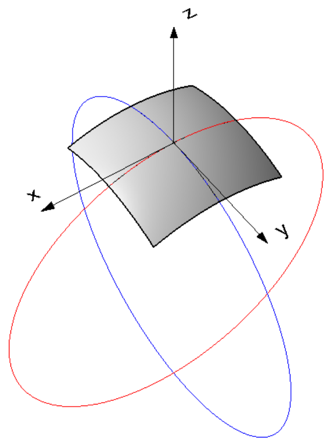

Fig.17. Oscillating circles in the x- and y-direction

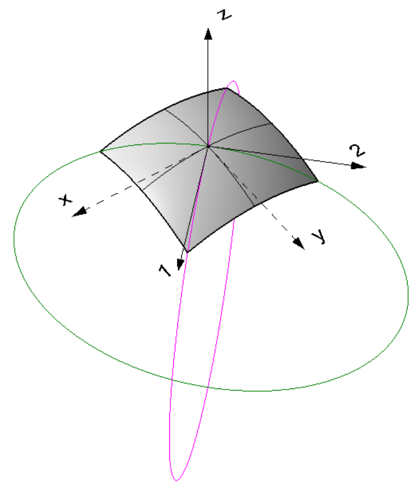

Fig.18. Oscillating circles for principle curvatures

The summation of either two principle curvatures ($\kappa_1 + \kappa_2$) or two planar curvatures in the orthogonal x- and y-directions ($\kappa_{xx} + \kappa_{yy}$) will by definition lead to an equal value sum of curvatures value $\bar{K}$ which means that the curvature is invariant with respect to rotations of the xy-coordinate system about its origin.

Curvature lines can be used to visualize the surface curvature directions. These lines are by definition the integral curves for the direction fields and in each surface point tangent to a principal or planar curvature direction (they are). There will be two lines of curvature through each non-umbilic point and the lines will cross at right angles.

2.6.3 Bending moments in x- and y-direction

By determining the ratio between the curvatures in respectively the x- and y-direction (k_{xx} and k_{yy}) and the sum of curvatures ($k_{xx} + k_{yy}$) of the membrane surface and subsequently multiplying this ratio with the sum of bending moments value $\bar{M}$, the bending moments m_{xx} and m_{yy} can be calculated as shown in the formula (2.xx). For reasons of clarity, the Greek curvature symbol kappa κ is changed into the symbol k. This is to avoid confusion between the curvature of the deflection field of plates and the curvature of the membrane surface.

$$m_{xx} = \frac{k_{xx}}{k_{xx} + k_{yy}} \cdot \bar{M} \quad ; \quad m_{yy} = \frac{k_{yy}}{k_{xx} + k_{yy}} \cdot \bar{M} \tag{2.46}$$

2.6.4 Principle moments

Because the sum of the bending moments value $\bar{M}$ is invariant with respect to the rotations of the xy-coordinate system about its origin, the ration between principle curvature values k_1 and k_2 and the sum of bending moments value $\bar{M}$ could in theory be used in the same way to determine the principle moments m_1 and m_2 by:

$$m_1 = \frac{k_1}{k_1 + k_2} \cdot \bar{M} \quad ; \quad m_2 = \frac{k_2}{k_1 + k_2} \cdot \bar{M} \tag{2.47}$$

Nevertheless this turns out not to be possible as the sum of bending moments value $\bar{M}$, being a summation of two moment values in orthogonal directions, can consist of either two positive or two negative values or out of one negative and one positive value. In the case of two positive or two negative values the summation delivers a results bigger (or equal, in case one of the values is zero) than the single values with the same sign. Both m_{xx} and m_{yy} are positive and therefore their sum can be used to calculate the ratio between one of the values and the sum as is show before in equation (2.xx). In the case of a summation of one negative and one positive value the result is smaller (or equal, in case one of the values is zero) than the single values with either a positive or negative sign. Therefore the ratio between the curvatures of the scaled sum of bending moment surface cannot be used to determine the m_1 and m_2 out of the sum of bending moments $\bar{M}$, as we know that the values for m_1 and m_2 can have an opposite sign.

For example, along the edges of a simply supported isotropic rectangular plate both m_{xx} and m_{yy} equal zero and m_1 and m_2 have the same absolute value as m_{xy} and m_{yx}, but their signs are opposite. As a result their sum equals zero. This can also be shown by using (rewritten) Mohr's equations:

$$m_{xy} = m_{yx} = \sqrt{\left(\frac{m_1 - m_2}{2}\right)^2 - \left(\frac{m_{xx} - m_{yy}}{2}\right)^2} \tag{2.48}$$

$$m_{xy} = \sqrt{\left(\frac{m_1 - m_2}{2}\right)^2} = |m_1| = |m_2| \qquad (m_{xx} = 0; m_{yy} = 0) \tag{2.49}$$

$$m_1 + m_2 = 0 \tag{2.50}$$

It must be noted that for a twistless plate, without torsional stiffness, the proposed method can be used directly to determine the principle bending moments in a simply supported plate.

2.7 *Finite difference method*

2.7.1 Introduction

The Finite Difference method (FDM) is a classical mathematical technique for approximating the solutions of differential equations by replacing them by finite difference equations (Blauwendraad, Plate Analysis, Theory and Application Volume 2, Numerical Methods, 2006). The FD-method is often seen as the predecessor of the widely used Finite Element Method (FEM).

Within the FD-method a grid is applied over the region (in this context formed by the boundaries of the plate) and the Partial Differential Equations are solved for each grid point (node) by approximating the derivatives via the Taylor series expansion and using the differences as an approximation. Solving the set of linear equations leads to an approximate solution of the problem, a solution which becomes more accurate as the mesh is chosen finer. The approximation error is exactly known in terms of the remainder from the Taylor series expansion of the derivatives.

For the FD-method it is important that a uniform grid is applied over the region to reduce the errors by the differencing method. Finite Difference methods are thus less robust for irregular shaped bodies than finite element methods which divide the region into separate arbitrary shaped elements to fit the region and use a variational approach to solving the partial differential equations. Furthermore, FEM-methods offer advantages to FD-methods with respect to modelling boundary conditions and abrupt changes in thickness are easier to deal with. The concept of springs and shear panels implemented into a computational model by J. Witteveen (Beranek, 1976) provides an elegant way to overcome the latter type of difficulties.

Reasons for using the FD-method instead of the FEM-method within this thesis are that this method offers a more straightforward formulation of the solution to the specific problem for which it is applied. This makes it easier to understand and implement into the envisioned parametric computational application. Furthermore, the advantages offered by FEM-methods with respect to modelling boundary conditions and the flexible approach in generating meshes within free form boundaries are not important as the scope of this thesis is confined to rectangular plates which are simply supported along their edges. Moreover, the equations for nodes which are not influenced by boundary conditions are similar to those found in the classical Finite Difference Method and, as will be explained in the upcoming chapters, the FD-method in cases where it is not necessary to model boundary conditions.

The next paragraphs first explain the finite difference method by deriving the (partial) finite difference equations for plates which are simply supported along their edges. Thereafter, it will be explained how the finite difference method is used for structural analysis purposes within this thesis.

2.7.2 Deriving the (partial) finite difference equations for plates

The first step in deriving the (partial) finite difference equations from the differential equations for simply supported plates is to transform the continuous displacement field into a discrete mesh consisting of a series of straight elements connected by nodes (grid points). An element of this mesh is shown in the figure below:

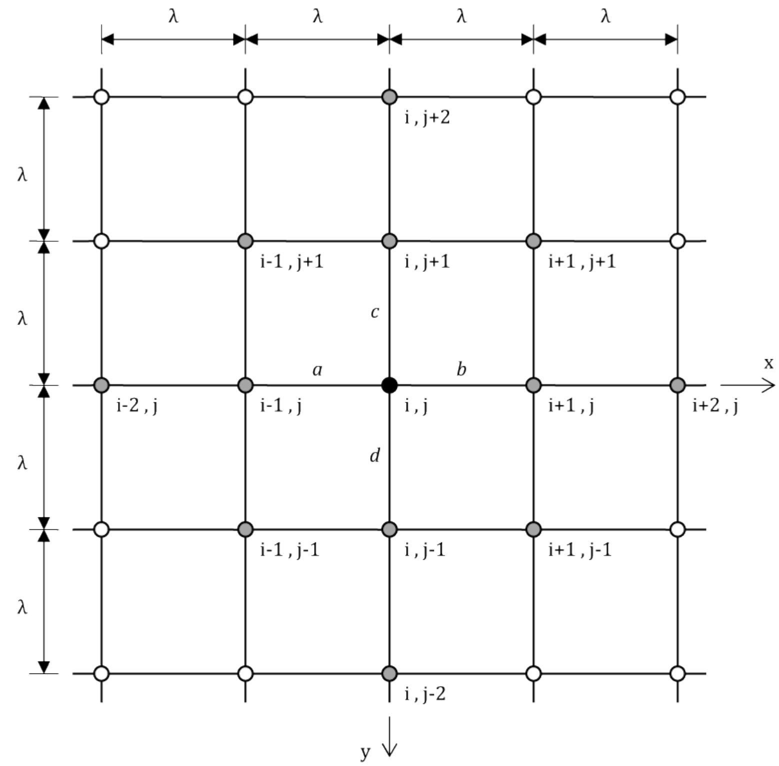

Fig.19. Part of the square calculation mesh

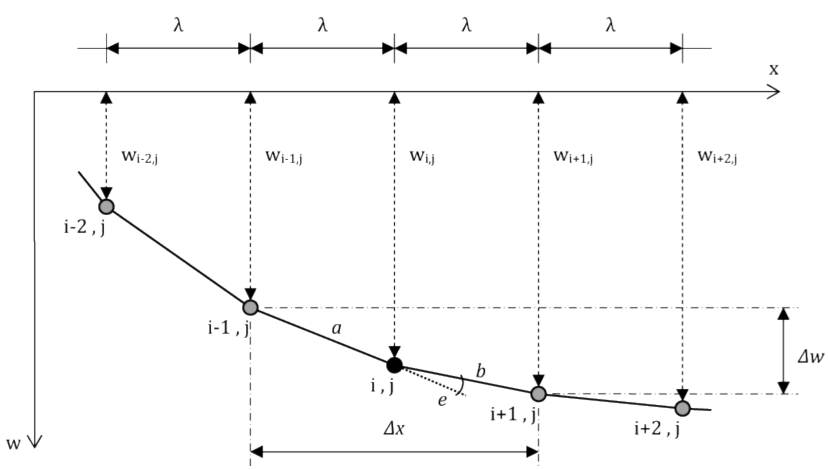

Fig.20. Discrete displacement curve along x-axis

De partial difference equation for respectively the generalised rotation φ, curvature κ, shears force V and load p for each grid point i, j in the x- and y-direction are derived by taking the n^{th} order derivatives of the displacement field for the x- and y-direction, analogously to the method for deriving the differential equations.

From the picture it can be concluded that the generalised rotations φ_a and φ_b in the x-direction of the elementary field elements a and b and the generalised rotations φ_c and φ_d in the y-direction of the elementary field elements c and d can be expressed in the displacements w by:

$$\varphi_a = \frac{1}{\lambda} \cdot (w_{i,j} - w_{i-1,j}) \quad ; \quad \varphi_b = \frac{1}{\lambda} \cdot (w_{i+1,j} - w_{i,j}) \quad \text{(rotations in x-direction)} \tag{2.51}$$

$$\varphi_c = \frac{1}{\lambda} \cdot (w_{i,j} - w_{i,j-1}) \quad ; \quad \varphi_d = \frac{1}{\lambda} \cdot (w_{i,j+1} - w_{i,j}) \quad \text{(rotations in y-direction)} \tag{2.52}$$

The generalised rotations in the x- and y-direction in point i, j are the first derivatives of the displacement field and can be expressed in the displacements w of the neighbouring grid points by:

$$\varphi_{x_{i,j}} = \frac{\partial w}{\partial x} = \frac{\Delta w}{\Delta x} = \frac{1}{2 \cdot \lambda} \cdot (w_{i+1} - w_{i-1}) \tag{2.53}$$

$$\varphi_{y_{i,j}} = \frac{\partial w}{\partial y} = \frac{\Delta w}{\Delta y} = \frac{1}{2 \cdot \lambda} \cdot (w_{j+1} - w_{j-1}) \tag{2.54}$$

The second derivative in a grid point i, j of the displacement field is defined as the curvature. This curvature is equal to the angle between the rigid rotations of the adjoining elements as is shown below:

$$\left.\begin{aligned} \varphi_a &= \frac{1}{\lambda}\left(w_{i,j} - w_{i-1,j}\right) \\ \varphi_b &= \frac{1}{\lambda}\left(w_{i+1,j} - w_{i,j}\right) \end{aligned}\right\} \rightarrow e = \varphi_a - \varphi_b = \kappa_{xx_{i,j}} = \frac{\partial^2 w}{\partial x^2} = \frac{\partial}{\partial x} \cdot \frac{\partial w}{\partial x} = \frac{1}{\lambda^2}\left(w_{i-1,j} - 2 \cdot w_{i,j} + w_{i+1,j}\right) \tag{2.55}$$

$$\left.\begin{aligned} \varphi_c &= \frac{1}{\lambda}\left(w_{i,j} - w_{i,j-1}\right) \\ \varphi_d &= \frac{1}{\lambda}\left(w_{i,j+1} - w_{i,j}\right) \end{aligned}\right\} \rightarrow e = \varphi_c - \varphi_d = \kappa_{yy_{i,j}} = \frac{\partial^2 w}{\partial y^2} = \frac{\partial}{\partial y} \cdot \frac{\partial w}{\partial y} = \frac{1}{\lambda^2}\left(w_{i,j-1} - 2 \cdot w_{i,j} + w_{i,j+1}\right) \tag{2.56}$$

The torsional curvatures can be defined as:

$$\kappa_{xy} = \kappa_{yx} = \frac{\partial^2 w}{\partial x \partial y} = \frac{1}{4 \cdot \lambda^2} \cdot (-w_{i+1,j+1} - w_{i-1,j-1} + w_{i-1,j+1} + w_{i+1,j-1}) \tag{2.57}$$

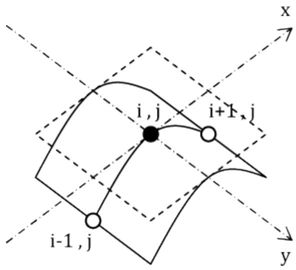

Fig.21. Curvature in x-direction

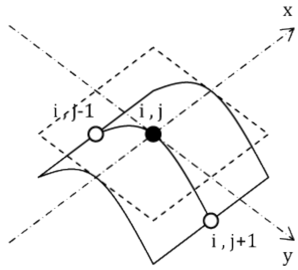

Fig.22. Curvature in y-direction

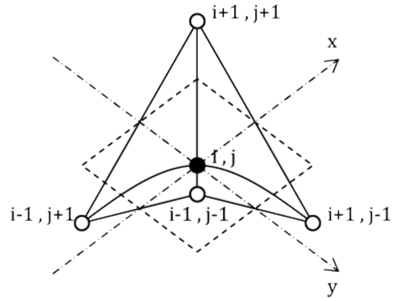

Fig.23. Torsion (plate of Nadai)

The shear forces in the x- and y-direction in point i, j are defined as the third derivative of the displacement field and thereby equal to the difference between the above determined curvatures of the grid points adjacent to the considered grid point i, j and therefore can be calculated as shown below:

$$V_{x_{i,j}} = \frac{\partial^3 w}{\partial x^3} = \frac{1}{2\cdot\lambda}\left[\left(\frac{\partial^2 w}{\partial x^2}\right)_{i+1,j} - \left(\frac{\partial^2 w}{\partial x^2}\right)_{i-1,j}\right] = \frac{1}{2\cdot\lambda^3}\cdot(-w_{i-2,j} + 2\cdot w_{i-1,j} - 2\cdot w_{i+1,j} + w_{i+2,j}) \qquad (2.58)$$

$$V_{y_{i,j}} = \frac{\partial^3 w}{\partial y^3} = \frac{1}{2\cdot\lambda}\left[\left(\frac{\partial^2 w}{\partial y^2}\right)_{i,j+1} - \left(\frac{\partial^2 w}{\partial y^2}\right)_{i,j-1}\right] = \frac{1}{2\cdot\lambda^3}\cdot(-w_{i,j-2} + 2\cdot w_{i,j-1} - 2\cdot w_{i,j+1} + w_{i,j+2}) \qquad (2.59)$$

The distributed load p is the fourth derivative of the displacement field and can be expressed in the displacements w for the x- and the y-direction by:

$$p_{x_{i,j}} = \frac{\partial^4 w}{\partial x^4} = \frac{\partial^2}{\partial x^2}\cdot\frac{\partial^2 w}{\partial x^2} = \frac{\left(\frac{\partial^2 w}{\partial x^2}\right)_{i-1,j} - 2\cdot\left(\frac{\partial^2 w}{\partial x^2}\right)_{i,j} + \left(\frac{\partial^2 w}{\partial x^2}\right)_{i+1,j}}{\lambda^2}$$

$$= \frac{1}{\lambda^4}\cdot(w_{i-2,j} - 4\cdot w_{i-1,j} + 6\cdot w_{i,j} - 4\cdot w_{i+1,j} + w_{i+2,j}) \qquad (2.60)$$

$$p_{y_{i,j}} = \frac{\partial^4 w}{\partial y^4} = \frac{\partial^2}{\partial y^2}\cdot\frac{\partial^2 w}{\partial y^2} = \frac{\left(\frac{\partial^2 w}{\partial y^2}\right)_{i,j-1} - 2\cdot\left(\frac{\partial^2 w}{\partial y^2}\right)_{i,j} + \left(\frac{\partial^2 w}{\partial y^2}\right)_{i,j+1}}{\lambda^2}$$

$$= \frac{1}{\lambda^4}\cdot(w_{i,j-2} - 4\cdot w_{i,j-1} + 6\cdot w_{i,j} - 4\cdot w_{i,j+1} + w_{i,j+2}) \qquad (2.61)$$

By combining these partial finite difference equations for respectively the x- and y-direction, the fourth order finite difference equation can obtained as shown in the equation below:

$$
\begin{aligned}
p_{i,j} &= \Delta\Delta w = \frac{\partial^4 w}{\partial x^4} + 2\cdot\frac{\partial^4 w}{\partial x^2 \partial y^2} + \frac{\partial^4 w}{\partial y^4} \\
&= \frac{1}{\lambda^4}\cdot\left(w_{i,j-2} - 4\cdot w_{i,j-1} + 6\cdot w_{i,j} - 4\cdot w_{i,j+1} + w_{i,j+2}\right) \\
&\ldots + 2\cdot\left(-w_{i+1,j+1} - w_{i-1,j-1} + w_{i-1,j+1} + w_{i+1,j-1}\right)^2 \\
&\ldots + \left(w_{i-2,j} - 4\cdot w_{i-1,j} + 6\cdot w_{i,j} - 4\cdot w_{i+1,j} + w_{i+2,j}\right) \\
&=
\end{aligned}
\tag{2.62}
$$

A molecule notation is a graphical representation of the derived equations for each grid point as finite difference quotients. The circles indicate the considered (surrounding) net points and the numbers inside them represent the quotients of the displacements of these points. The quotients shown in the middle represent the distance between the grid points.

$$\varphi_{x_{i,j}} = \frac{\partial w}{\partial x} = \frac{1}{2\cdot\lambda}\cdot \begin{bmatrix} -1 & 0 & +1 \end{bmatrix} \tag{2.63}$$

$$\kappa_{xx} = \frac{\partial^2 w}{\partial x^2} = \frac{1}{\lambda^2}\cdot \begin{bmatrix} +1 & -2 & +1 \end{bmatrix} \tag{2.64}$$

$$\kappa_{xy} = \frac{\partial^2 w}{\partial x \partial y} = \frac{1}{4\cdot\lambda^2}\cdot \begin{bmatrix} +1 & 0 & -1 \\ 0 & 0 & 0 \\ -1 & 0 & +1 \end{bmatrix} \tag{2.65}$$

$$V_{x_{i,j}} = \frac{\partial^3 w}{\partial x^3} = \frac{1}{2\cdot\lambda^3}\cdot \begin{bmatrix} -1 & +2 & 0 & -2 & +1 \end{bmatrix} \tag{2.66}$$

$$p_{x\,i,j} = \frac{\partial^4 w}{\partial x^4} = \frac{1}{\lambda^4}\cdot \begin{bmatrix} +1 & -4 & +6 & -4 & +1 \end{bmatrix} \tag{2.67}$$

$$p_{i,j} = \Delta\Delta w = \frac{\partial^4 w}{\partial x^4} + \frac{\partial^4 w}{\partial x^2 \partial y^2} + \frac{\partial^4 w}{\partial y^4} = \frac{1}{\lambda^4}\cdot \begin{bmatrix} & & +1 & & \\ & +2 & -8 & +2 & \\ +1 & -8 & +20 & -8 & +1 \\ & +2 & -8 & +2 & \\ & & +1 & & \end{bmatrix} \tag{2.68}$$

2.7.3 Boundary conditions

For points on the edge or next to the edge some of the 'molecules' fall outside the boundaries of the plate, four types of such situations are indicated in figure 24. Therefore, the finite difference equations for these points must be modified by eliminating the points outside the plate boundaries on basis of the associated boundary conditions. Since this thesis is confined to plates which are simply supported along their edges, the displacements w along the edges are equal to zero (and so in points A and C) and only the finite difference equations for points B and D have to be modified. For points B and D, the points outside the plate boundaries are eliminated by applying the applying the boundary conditions as specified in equation (2.71 and 2.72).

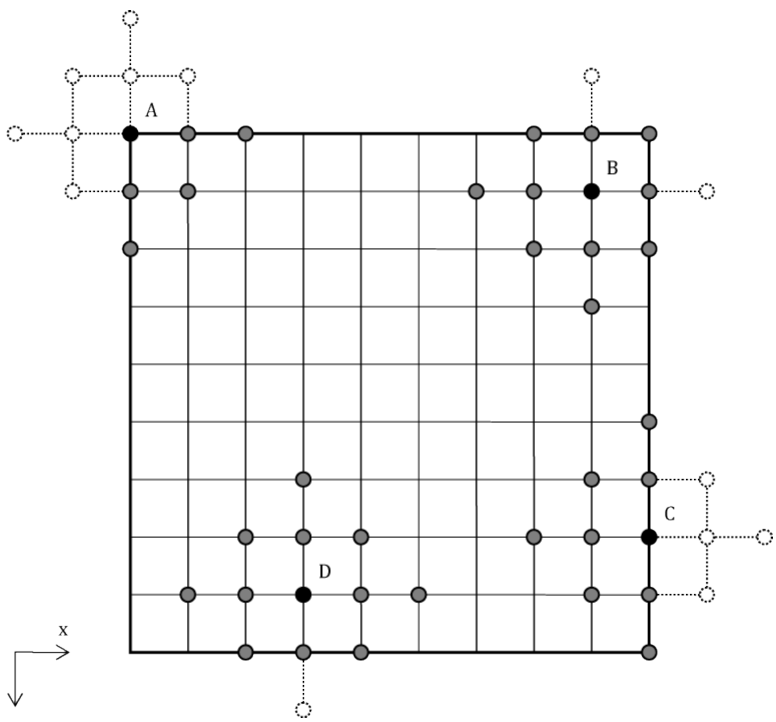

Fig.24. Points on the edge (A and C) and next to the edge (B and D)

$$\mathrm{A} \rightarrow \left\{ w_A = 0 \right. \tag{2.69}$$

$$\mathrm{C} \rightarrow \left\{ w_B = 0 \right. \tag{2.70}$$

$$\mathrm{B} \rightarrow \begin{cases} \kappa_{xx} = \dfrac{\partial^2 w}{\partial x^2} = 0 \\ \kappa_{yy} = \dfrac{\partial^2 w}{\partial y^2} = 0 \end{cases} \tag{2.71}$$

$$\mathrm{D} \rightarrow \left\{ \kappa_{xx} = \dfrac{\partial^2 w}{\partial x^2} = 0 \right. \tag{2.72}$$

Fig.25. Boundary conditions in point A-D

This results in the modified partial difference equations for point B (2.73) and D (2.74) shown below:

$$\mathrm{B} \rightarrow \begin{cases} \kappa_{xx} = \dfrac{\partial^2 w}{\partial x^2} = 0 \rightarrow w_{i,j} - 2 \cdot w_{i+1,j} + w_{i+2,j} = 0 \rightarrow w_{i+2,j} = -w_{i,j} + 2 \cdot w_{i+1,j} \\ \kappa_{yy} = \dfrac{\partial^2 w}{\partial y^2} = 0 \rightarrow w_{i,j} - 2 \cdot w_{i,j+1} + w_{i,j+2} = 0 \rightarrow w_{i,j+2} = -w_{i,j} + 2 \cdot w_{i,j+1} \end{cases} \tag{2.73}$$

$$\mathrm{D} \rightarrow \left\{ \kappa_{yy} = \dfrac{\partial^2 w}{\partial y^2} = 0 \rightarrow w_{i,j} - 2 \cdot w_{i,j+1} + w_{i,j+2} = 0 \rightarrow w_{i,j+2} = -w_{i,j} + 2 \cdot w_{i,j+1} \right. \tag{2.74}$$

These equations (2.73 and 2.74) can be used to modify the molecules which relate the load p to the displacements w as is shown in equations (2.55) and (2.56).

$$\mathrm{B} \rightarrow p_{i,j} = \Delta\Delta w = \frac{\partial^4 w}{\partial x^4} + \frac{\partial^4 w}{\partial x^2 \partial y^2} + \frac{\partial^4 w}{\partial y^4} \quad = \frac{1}{\lambda^4} \cdot \tag{2.75}$$

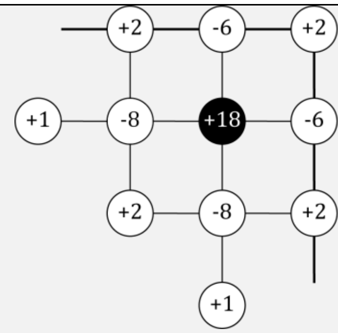

$$\mathrm{D} \rightarrow p_{i,j} = \Delta\Delta w = \frac{\partial^4 w}{\partial x^4} + \frac{\partial^4 w}{\partial x^2 \partial y^2} + \frac{\partial^4 w}{\partial y^4} \quad = \frac{1}{\lambda^4} \cdot \tag{2.76}$$

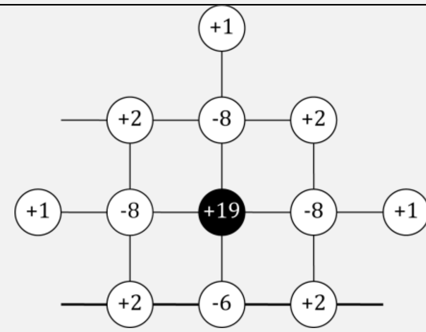

2.7.4 Solving the system of linear equations

The finite difference equations for each grid point for which $w \neq 0$ expresses the loads in the quotients of the considered, and several surrounding, points together form a system of n linear equations with n unknown displacements. By solving this system, the displacements for the considered grid points can be obtained, which subsequently can be used to calculate the stress resultants by using the partial difference equations.

The set of linear finite difference equations can be displayed in matrix notation by specifying a quotient matrix **A**, a column matrix w and another column matrix p as shown below:

$$\mathbf{A} \times \mathbf{w} = \mathbf{p} \tag{2.77}$$

Since the displacements w for the edge points of a simply supported plate are equal to zero, the corresponding rows and columns can be left out of the matrix by which the matrix size is reduced and simplified into a square $n \ x \ n$ matrix which can be solved by:

$$\mathbf{A}^{-1} \times \mathbf{p} = \mathbf{w} \tag{2.78}$$

2.8 Sand hill method

2.8.1 Introduction

Physical sand hill models can be used to determine the yield lines of plates with different support conditions. The models are produced by dropping fine grained dry sand on a plate with high edges with openings corresponding to the support conditions (Beranek, 1976). The sand grains will flow partially off the plate through the openings until the produced sand hill doesn't change anymore. The ridges of the sand hill figures represent the discrete yield lines of the considered plate structure. An example of such a sand hill model for a plate structure is shown in figure 26. The correspondence between the ridges of the sand hill model and the yield lines can be recognized by comparing figures 26 and 27.

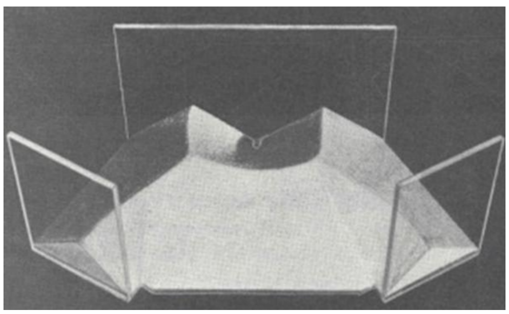

Fig.26. Physical sand hill figure

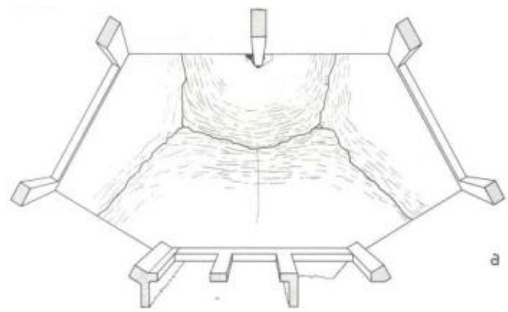

Fig.27. Yield lines of structure

The support conditions modelled as openings determine how the sand will flow of the plate and thereby the corresponding sand hill geometry. The openings are modelled in this way:

- a simply supported edge is modelled by a free plate edge
- an unsupported edge is modelled by a high edge
- a line support is modelled by a slotted hole
- a point support is modelled by a hole

Due to the mechanical behaviour of the fine dry sand grains, the resulting sand hill models will have slopes of approximately 45 degrees, which is the natural slope of sand hills. This will even be the case with inclined plate surfaces as is shown by the examples shown in figure 28.

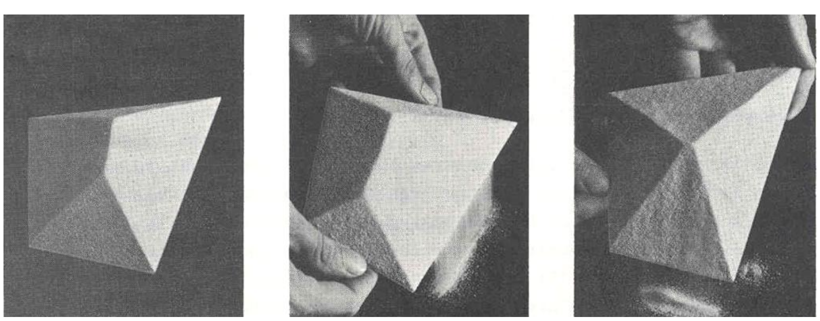

Fig.28. Sand hill models for horizontal and inclined surfaces

2.8.2 *Resemblance between sand hill models and Voronoi diagrams*

The planar yield lines for plates represented by the crests of the physical sand hill models show a clear resemblances with mathematical equidistance diagrams (often referred to as Voronoi tessellations, named after Gregory Voronoi or a Dirichlet tessellation after Lejeune Dirichlet) for a planar set of points or lines (collection of points) on the boundaries of the plate (Weisstein, Voronoi Diagram). Such a Voronoi diagram represents a partitioning of the plane into regions of equal nearest neighbours. The segments of the Voronoi diagram are all the points in the plane that are equidistant to the two nearest sites. The Voronoi nodes are the points equidistant to three (or more) sites. The dual graph for a Voronoi diagram corresponds to the Delaunay triangulation for the same set of points *P.*

Mathematical definition:

Let P be a set of n distinct points (sites) in the plane. The Voronoi diagram of P is the subdivision of the plane into n cells, one for each site. A point q lies in the cell corresponding to a site $p_i \in P$ if Euclidean_Distance(q, p_i) < Euclidean_distance(q, p_j), for each $p_i \in P, j \neq i$.

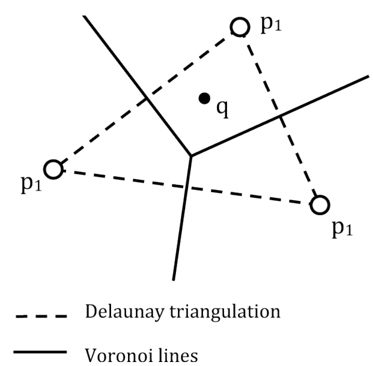

2.9 Application of the theoretical framework

2.9.1 Introduction

The just described structural analysis methods will be used in two steps to obtain insight in the mechanical behaviour of thin plate structures, in correspondence with objective 1a and the corresponding approach as defined within chapter 1. The first step is to implement the different methods in their original form into different parametric computational components. The next step was to combine methods into (novel) structural analysis sequences. This resulted in the following analysis sequences:

a) Force Density method(3) + Elastic membrane analogy(2)
b) Force Density method(3) + Elastic membrane analogy(2) + Differential equations(1)
c) Force Density method(3) + Elastic membrane analogy(2) + Rain flow analysis(4)
d) Force Density method(3) + Elastic membrane analogy(2) + Curvature ratio method(5)
e) Force Density method(3) + Elastic membrane analogy(2) + Finite Difference method(6) + Differential equations(1)

A combination between the sand hill method and other structural analysis methods was considered not feasible. The potential with respect to this method lies mainly in the computational application and extending its functionality (e.g. by exploring the relation between sand hill models and Voronoi tessellations). For these reasons this method is conceived as standalone structural analysis sequence.

In the upcoming paragraphs it will be explained how the different structural analysis sequences will presumably contribute to determining/calculating the deformations and the flow- and magnitude of forces within thin plate structures.

2.9.2 Elastic membrane analogy & Force Density method

The elastic membrane analogy will be used in combination with the Force Density form finding method to generate sum of bending moment mesh for $\bar{M}$ by generating the corresponding membrane mesh on basis of the theory presented in paragraph 2.xx. By applying a NURBS surface interpolation a sum bending moments surface is obtained, which is subsequently used to determine deformations and flow- and magnitude of forces by establishing the before mentioned structural analysis sequences b, c, d and e.

2.9.3 Elastic membrane analogy, Force Density method & Differential equations

The sum of bending moments surface (determined within sequence a) and the analytical equations which define the relation between the sum of bending moments and the shear forces (2.12-2.14) will be combined to calculate the magnitude- and direction of the (principle) shear forces v_n, v_x and v_y.

2.9.4 Elastic membrane analogy, Force Density method & Rain flow analysis

The sum of bending moments surface (determined within sequence a) will be used in combination with the rain flow analogy to generate rain flow stream lines which represent the trajectories the principle shear forces v_n. Subsequently, these trajectories will be used to determine the principle shear forces in arbitrary sections within plate structures by integrating the load between two trajectories towards the associated section or support. Furthermore, the rain flow analogy (again in combination with the sum of bending moments surface) will be used to generate 3D principle shear force v_n diagrams by simulating the load accumulation analogous to x- and y-components of the rain flow vectors in a series of points.

2.9.5 Elastic membrane analogy, Force Density form finding method & Curvature ratio method

The sum of bending moments surface (determined within sequence a) will be used in combination with the novel curvature ratio method to determine the bending moments in the x- and y-direction (m_{xx} and m_{yy}).

2.9.6 Elastic membrane analogy, Force Density method, Finite Difference method & Differential equations

The sum of bending moments surface (determined within sequence a) in combination with the Finite Difference method is used to determine the displacement field and the magnitude of the stress resultants.

The displacements in a grid of points will be calculated by assembling a system of linear partial finite difference equations, which relate the concerning displacements to the sum of curvature values $\bar{K}$, as shown in equation (2.79).

$$\bar{K} = \kappa_{xx} + \kappa_{yy} = \frac{\partial^2 w}{\partial x^2} + \frac{\partial^2 w}{\partial y^2} = \Delta w \tag{2.79}$$

In case the plate stiffness $D = 1$, both bending moments m_{xx} and m_{yy} are equal to the curvatures κ_{xx} and κ_{yy} in the corresponding directions and thereby the sum of curvatures $\bar{K}$ is equal to the sum of bending moments $\bar{M}$. Therefore, the sum of bending moments can be expressed by combining the before derived partial finite difference equations for κ_{xx} and κ_{yy} as shown in equation (2.80)

$$\kappa_{xx} + \kappa_{yy} = (m_{xx} + m_{yy}) = \bar{M} = \frac{1}{\lambda^2} \cdot (-4 \cdot w_{i,j} + w_{i-1,j} + w_{i+1,j} + w_{i,j-1} + w_{i,j+1}) \tag{2.80}$$

This equation can be represented graphically by using the molecule notation as shown in (2.81).

$$\kappa_{xx} + \kappa_{yy} = \frac{\partial^2 w}{\partial x^2} + \frac{\partial^2 w}{\partial y^2} = \bar{M} \qquad = \frac{1}{\lambda^2} \cdot$$

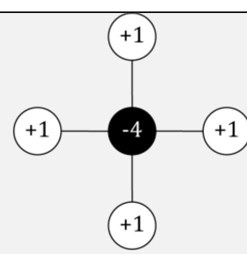

(2.81)

By solving the obtained set of linear equations and relating the displacements w of the grid points to the sum of bending moment values $\bar{M}$, the displacement field is obtained. This displacement field is subsequently used to determine the stress resultant in the points by solving the partial difference equations (2.55), (2,56) and (2,57) for each grid point.

The concentrated shear forces V will be calculated by taking the first derivative of the torsional moments along the edges on basis of differential equation (2.8). Finally Mohr's equations for the principle moments (2.20 & 2.21) will be used to determine the principle moments m_1 and m_2.

2.9.7 Sand hill models and Voronoi tessellations

The principles which determine the formation of physical sand hill models (defined on basis of experiments with these models), will be used to construct a computational application which can be used to generate sand hill models. Furthermore, it will be investigated if (and if yes, to what extend) inverted sand hill diagrams can be used as (discrete) principle shear force diagrams. This will be tested by using them to determine the corresponding bending moments along an axis by numerical integration methods. Moreover,

The presumed relationship between sand hill models and Voronoi tessellations will be used to determine the magnitude of principle shear forces along the edges of simply supported plates.

2.9.8 Application of the structural analysis sequences

Since the just described structural analysis sequences are mainly unprecedented it is not known in advance what their individual contribution will be with respect to obtaining insight in the flow- and magnitude of forces within thin plate structures. The actual contribution of the just described structural analysis sequences will be explored by implementing them into a series of parametric structural analysis components as part of the development of the covering structural design tool. The development of the different components will be explained in next chapter. In figure 2.xx a flow chart of the conceived structural analysis sequences, as part of the theoretical framework, is shown.

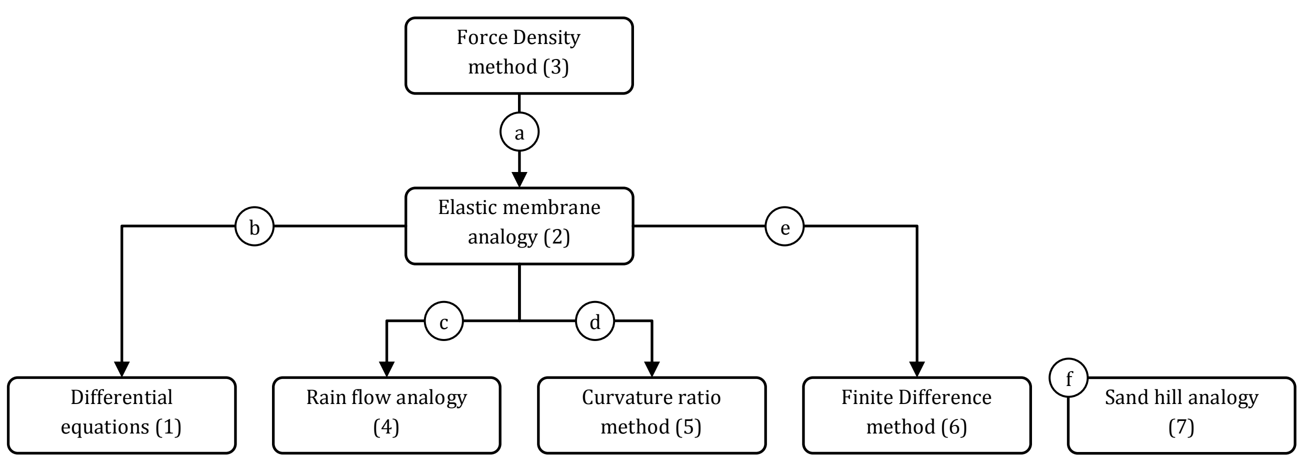

Fig.29. Flow chart of the conceived theoretical framework

3 Parametric structural design tool

3.1 Introduction

This chapter will elaborate on the development of the parametric structural design tool for thin plate structures, which was guided by the objectives 1b, 1c and 1d. First, the demands for the parametric structural design tools will be discussed in chapter 3.2, with respect to functionality and usability from the perspective of the envisioned users (objective 1b). Second, the general outline and structure of the structural design tool will be defined (objective 1c) within chapter 3.3 by giving a description of the parametric associative design approach, the software framework (and its functionality) and the structure of the conceived structural design tool which directly relates to the theoretical framework (defined in chapter 2). Third, it will be explained in chapter 3.4 how the theoretical framework was implemented into the conceived general structure of the design tool (objective 1d) by describing how the different structural analysis methods were applied within the corresponding structural analysis components. It will also be mentioned how each component relates to structural analysis sequence of which it forms a part. The actual contribution of the concerned structural analysis sequences will be given in the form of the output results generated by the different components. Fourth, the total performance of the structural design tool will be evaluated within chapter 3.5 with respect to the demands concerning functionality and usability (defined within paragraph 3.2).

3.2 Functionality and usability

In correspondence with objective 1b, it will be defined which demands concerning functionality and usability have to be fulfilled within the parametric structural design tool on basis of a concise enquiry amongst experts from practice (Witteveen+Bos). The objective was stated as:

"Define which demands, concerning functionality- and usability, have to be fulfilled by the parametric structural design tool."

3.2.1 Users

As mentioned in paragraph 1.3, the envisioned users of the structural design tool are both the architect and the structural engineer. As they have both a different task within- and approach to the design process, it is important to identify how they might use the parametric structural design tool within a conceptual design process. This knowledge can subsequently be used to create a parametric structural design tool that may even contribute to the collaboration between the architect and the structural engineer by introducing structural evaluation into the conceptual design process.

3.2.2 Characteristics of the conceptual design stage

During a conceptual design stage, both an architectural- and a structural conceptual design must be conceived in a relative short time. A series of different design concepts will be generated and evaluated with respect to architectural, technical, economical and legal feasibility within a cyclic design process. Within this design stage, the architect is mainly concerned with achieving a certain aesthetical appearance as part of an architectural concept and the structural engineer is more concerned with the structural feasibility determined on basis of information on for example stress distribution and deformations as part of a structural concept. The considerations made by both parties should converge into conceptual design in which both architectural and structural aspects are taken into account: an integrated design. The architectural quality and structural performance of this design is directly depended on the collaboration between the architect and the structural engineer. The parametric structural design tool, developed within this thesis project, is supposed to assist within this process by providing necessary information on the relation between form and forces (within plate structures) which can be used to make informed architectural- and structural design decisions and/or to perform manual optimizations.

The envisioned role of the parametric structural design tool, regarded from the perspective of both users, in combination with the just described character of the conceptual design stage has led to several demands concerning functionality and usability.

3.2.3 Functionality

The functional demands are directly related to the calculation procedures- and results (output) and how they contribute to quantitative and qualitative insight into the structural behaviour of thin plate structures. Concerning the quantitative insight the structural analysis tool must at least be able to calculate the numerical magnitudes of the following quantities:

- Shear forces (v_n, v_x, v_y)
- Bending and torsional moments (m_{xx}, m_{yy}, m_{xy})
- Concentrated shear forces (V)
- Principle moments (m_1, m_2)
- Displacements (w)

Qualitative insight relates, at least within this thesis, to the relationship between the different structural aspects: structural geometry, flow of forces, magnitude of forces and deformations. This is illustrated in figure 3.1, shown below.

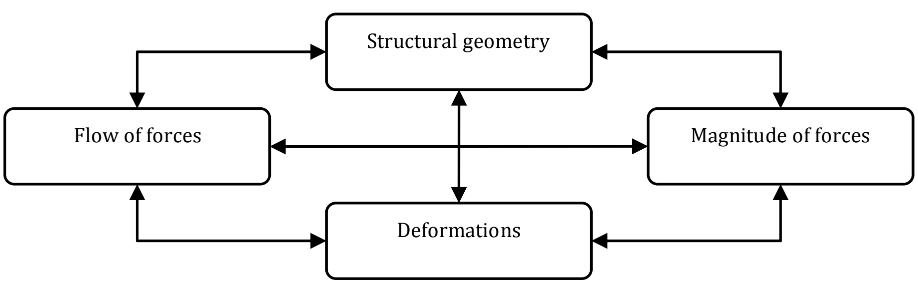

Fig.30. Relationships between the different structural aspects

Achieving this kind of insight in the mechanical behaviour of structures plays an important role within this thesis project, as mentioned within paragraph 1.1 concerning the background of this thesis project: this kind of information is often not obtained by using the widely used FEM methods (Borgart, Hoogenboom, & De Leeuw, 2005).

3.2.4 Usability

The envisioned flexible and intuitive process of exploring different design alternatives and/or (simultaneous) manual optimization demands a fast and flexible structural analysis procedure, characterized by several features concerning its usability:

- The structural design tool should be able to provide real-time results during the (architectural) design (modelling) process by which the influence of the structural parameters can be assessed.
- Ability to change the structural geometry, load cases, support conditions or material properties
- Ability to compose geometrical and analysis components in such a way that compose user defined structural analysis sequences
- Ability to define which- and how calculation results are presented
- Ability to extend the functionality of the structural design tool by adding (parametric) components or procedures

3.3 General outline and structure of the structural design tool

In correspondence with objective 1c, it will be explained within this paragraph how the general setup for the parametric structural design tool is conceived by giving a description of the software framework (and its functionality) and the structure of the conceived structural design tool which directly relates to the theoretical framework (defined in chapter 2). The objective was stated as:

"Define an appropriate general software framework and structure for the parametric structural design tool with respect to the demands concerning functionality and usability."

3.3.1 Parametric associative design approach

The parametric design approach is ideally suited to a simultaneous process of exploring and optimizing (complex) geometries as part of an architectural and structural design. The aim of parametric associative design is to capture a design into logical definitions, related by geometrical, mathematical or logical associations which are controlled by parameters.

3.3.2 Software framework

As software framework for the implementation of the structural analysis methods (part of the theoretical framework) a parametric design application named Grasshopper running within the 3D modelling environment Rhinoceros is presumed to be a good option. The main reason for choosing Grasshopper amongst other software applications is that this programme offers in comparison to other parametric design applications (for example Generative Components) a more intuitive, and thereby a very user friendly approach for building parametric models. At the moment only a work-in-progress version of the applications exists, features and procedures are added and or changed very often, but it is already being used by thousands of people world-wide.

Parametric models within Grasshopper can be set up by using either predefined components consisting out of a wide range of geometrical, mathematical and logical definitions and operations. In the case it is not possible to achieve certain functionality by using the pre-defined components, custom script components can be composed, based on the programming languages VB.NET or C#. The possibility of programming extends the possibilities of the Grasshopper application enormously as every procedure can be performed as long as it is programmable. Another argument to use scripted components instead of an assembly of pre-defined components could be reducing the size of the total model and thereby the apprehension. A disadvantage of scripted components is that the user must be familiar with the programming language used, in order to gain insight in the routines and algorithms.

As it was sometimes necessary to solve systems of linear equations, an external matrix class library for basic linear algebra computations was used, named Mapack for .NET, developed by Lutz Roeder (Roeder, 2002). The Mapack library can be accessed by referencing from within the script components to the external library, this was very useful since it was not necessary to incorporate the source code into the script.

3.3.3 Conceived general outline and structure of the structural design tool

The conceived general outline and structure of the parametric structural design tool, in correspondence with the software framework and demands concerning functionality and usability is shown in figure 3.xx. The structure of the design tool is build up analogous to the flow chart of the structural analysis sequences presented (theoretical framework) (figure 30) which was derived at the end of the previous chapter. Additions to this flowchart are made by defining which operations take place in the two software programs (Rhinoceros & Grasshopper). As can be seen in figure 31, a mesh component is added which generates the necessary calculation mesh within the boundary curves defined within Rhinoceros (representing the outlines of the structural geometry) for the structural analysis components.

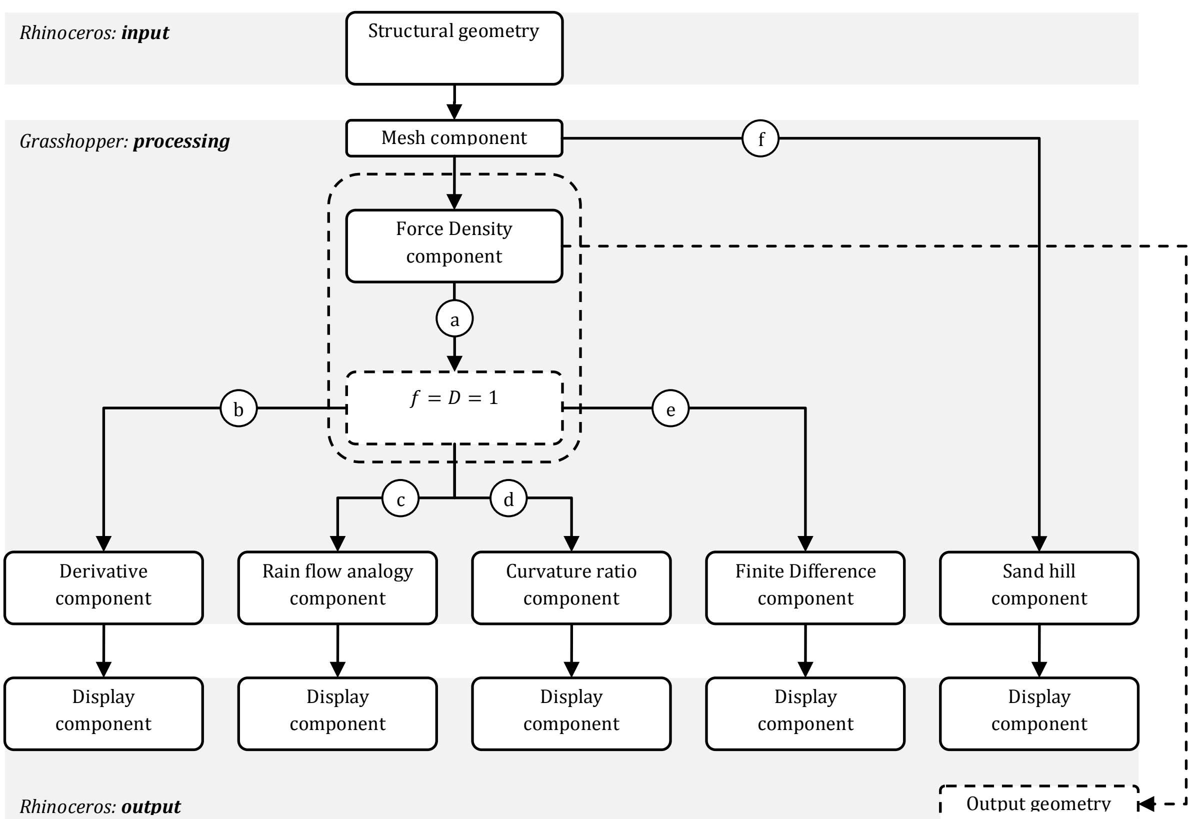

Fig.31. General outline and structure of the parametric structural design tool

3.4 Implementation of the theoretical framework

Within this paragraph is will it will be explained how the theoretical framework was implemented into the conceived general structure of the design tool (see paragraph 3.3.3), by describing how the different structural analysis methods were applied within the corresponding structural analysis components in association with objective 1d:

"Implement the theoretical framework into the defined general setup."

For each component it will be explained how the concerned component relates to structural analysis sequence of which it forms a part. The actual contribution of the concerned structural analysis sequences will be given in the form of the output results generated by the different components.

3.5 Mesh Component

3.5.1 Introduction

The mesh component generates a mesh within a set of curves representing the boundaries (edges) of the concerned plate structure which are defined within the Rhinoceros environment and imported into Grasshopper as reference curves. The generated mesh is subsequently used in almost every other component.

3.5.2 Generating the mesh

For calculation purposes a square grid consisting of a grid of points connected by lines of the same length seemed the most appropriate as it considerably simplifies the numerical calculation sequence within both the (reverse) finite difference component and the numerical calculation methods. Although there are some predefined meshing and grid generating components present with the Grasshopper application these components were not considered as useful since their output, a series of closed polygons (grid cells) and points, turned out to be less convenient than a square grid of points connected by single lines. For these reasons a scripted grid component was developed.

The generation of (free form) meshes is performed in three steps. First, the domain of the planar curve was determined to generate a rectangular grid covering the curve's region. Second, the grid lines located totally outside the domain were deleted. Third, the grid lines intersecting the boundary curves were trimmed using the intersection point between the boundary curve and the concerned grid line.

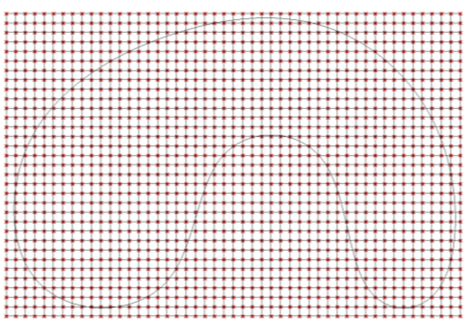

Fig.32. Rectangular mesh over free form boundary curve

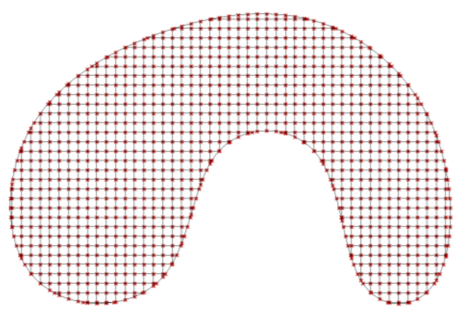

Fig.33. Trimmed mesh within free form boundary curve

Apart from the generation of a mesh, the grid component also assembles a list containing the free points, fixed points and semi free points. This subdivision is useful for streaming the output of the grid component into the form finding component which will be shown later. An extra option which was later added to the grid component makes it possible to generate diagonal lines between the grid points by which every point is connected to eight other points, instead of four.

3.6 Force Density component

3.6.1 Introduction

The form finding component, based on the force density method (Schek, 1973), generates the equilibrium state of a predefined net structure by transforming a system of non linear equilibrium equations into a system of linear equations. This is done by prescribing a constant "force density" value, an optional load case and a series of boundary conditions concerning the geometrical constraints. The resulting equilibrium meshes are mainly used within this thesis as part of a calculation sequence for determining the stress resultants and deformations in thin plate structures within a series of structural analysis components. In order to achieve this, it was in necessary to incorporate the possibility to interpolate a mesh through the equilibrium mesh. Apart from this, the forming component could also be used as standalone design tool for membrane and shells structures.

3.6.2 Development process

The form finding component was developed by implementing the force density method in a component by scripting an algorithm in the VB.NET programming language following the steps as presented in chapter two. Since this method is mainly based on performing a series of matrix operations, two options were considered for performing this kind of mathematical operations. The first option was to incorporate the essential numerical matrix calculation algorithms into the parametric component itself. Several attempts were made to implement the required matrix operations within the component based on several numerical algorithms (Press & William, 2007). Since a lot of time is involved with this method, it was decided to use an external matrix class library named Mapack (Roeder, 2002) to perform the matrix operations by using it as an external reference assembly.

Whereas the first version of the component could only generate the equilibrium mesh for a collection of fixed points and free points by defining the force density ratio and an optional distributed load, the second version of the parametric component also offered the possibility of defining points with a limited degree of freedom. Within the third version of the component it was made possible to implement diagonal connections (lines) between the points and the fourth version also allows the definition of point loads with a certain magnitude.

3.6.3 Generating the equilibrium mesh

The geometrical input for the force density component consists of two lists containing collections of points and lines which together describe the initial mesh topology. Besides this, two additional point lists are required, containing the free points and fixed points. The first structural parameter consists of the magnitude and direction of the external loads (lumped in the mesh nodes) which have to be defined by specifying the load components for the x-,y- and z-direction, together forming a load vector. The second structural parameter is the force-density ratio.

After defining the inputs, the force density algorithm assembles the necessary matrixes as specified in chapter two and uses these matrixes to assemble the equilibrium equations for the x-,y- and z-direction. These equilibrium equations are then solved yielding the equilibrium coordinates. Afterwards, the branch node matrix is used to generate the corresponding equilibrium mesh. On the next page, the force density algorithm inside the parametric form finding component is presented as flow chart (figure 34). The gray hatched boxes represent the parameters.

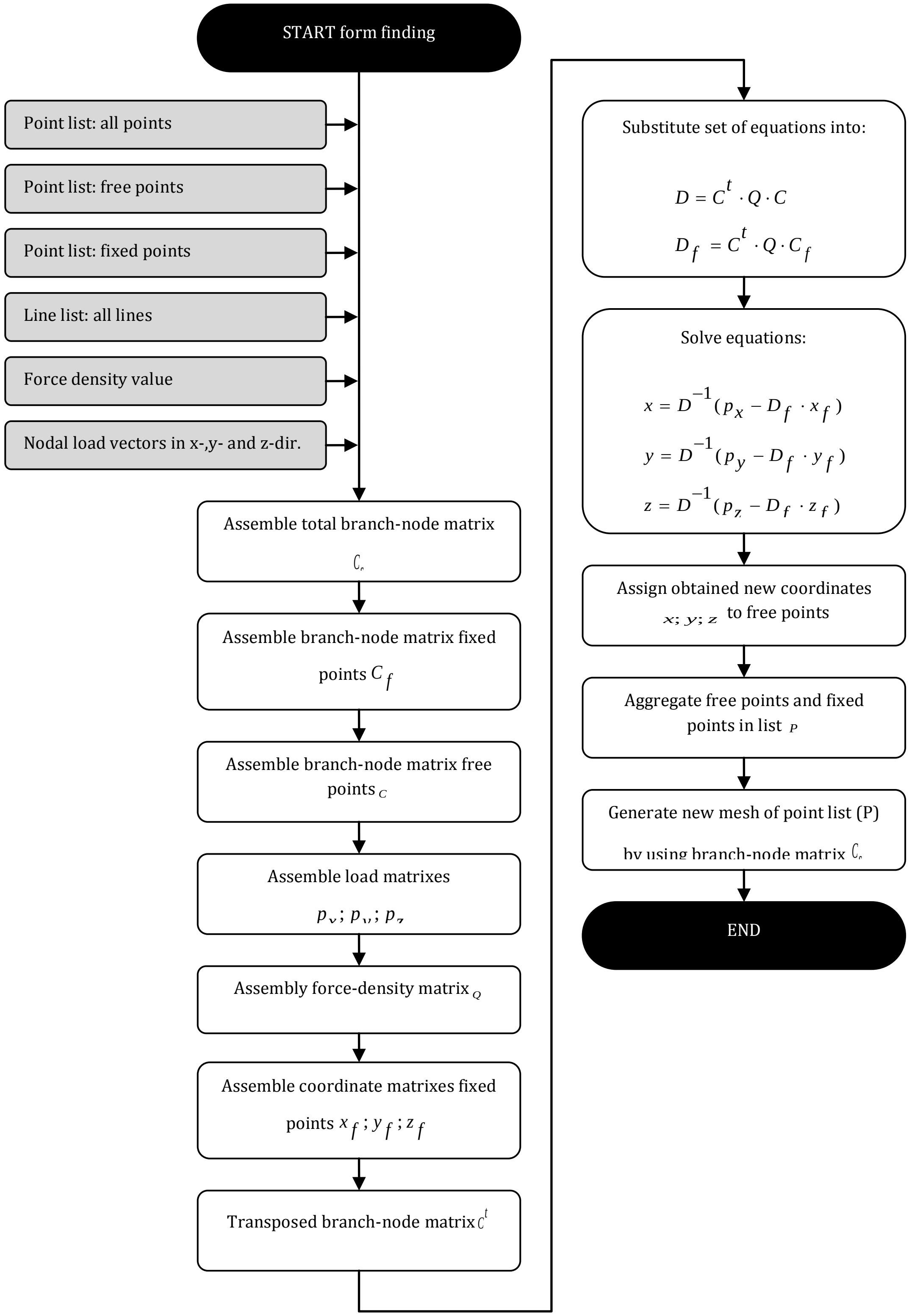

Fig.34. Flowchart of the force density form finding component

3.6.4 Equilibrium mesh results

Below, the form finding procedure is illustrated graphically for a rectangular mesh with fixed points along the edges, subjected to a distributed vertical load. It can be seen that first the equilibrium positions of the free points are calculated by solving the system of linear equilibrium equations and subsequently a corresponding mesh is generated for the initial mesh.

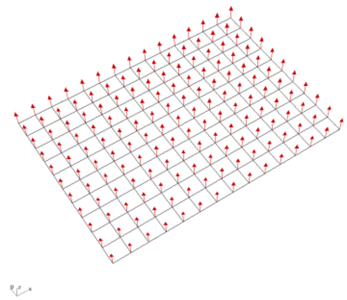

Fig.35. Initial grid with distributed load

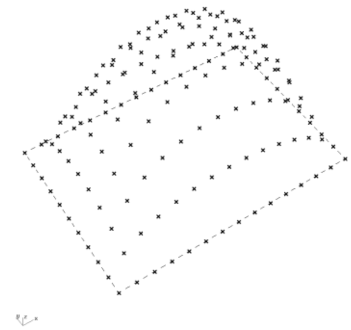

Fig.36. Equilibrium position of points

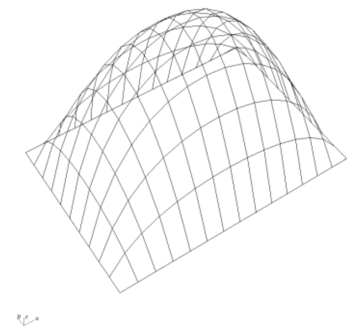

Fig.37. Mesh generation

In the pictures below the influence of the freedom of movement is illustrated by varying them for the points along the edges of the mesh (except from the corner points). In figure 38 the points along the edges are fully fixed, in figure 39 the points along the edges are totally free and in figure 40 the points along the edges are fixed into a vertical plane, determined by the direction of the edge and the vertical z-direction.

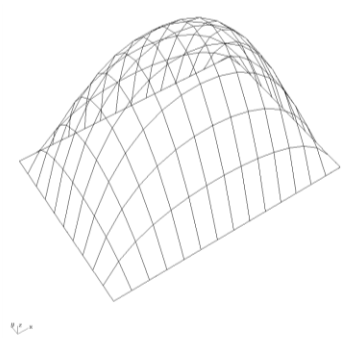

Fig.38. Fully fixed points along edges

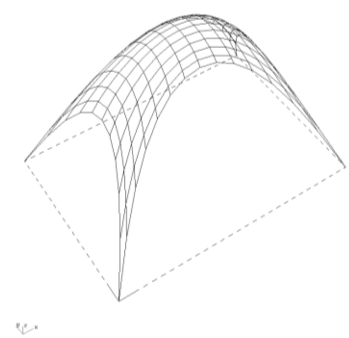

Fig.39. Fixed corner points

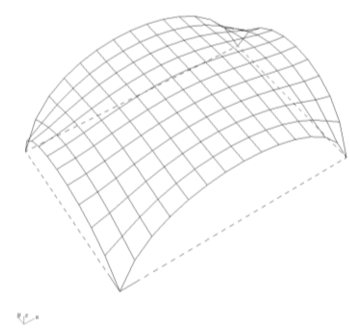

Fig.40. Points along edges free in z-direction, fixed corner points

The influence of the position of the fixed points is illustrated by figure 41 which shows the equilibrium mesh for a membrane between four corner points at different heights of which the shape is only determined by internal forces. Figures 42 and 43 show the equilibrium meshes for membranes which are respectively subjected to a concentrated load and a combination of a concentrated load and a distributed load acting in opposite directions.

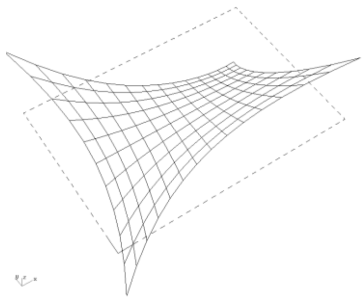

Fig.41. *Fixed corner points*

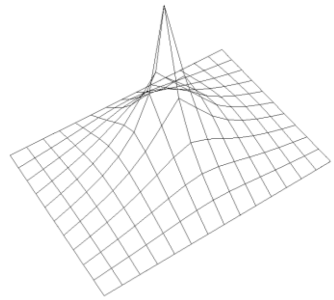

Fig.42. *Point load in mid point*

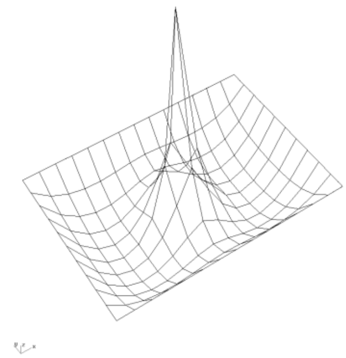

Fig.43. *Load combination*

The square meshes generated by the mesh component within free form planar boundary curves can also be used as input for the form finding component in the same way as was done for the rectangular geometries as is shown in picture 44.

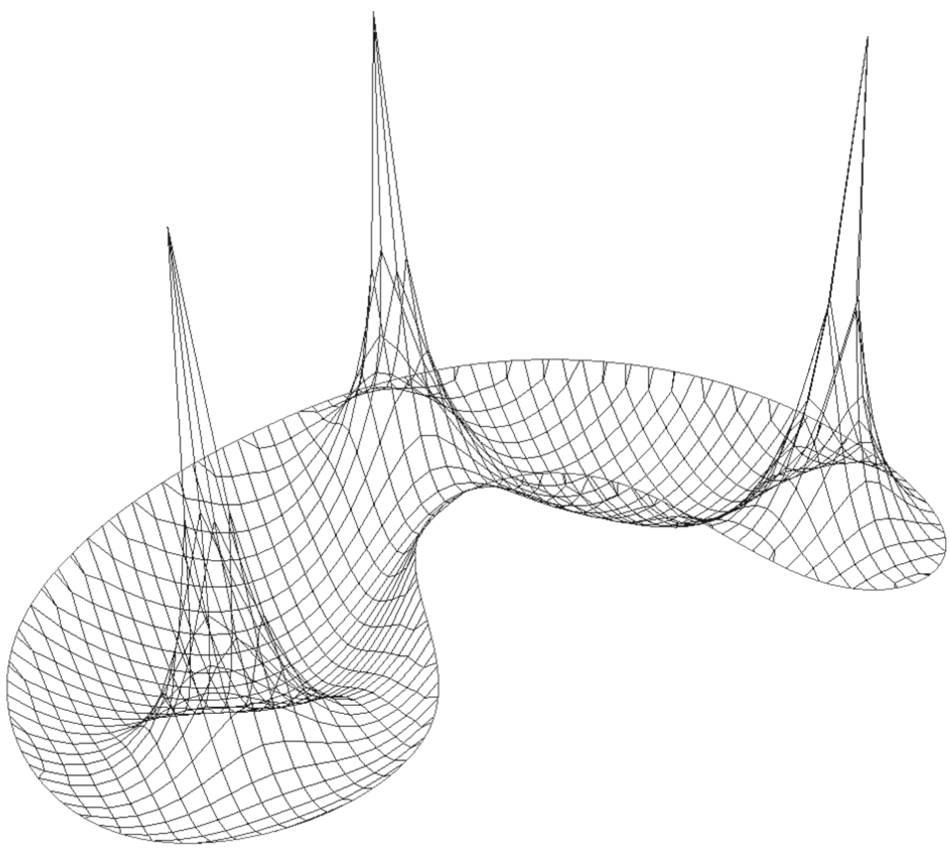

Fig.44. *Equilibrium mesh for a free form membrane subjected to a distributed load and three concentrated loads*

3.6.5 Surface interpolation

As explained in chapter two, the membrane analogy describes the relation between the sum of bending moments surface and the displacement field of air inflated membranes when the force density ratio is specified as 1 (analogous to the plate stiffness D). This knowledge is used within this thesis to generate membrane surfaces which are equal to sum of bending moments surfaces. These surfaces are subsequently used as the basis for the derivative component, the rain flow analogy component, the curvature ratio component and the finite difference component.

An interpolated NURBS surface is generated on basis of the equilibrium mesh. The generation of this NURBS surface can be achieved for surfaces with a rectangular or right-angle polygon base by using the predefined surface interpolation component provided by the Grasshopper application. For membrane surfaces generated based on a free form boundary curve this surface interpolation component cannot deliver an appropriate result, because this component requires a rectangular grid of UV points. An alternative for generating a continuous surface based on of a free form membrane mesh was found by developing a script component which exports the membrane mesh to Rhinoceros, generates a surface by utilizing the surface patch function and subsequently imports the generated surface back into Grasshopper. The resulting surface for a membrane geometry fixed along its edges is shown in figure 3.xx.

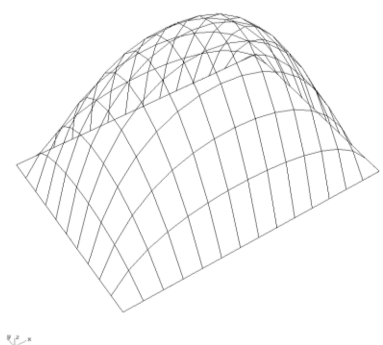

Fig.45. Equilibrium mesh

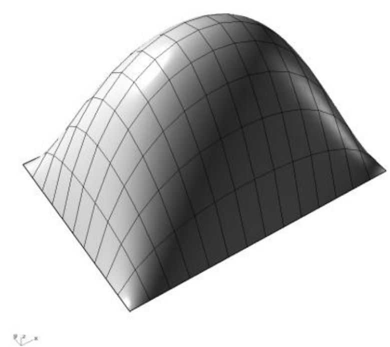

Fig.46. Surface interpolation

3.6.6 Validation of the results

The output of the form finding component was compared to the output provided by an established software package named EASY, which is also based on the force density method. The exact similarity of the two equilibrium meshes generated from the same boundary conditions and parameters validated the output of the parametric component.

3.7 Derivative component

3.7.1 Introduction

The derivative component calculates the magnitude and direction of the principle shear forces (and its components in the x- and y-direction) based on the analytical relation between the sum of bending moment surface and the shear force: the shear force in a certain direction in a particular point is the first derivative of the sum of bending moments surface in that direction (see paragraph 2.2). Several display components have been developed for rendering the results.

3.7.2 Development of the derivative component

The derivative component is developed by combining a set of predefined components provided by the Grasshopper application for mathematical and geometrical operations, which together provide the solution to the differential equations (2.12), (2.13) and (2.14). The hereafter presented solutions all relate to a simply supported rectangular plate subjected to a distributed load.

The required input for derivative component consists of the sum of bending moments surface (provided by the form finding component) and a grid of points (provided by the mesh component). The magnitude and direction of the principle shear force in a series of grid points is determined by calculating the derivative (slope) of the sum of bending moments surface in the direction of the steepest descent. First, the steepest descent direction is determined by using the surface normal vector. By multiplying this normal vector with the global z-vector the cross vector is obtained, which is subsequently used to rotate the normal vector around over 90˚ and thereby becomes the steepest descent vector. The steepest descent vector is tangential to the sum of bending moments surface in the considered point and points in the direction of the steepest descent. The resulting vector collection plotted on the sum of bending moments surface is shown in figure 48. The vector collection can also be represented by a planar vector field as shown in figure 47.

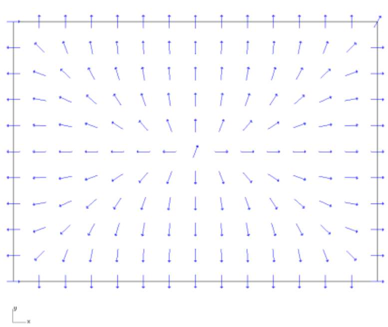

Fig.47. Vector field with directions of principle shear forces (simply supported rectangular plate subjected to a distributed load)

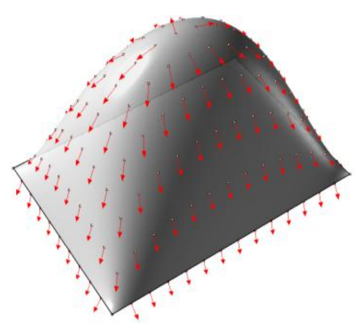

Fig.48. Steepest descent vectors on sum of bending moments surface

Next, the magnitude of the principle shear force is calculated by calculating the slope (derivative) of the steepest descent vector. Subsequently the shear forces in the x- and y-direction are calculated by determining the corresponding planar components of the principle shear force as illustrated in figure 49.

3.7.3 Results

The output of the derivative component consists of the direction and magnitude of the (principle) shear force for a grid of points. Two display components are designed for displaying the numerical and graphical information concerning the shear forces.

The first display component generates a planar vector field in which the direction of the (principle) shear forces is indicated by a small arrow and the magnitude of the shear force is represented by the thickness of the arrow. This is illustrated in figures 49, 50 and 51.

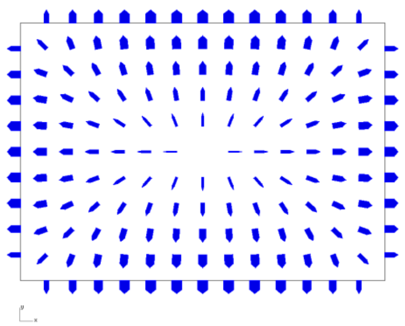

Fig.49. Principle shear force represented as scaled arrows (simply supported rectangular plate subjected to a distributed load)

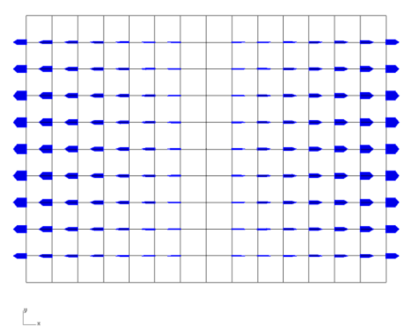

Fig.50. Shear force in x-direction represented as scaled arrows (simply supported rectangular plate subjected to a distributed load)

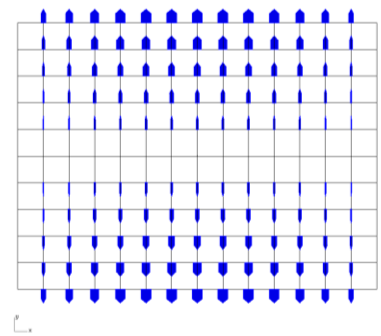

Fig.51. Shear force in y-direction represented as scaled arrows (simply supported rectangular plate subjected to a distributed load)

The second display component generates a 3D mesh or surface which represents the magnitude of the shear forces. This is done by translating the initial grid of points in the z-direction over a distance equal to the magnitude of the shear force and optinally generating a mesh or (NURBS) surface through these points. The 3D meshes are presented in figures 52, 53 and 54.

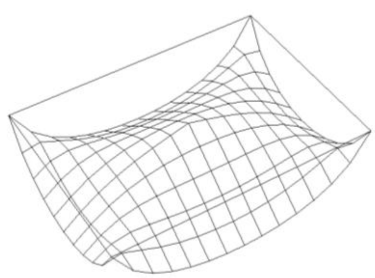

Fig.52. Principle shear force represented as 3D mesh (simply supported rectangular plate subjected to a distributed load)

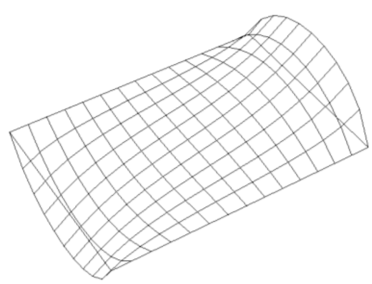

Fig.53. Shear forces in x-direction represented as 3D mesh (simply supported rectangular plate subjected to a distributed load)

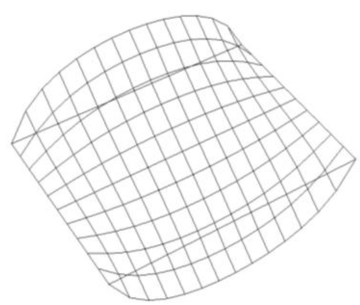

Fig.54. Shear forces in y-direction represented as 3D mesh (simply supported rectangular plate subjected to a distributed load)

3.8 Curvature ratio component

3.8.1 Introduction

The curvature ratio component is based on the curvature ratio method (see paragraph 2.xx) which was developed during this thesis. This method determines the bending moments in the x- and y-direction in a series of grid points by using the ratio between the curvatures in the corresponding directions of the scaled sum of bending moments surface (for which ... is true) multiplied by the sum of bending moment value.

3.8.2 Development of the curvature ratio component

The input required for the curvature ratio component involves a surface (provided by the surface interpolation component), the sum of bending moments values (provided by the form finding component) and a grid of points (provided by the mesh component). Since the Grasshopper application offers all the required components which are needed for the calculation sequence no scripting was necessary in this case.

The first step in the calculation sequence consists of determining the (planar) curvatures of the scaled membrane surface in the x,z- and the y,z-plane for a set of grid points on the surface (vertical projections of the planar grid points). These curvatures can be determined by generating iso-curves (mathematical intersection events for a surface and a (vertical) plane) on the surface. The curvature in the examined points can subsequently be determined with the predefined curvature analysis component. With the curvature ratio and the sum of bending moments value, the bending moments in the x- and y-direction can be calculated by using equation (2.47).

3.8.3 Results

The result of the curvature ratio component is a series of numerical bending moment values corresponding to a series of grid points. For Several display components could be used to display the calculation results of the curvature ratio component. First, a 3D mesh or surface which represents the magnitudes of the bending moments could be used as shown in figures 55 and 56.

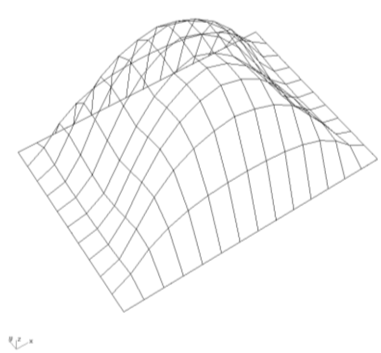

Fig.55. Bending moments in y-direction represented as 3D mesh

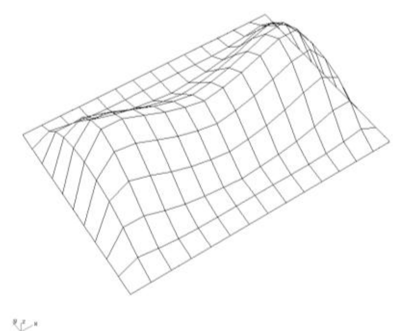

Fig.56. Bending moments in x-direction represented as 3D mesh

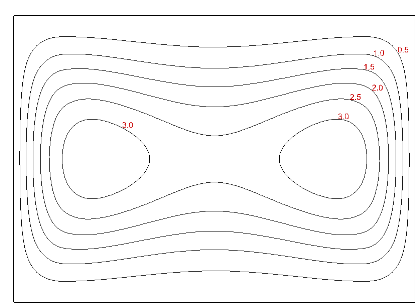

Fig.57. Contour plot sum bending moments in x-direction (m_{xx})

Second, for a planar representation of the calculation results, a component which generates a contour plot on the basis of the interpolated NURBS surface could be used as shown in figure 57.

3.9 Rain flow analogy component

3.9.1 Introduction

The rain flow analogy can be used to determine continuous principle shear force trajectories along which the principle shear forces will flow to the supports in plate structures. These trajectories can subsequently be used to determine the magnitude of the principle shear forces in sections in a graphical manner by integrating the associated load, which is equal to the surface area between two trajectories (the part of the load which flows to the section). Another method for calculating the principle shear forces in a grid of points on the plate is by simulating the discrete accumulation of loads by using the steepest descent vectors in the grid points.

3.9.2 Gradient descent algorithm

The rain flow analogy component generates 'continuous' rain flow trajectories on a surface by using the gradient descent algorithm. This algorithm starts from a predefined starting point and iteratively determines the steepest descent vector on the considered surface and defines the next point by translating the start point over a (very small) distance in this direction. The sequence is repeated until a local (or global) minimum is reached or a predefined stopping condition is met.

Mathematical definition

An algorithm for finding the nearest local minimum of a function which presupposes that the gradient of the function can be computed. The method of steepest descent, also called the gradient descent method, starts at a point P_0 and, as many times as needed, moves from P_i to P_{i+1} by minimizing along the line extending from P_i in the direction of $-\nabla f(P_i)$, the local downhill gradient until a local minimum is reached. This process is illustrated in the picture to the right. Here f is assumed to be defined on the plane, and its graph to have a bowl shape. The dotted lines are the contour lines along which the value of f is constant. An arrow originating at a point p_i shows the direction of the negative gradient at that point. Note that the (negative) gradient at a point is orthogonal to the contour line going through that point.

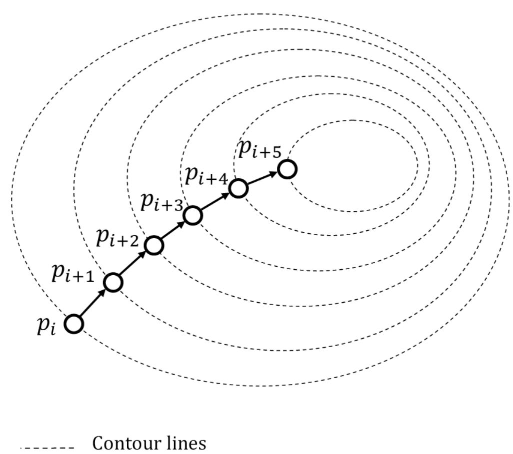

The steepest descent algorithm was implemented in the rain flow analogy component by using scripting components within Grasshopper. The steepest descent vector is determined by using the associated normal vector in a point on the surface, which can be easily determined with a Rhinoceros command. By multiplying this normal vector with the (vertical) global z-vector, the result is the cross vector, which is perpendicular to the plane containing the two input vectors. When the normal vector is rotated over 90 degrees around the cross vector it points in the direction of the steepest descent. By scaling this factor to a length which equals the step size (sampling accuracy) as defined by the user it can be used to translate the start point into this direction. Subsequently, the point is pulled back to the surface and forms the starting point for the next iteration (which is a repetition of the just described procedure). By this means a collection of points is defined which is used to generate a polyline which represents the rain flow trajectory.

It is important to determine a stopping criterion for the algorithm to prevent it from endlessly continuing to reach the exact position of the local minimum, which is often impossible due to the finite constant step size, resulting in an endless process of overshooting the exact mathematical minimum (often referred to as the 'ping pong effect'). Three stopping criterions are specified within the designed algorithm to prevent this:

1) Surface normal vector is (almost) vertical
2) Point p_{i+1} is outside 3D bounding box of surface
3) Iteration number is larger than predefined maximum number of iterations

Since the surface angle in the steepest descent direction (as principle derivative) in each point on the sum of bending moments surface is directly related to the magnitude of the principle shear force an extension was made to the rain flow analogy component which indicates the descent along the trajectories by applying a colour gradient to the trajectory. Along the lines of the rain flow analogy, the colour indicates the flow speed of the rain water and thereby forms a measure for the relative magnitude of the principle shear force.

At the end of this chapter, on page xx, a flowchart of the rain flow analogy algorithm is shown which illustrates the steps performed within the rain flow analogy component.

3.9.3 Rain flow trajectories

The output results of the rain flow analogy component for an arbitrary surface are shown in figures 60 to 61.

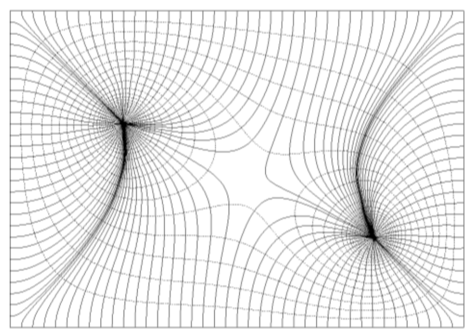

Fig.58. Planar rain flow trajectories and contour lines

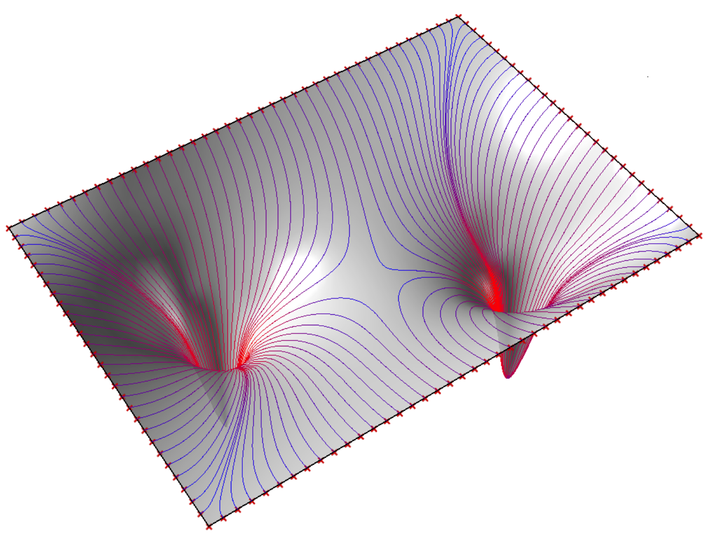

Fig.59. Rain flow trajectories plotted on arbitrary s surface

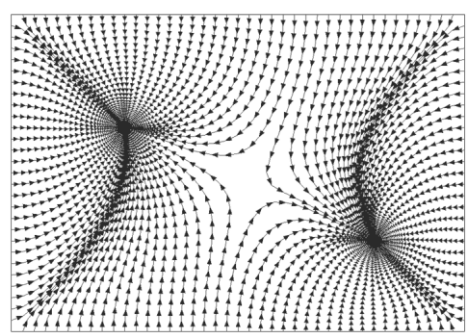

Fig.60. Planar rain flow stream directions indicated along trajectories

3.9.4 Principle shear force trajectories

When a series of rain flow trajectories is plotted on a sum of bending moments surface, corresponding to a collection of equally spaced division points along the edges of a plate, excellent insight can be obtained on how the principle shear forces (loads) flow to the plate supports (as illustrated by professor Beranek). The sum of bending moments surfaces are generated by using the form finding component (paragraph 3.4) based on the analogy between these surfaces and air inflated membranes (paragraph 2.3). The rain flow analogy component is subsequently used to generate the principle shear force trajectories.

In figure 63, the generated principle shear force trajectories are generated for a collection of evenly distributed points along the edge of the sum of bending moment surface belonging to a simply supported plate, subjected to a distributed load. In figure 64, the planar trajectories are displayed together with the contour lines of the same sum of bending moments surface. In this picture it can be clearly seen that the principle shear force trajectories are always perpendicular to the contour lines. When this picture is compared to figure 11 in paragraph 2.5, it can be concluded that the shape of the trajectories is correct.

Fig.61. Rain flow trajectories plotted on sum of bending moment s surface (plate simply supported along edges subjected to distributed load)

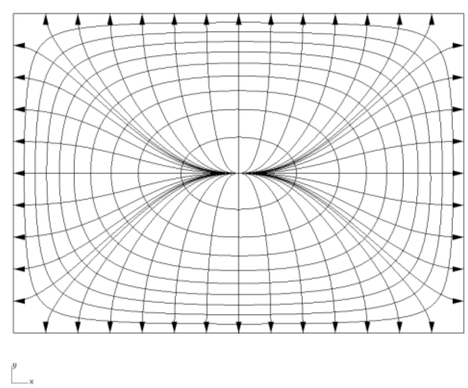

Fig.62. Corresponding contour plot of sum of bending moments surface with rain flow trajectories

It is interesting to see what happens if the plate is shaped as a polygon with 90 degree edges instead of a rectangle. In these cases the global maximum of the sum of bending moments surface is no longer clearly a single point but rather a ridge along which the slope is nearly zero degrees. This is shown in figures 65 and 66.

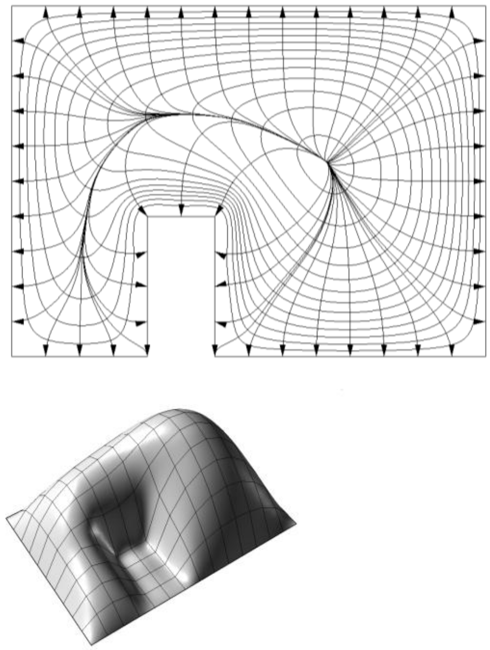

Fig.63. Rain flow trajectories and sum of bending moment surface (plate simply supported along edges subjected to distributed load)

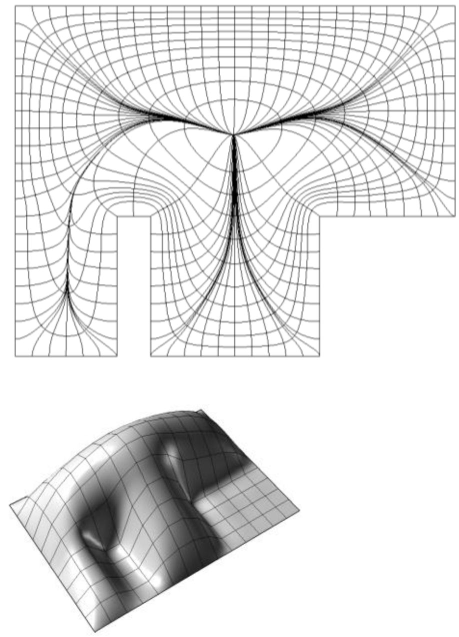

Fig.64. Rain flow trajectories and sum of bending moment surface (plate simply supported along edges subjected to distributed load)

Depending on the shape of the shape of the plate boundaries it is even possible that instead of one, two local maxima occur in the sum of bending moments surface as is shown in figure 67 below. The influence of a point support placed in the midst of the plate on the shape on the sum of bending moments surface and the corresponding principle shear force trajectories is shown in figure 68.

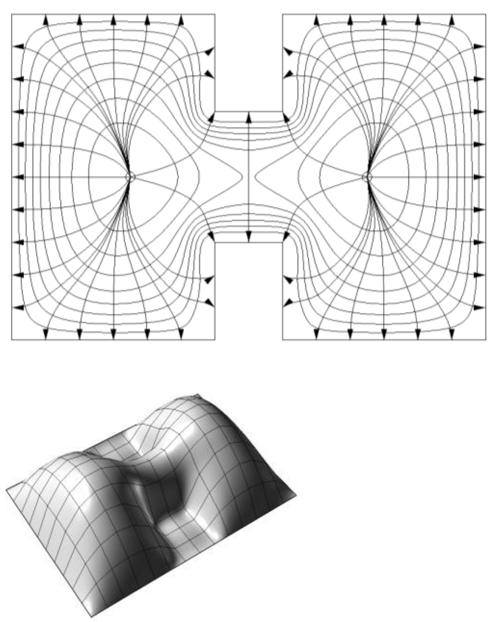

Fig.65. Rain flow trajectories and sum of bending moment surface: 2 local maxima (plate simply supported along edges subjected to distributed load)

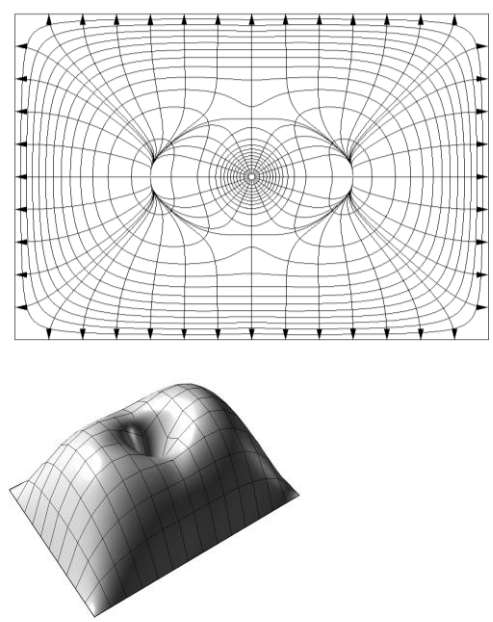

Fig.66. Rain flow trajectories and sum of bending moment surface: point support in midst of plate (plate simply supported along edges subjected to distributed load)

The effect of a point support on the sum of bending moments surface shape and the corresponding principle shear force trajectories is shown in figure 68.

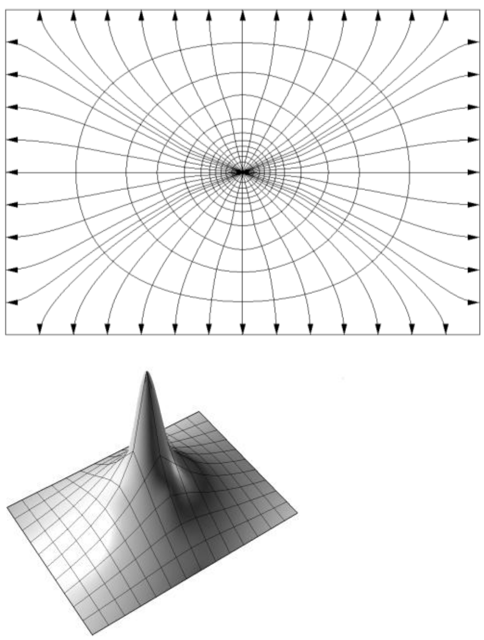

Fig.67. Rain flow trajectories and sum of bending moment surface: (plate simply supported along edges subjected to point load in midst of plate)

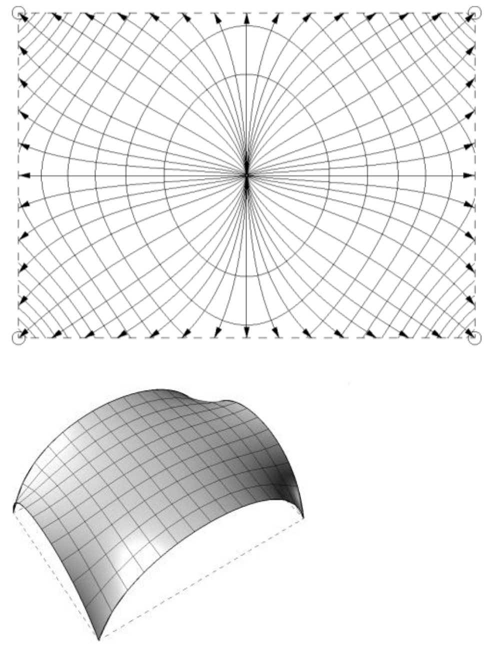

Fig.68. Rain flow trajectories and sum of bending moment surface: plate supported in corners (plate simply supported along edges subjected to distributed load)

In figures 69 the relation between the sum of bending moments surface and the corresponding principle shear forces trajectories for a simply supported plate subjected to a point load. Furthermore, the generated sum of bending moments surface for a plate (subjected to a distributed load) supported in its corners and the corresponding principle shear force trajectories are shown in figure 70. With respect to such topologies it was found that a different force density ratio f for respectively the edges and the midfield must be specified to obtain a correct sum of bending moments surface. This ratio was approximately 1:3.

3.9.5 Magnitude of shear forces

The membrane surface geometry in combination with the principle shear force trajectories can be used to determine the magnitude of the shear forces in a collection of points or sections. In order to achieve this, two different algorithms are developed and implemented into a parametric component to calculate the magnitude (and direction) of the principle shear forces.

The first algorithm was developed in an early stage of this thesis project. It determines the x- and y-components of the principle shear force in a collection of grid of points by simulating the accumulation loads in the x- and y-direction towards the supports in compliance with the corresponding components of the steepest descent vector. First, in each grid point the steepest descent (on the sum of bending moment surface) is determined in the same way as was done within the rain flow analysis. Next, the x- and y-components of this vector are determined. The ratio between the lengths of these components is used to determine which part of the load acting on this grid point will be carried in the corresponding directions:

$$q_x = \frac{q_x}{q_y + q_x} \cdot q_n \qquad ; \qquad q_y = \frac{q_y}{q_y + q_x} \cdot q_n \tag{3.1}$$

When it is known which part of the load will be carried in the x and the y direction, this load is added to all points which are located in the corresponding direction; from the concerned grid point towards the edge of the plate. This procedure is conducted for each grid point. With this, it is essential that the grid points are examined in an order determined by the height of the points, where the highest is examined first and the lowest point last, as this directly influences the outcome of the calculation. If this order is not followed, then the summation is incorrect and so will be the outcome of the calculation.

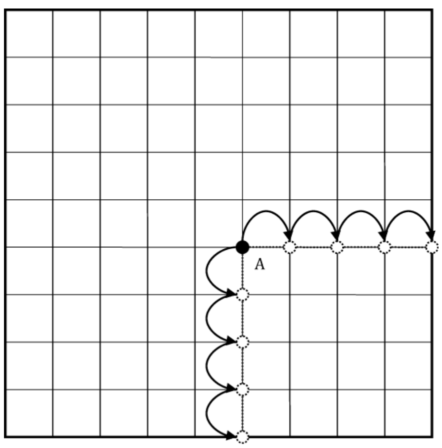

Fig.69. Calculation procedure for a set of grid points within rain flow component (method 1)

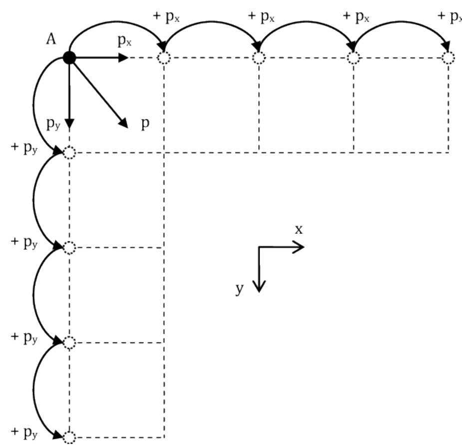

Fig.70. Summation of load in the x- and y-direction for an arbitrary point (method 1, rain flow component)

The output of the algorithm consists of a shear force value for each grid point. This information can be represented graphically as 3D mesh or a contour plot as presented in figures 73 and 74.

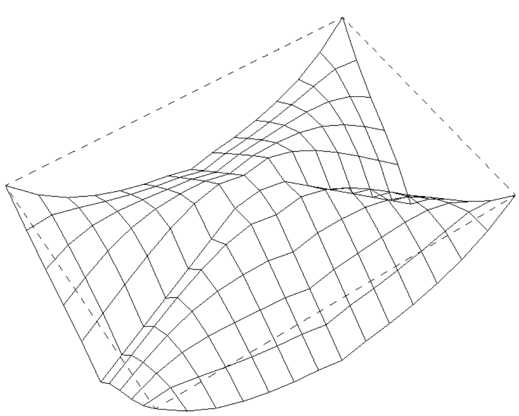

Fig.71. Output of rain flow component (method 1): 3D mesh representation of principle shear forces

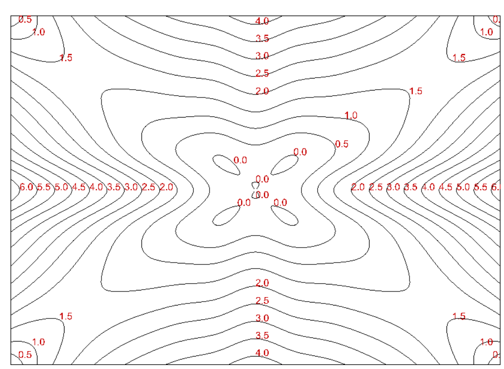

Fig.72. Output of rain flow component (method 1): Contour plot of principle shear force distribution

The second algorithm for determining the magnitude of the principle shear force in a certain section is based on the integration of the load flowing towards a particular section as indicated in figure 75. This method requires a user defined section on the plate surface as input, generates the shear force trajectories associated to the start and end point of a series of sub sections, then generates a planar surface between these curves and determines the area of this surface. This surface area value is subsequently used to generate a principle shear force vector with the magnitude of the principle shear force pointing in the direction of the steepest descent of the sum of bending moments surface. The results for some sections on a plate supported along its edges are shown in figures 76, 77 and 78.

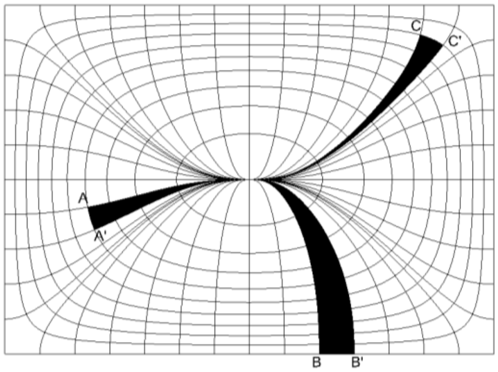

Fig.73. *Sections with associated load between trajectories*

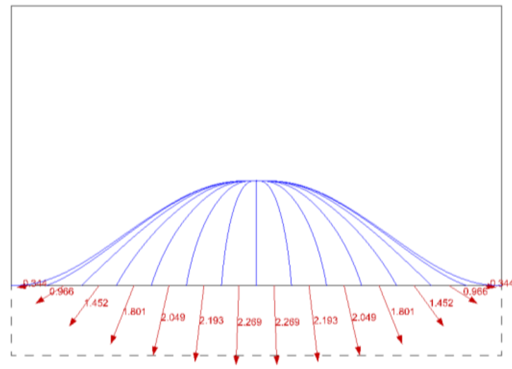

Fig.74. *Output of rain flow component (method 2): arbitrary section with associated load between trajectories and shear force vectors*

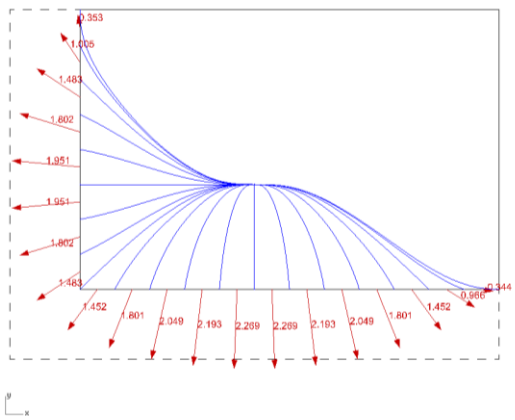

Fig.75. *Output of rain flow component (method 2): arbitrary straight angle section with associated load between trajectories and shear force vectors*

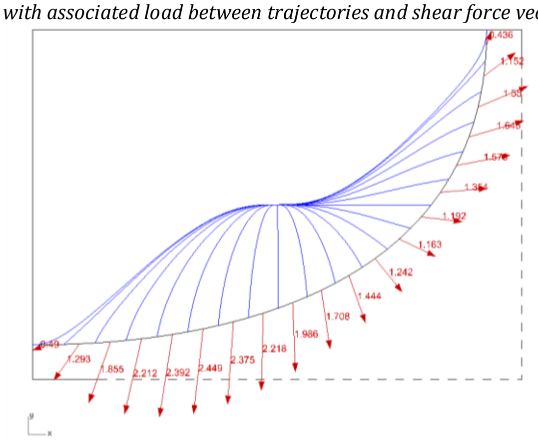

Fig.76. *Output of rain flow component (method 2): arbitrary free form section with associated load between trajectories and shear force vectors*

On the next page a flow chart is presented of the conceived rain flow algorithm (figure 79).

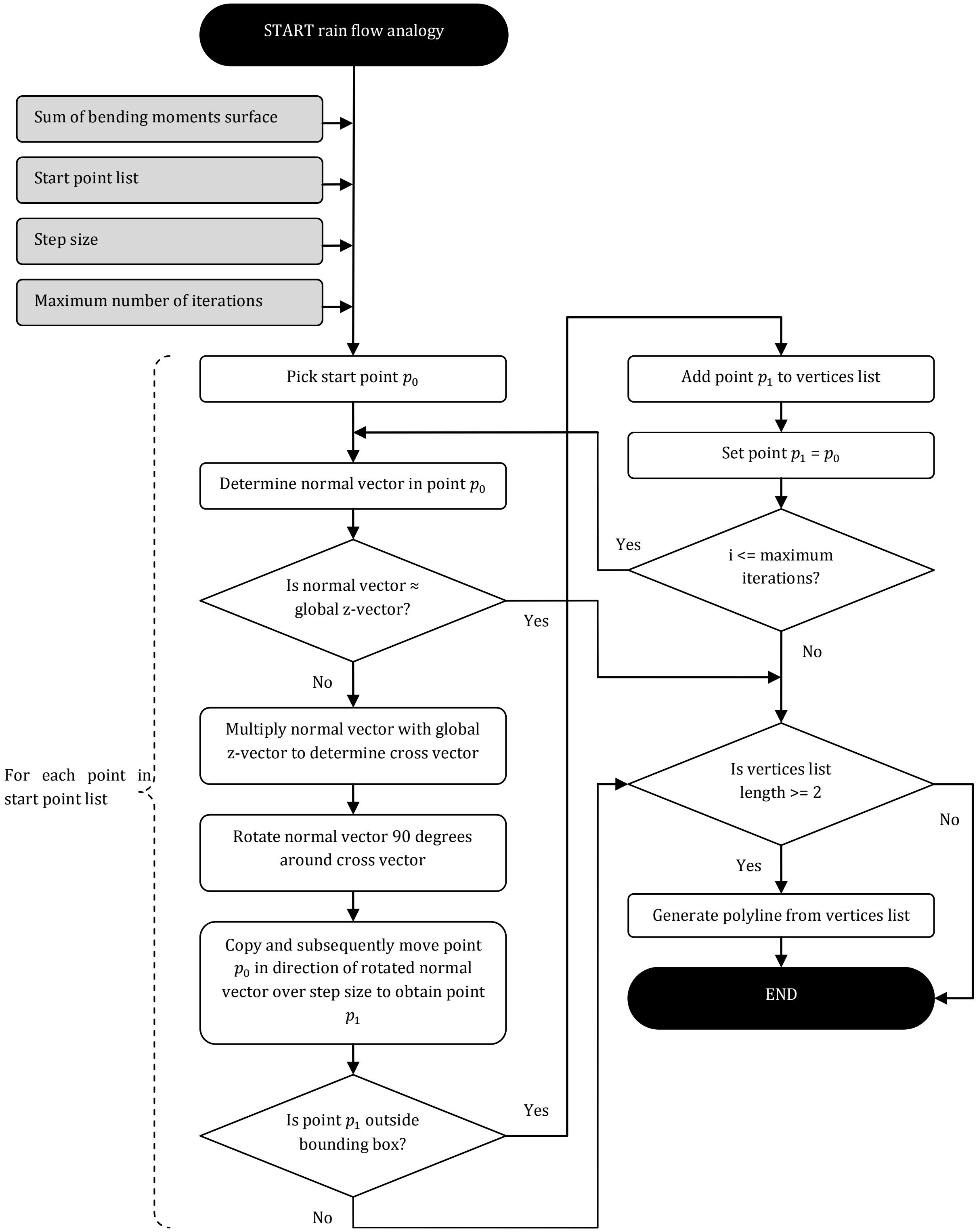

Fig.77. *Flowchart of the rain flow analogy component*

3.10 Finite difference component

3.10.1 Introduction

In this thesis the numerical finite difference method is used for plates, simply supported along their edges and subjected to a distributed load, in two steps. First, it is used to determine the displacements in a series of grid points for which the sum of bending moments is provided by the form finding component. Through assembling and solving a set of linear partial finite difference equations and relating the displacements of the grid points to the sum of bending moment values in the grid points, the displacement field is obtained. Subsequently this displacement field is used to determine the stress resultant in the point by solving the partial difference equations. Finally, the concentrated shear force is determined by taking the derivative of the torsional moments along the edges of the plate. Several options are developed to display the numerical output of the component.

3.10.2 Development of the finite difference component

The finite difference method was implemented into the finite difference component by programming in the VB.NET language. Since the method also involves a series of matrix operations Mapack (Roeder; 2002) was used as external reference library. The theoretical aspects of the implementation process were mainly facilitated by a reader written by professor Beranek, which features a comprehensive description of the finite difference method.

The finite difference component requires a planar square calculation mesh as input, which is provided by the mesh component. For calculation purposes it is important to determine the point conditions of the mesh points. For the considerd, simply supported, plate this means that there are three types (collections) of grid points p, mid points, edge points and corner points as illustrated in figure 60.

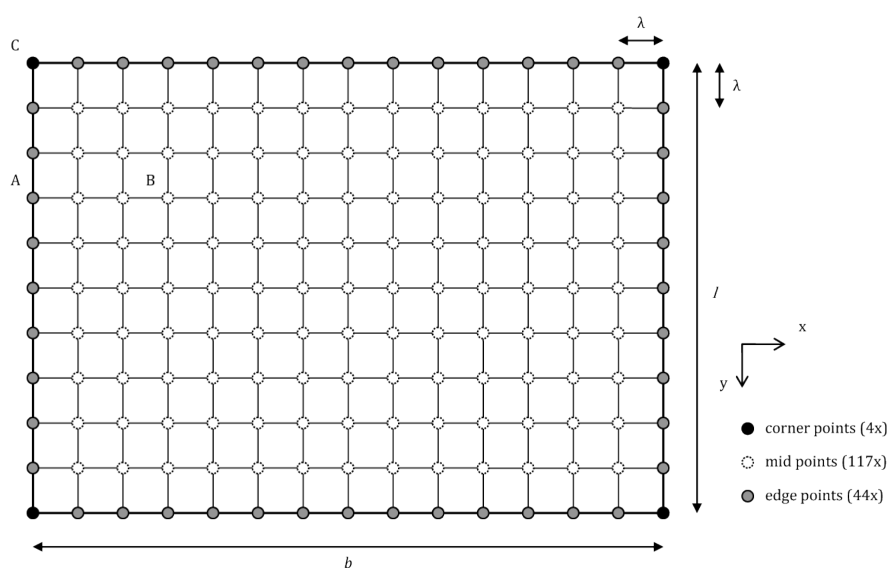

Fig.78. Calculation mesh used for the finite difference component

The sum of bending moment values for all grid points p are required, this data is provided by the form finding component. Also a calculation mesh width λ, equal to the mesh width of the input mesh, should be specified which determines the accuracy of the calculation results (a finer mesh leads to more accurate results).

The first step within the algorithm consists of assembling a branch node matrix (see paragraph 2.xx) which is a mathematical description of the mesh topology. This branch node matrix is used in a later stadium to generate meshes which represent the calculation results. Within the next steps, matrixes **Q** and **m** (3.xx) are assembled relating to the p grid points, part of equation (3.2).

$$\mathbf{m} = \left(\frac{1}{4 \cdot \lambda^2}\right) \cdot \mathbf{Q} \cdot \mathbf{w} \tag{3.2}$$

The initial $p \times p$ dimensional quotient matrix **Q** contains the coefficients of the displacements of all grid points. In contradiction to the collection of mid points n, the points along the edges are fixed and their displacement w equals zero. Therefore, the size of matrix **Q** can be reduced to an $n \times n$ dimensional matrix, containing the coefficients for the displacements of the mid points only. The n dimensional matrix **m** contains the sum of bending moment values for the corresponding collection of mid points.

$$\mathbf{m} = \begin{bmatrix} m_1 \\ \vdots \\ m_1 \end{bmatrix} \quad ; \quad \mathbf{Q} = \begin{bmatrix} q_{11} & 0 & 0 \\ 0 & \ddots & 0 \\ 0 & 0 & q_{ij} \end{bmatrix} \quad ; \quad \mathbf{w} = \begin{bmatrix} w_1 \\ \vdots \\ w_1 \end{bmatrix} \tag{3.3}$$

Now, the necessary matrixes **Q** and **m** are assembled, the displacements of the mid points n can be calculated by using equation (3.4).

$$\mathbf{w} = \mathbf{m} \cdot (4 \cdot \lambda^2) \cdot \mathbf{Q}^{-1} \tag{3.4}$$

The displacements of the mid points and the edge- and corner points together form the displacement field of the plate. This displacement field can subsequently be used to calculate the stress resultants with the partial finite difference equations (because $D = 1$, the curvatures of this displacement field are equal to the corresponding stress resultants) , the bending moments in the x- and y-direction m_{xx} and m_{yy} (equations 2.55 and 2.56) and the torsional moments m_{xy} (equation 2.57). With this, it is important to pay extra attention to edge points and corner points as these require a modified partial finite difference equation (see paragraph 2.7.3).To achieve this, the finite difference algorithm is designed in such a way that it recognizes these points by determining the number of surrounding grid points and subsequently uses a modified partial finite difference equation to calculate the stress resultants. The torsional moments m_{xy}, in contradiction to the bending moments m_{xx} and m_{yy}, are not zero along the simply supported edges which leads to the modified molecule notations of (3.5).

$$m_{xy\,i,j} = \frac{\partial^2 w}{\partial x \partial y} = \frac{1}{4 \cdot \lambda^2} \cdot \qquad (3.5)$$

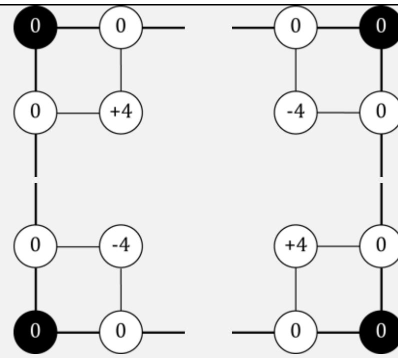

When the bending- and torsional moments m_{xx}, m_{yy} and m_{xy} are calculated for each grid point, the principle moments m_1 and m_2 can be calculated by using Mohr's equations (2.20 and 2.21). Next, the concentrated shear forces V_e for the edge points are calculated by taking the derivative of the torsional moments in directions parallel to the edges. For respectively the edges parallel to the x-axis and the edge parallel to the y-axis yields:

$$V_{x\,i,j} = \frac{m_{xy\,i+1,j} - m_{xy\,i-1,j}}{2 \cdot \lambda} \quad ; \quad V_{y\,i,j} = \frac{m_{xy\,i,j+1} - m_{xy\,i,j-1}}{2 \cdot \lambda} \qquad (3.6)$$

We know that the concentrated shear force in the corners V_c is equal to: $2 * m_{xy}$.

$$V_{c\,i,j} = 2 \cdot m_{xy\,i,j} = 2 \cdot m_{yx\,i,j} \qquad (3.7)$$

There are three options for calculating the shear forces in the x- and y-direction in a certain grid point. The first option is to calculate the summation of the derivatives of the bending moment and the torsional moment (equation 2.3). This results in the following partial finite difference equations (3.8) for mid points:

$$v_{x\,i,j} = \frac{m_{xx\,i+1,j} - m_{xx\,i-1,j}}{2 \cdot \lambda} + \frac{m_{xy\,i+1,j} - m_{xy\,i-1,j}}{2 \cdot \lambda}$$

$$v_{y\,i,j} = \frac{m_{yy\,i+1,j} - m_{yy\,i-1,j}}{2 \cdot \lambda} + \frac{m_{yx\,i,j+1} - m_{yx\,i,j-1}}{2 \cdot \lambda} \qquad (3.8)$$

For points on the edges, the finite difference equations are modified as:

$$v_{x\,i,j} = \frac{m_{xx\,i+1,j} - m_{xx\,i,j}}{2 \cdot \lambda} + \frac{m_{xy\,i,j+1} - m_{xy\,i,j-1}}{2 \cdot \lambda} \; or \; \frac{m_{xx\,i,j} - m_{xx\,i-1,j}}{2 \cdot \lambda} + \frac{m_{xy\,i+1,j} - m_{xy\,i-1,j}}{2 \cdot \lambda} \quad \text{(for edges parallel to the x-axis)}$$

$$v_{y\,i,j} = \frac{m_{yy\,i+1,j} - m_{yy\,i,j}}{2 \cdot \lambda} + \frac{m_{yx\,i,j+1} - m_{yx\,i,j-1}}{2 \cdot \lambda} \; or \; \frac{m_{yy\,i,j} - m_{yy\,i-1,j}}{2 \cdot \lambda} + \frac{m_{yx\,i+1,j} - m_{yx\,i-1,j}}{2 \cdot \lambda} \quad \text{(for edges parallel to the y-axis)} \qquad (3.9)$$

The second option is to use the partial finite difference equation of (3.10). This method is slightly more difficult as it also requires modifications to the finite difference equations for points next to the edges. The third option is to determine the derivative in the x- and y-direction of the sum of bending moments mesh/field instead of the displacement field to determine the shear forces in the corresponding direction (similar to the derivative method) by using equations (3.13) and (2.15).

$$v_{x_{i,j}} = \frac{\bar{m}_{i+1,j} - \bar{m}_{i-1,j}}{2 \cdot \lambda} \quad ; \quad v_{y_{i,j}} = \frac{\bar{m}_{i,j+1} - \bar{m}_{i,j-1}}{2 \cdot \lambda} \tag{3.10}$$

As all of the before mentioned methods are based on a discrete mesh instead of an interpolated surface, the principle shear forces cannot be determined directly, therefore equations (2.15) and (2.16) must be used.

The conceived finite difference component is represented as a flow chart in figure 81.

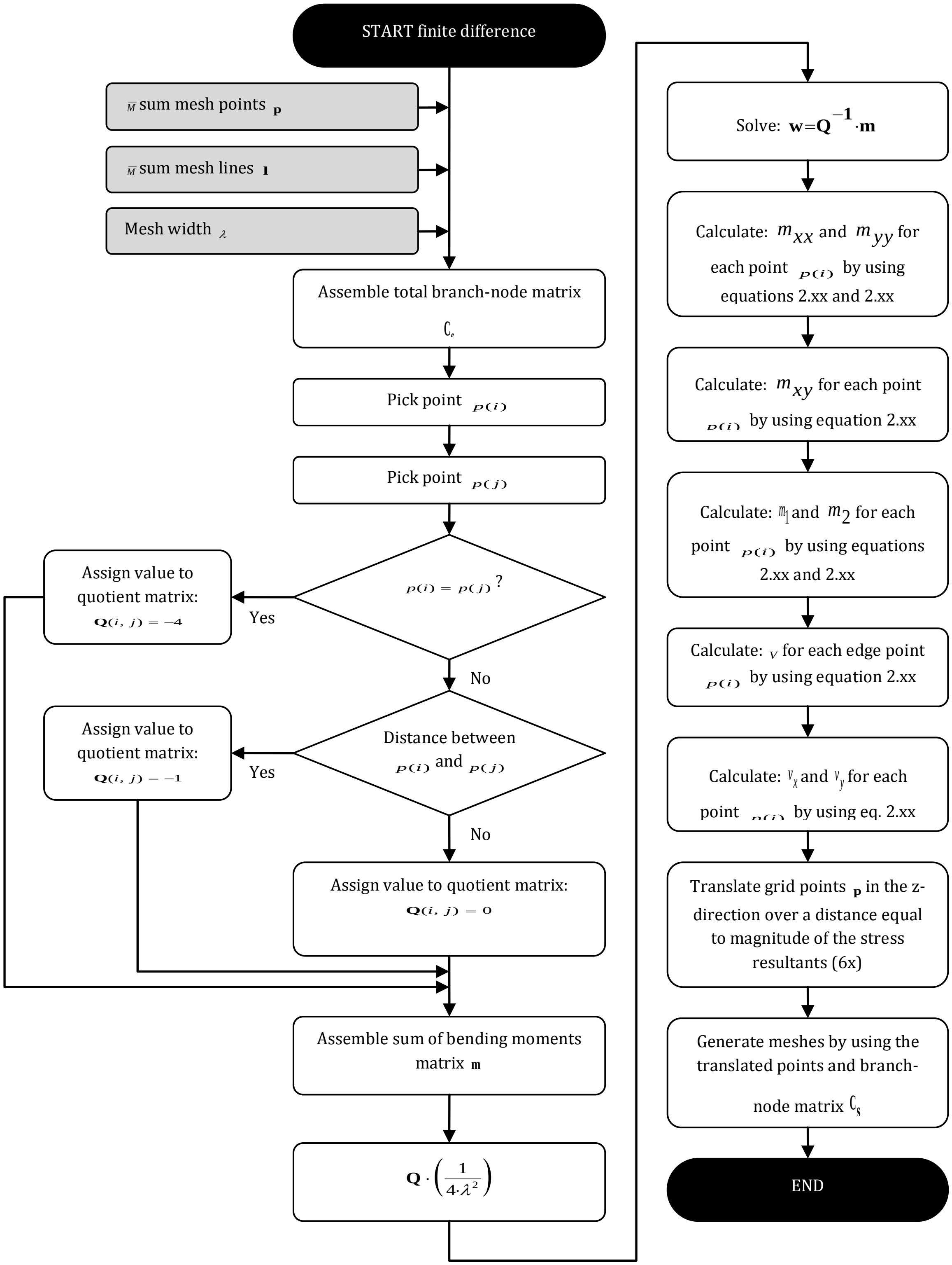

Fig.79. Flow chart of the finite difference component

3.10.1 Results

In order to display the output values (stress resultants and deformations) of the finite difference component, a separate display component was developed out of predefined components provided by the Grasshopper application. This component offers different options for displaying the numerical calculation results: (coloured) 3D mesh, 3D (interpolated) surface, contour plots and value tags. Below the results for a simply supported plate (plate stiffness $D = 1$; $l = 1{,}4$; $b = 1{,}0m$; $\lambda = 0{,}1m$) subjected to a distributed load $p = 1kN$ are displayed as 3D meshes.

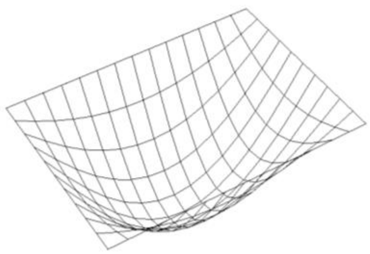

Fig.80. Displacement field (w)

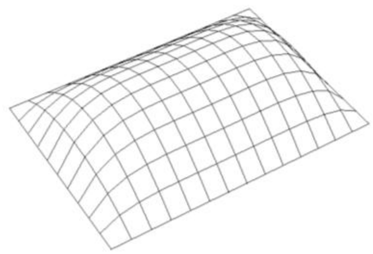

Fig.81. Bending moments in x-direction (m_{xx})

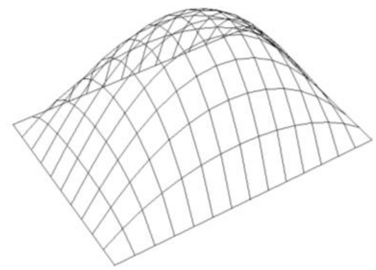

Fig.82. Bending moments in y-direction (m_{yy})

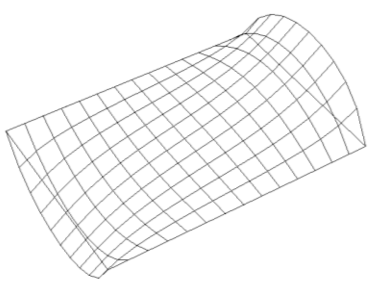

Fig.83. Shear forces in x-direction (v_x)

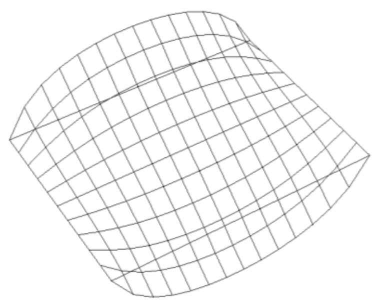

Fig.84. Shear forces in y-direction (v_y)

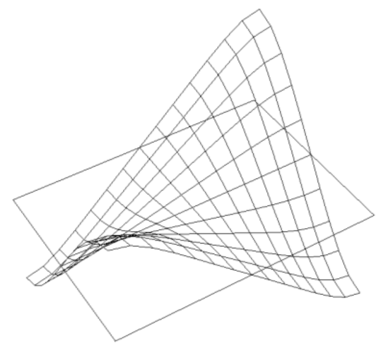

Fig.85. Torsional moments (m_{xy})

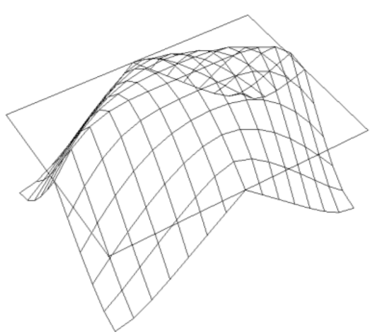

Fig.86. Minimum Principle moments (m_1)

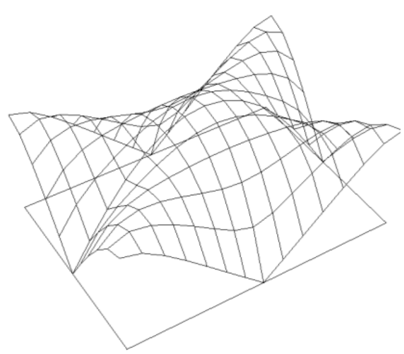

Fig.87. Maximum Principle moments (m_2)

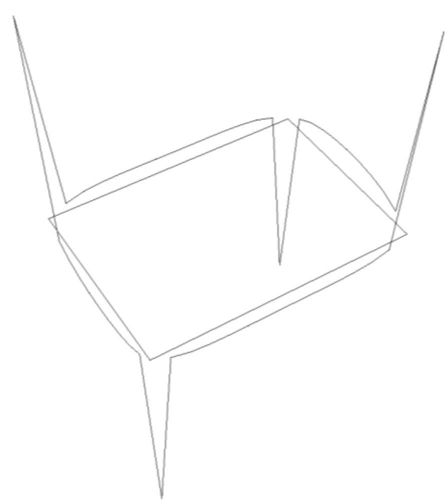

Fig.88. Concentrated shear forces (V)

The same results can also be displayed as contour plots with value tags as shown below:

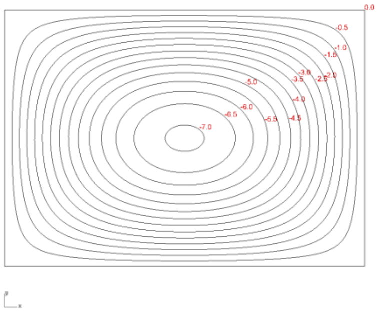

Fig.89. Displacement field (w)

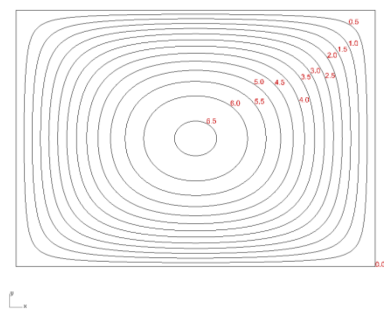

Fig.90. Bending moments in x-direction (m_{xx})

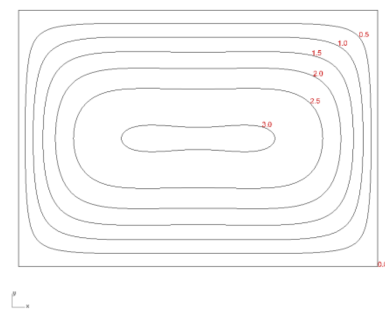

Fig.91. Bending moments in y-direction (m_{yy})

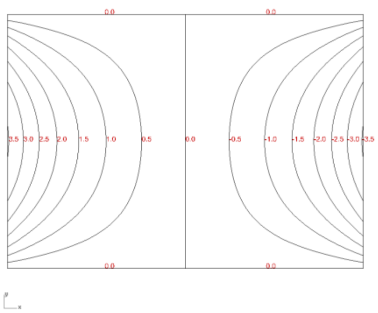

Fig.92. Shear forces in x-direction (v_x)

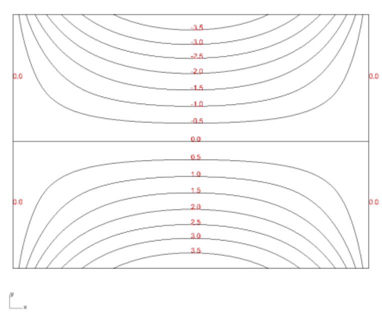

Fig.93. Shear forces in y-direction (v_y)

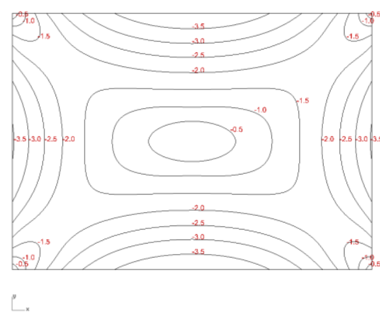

Fig.94. Principle shear forces (v_n)

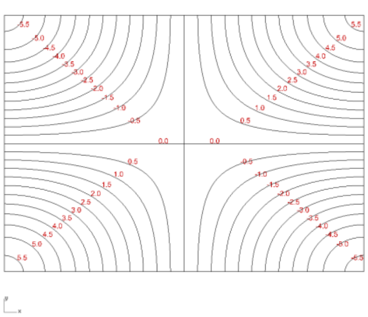

Fig.95. Torsional moments (m_{xy})

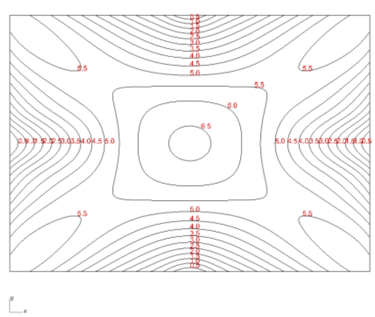

Fig.96. Maximum Principle moments (m_1)

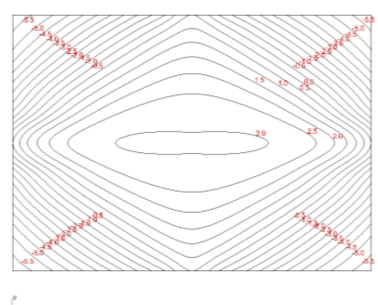

Fig.97. Minimum Principle moments (m_2)

Another case study was performed for a simply supported plate subjected to a point load $P = 10kN$, positioned in the centre of the (plate stiffness $D = 1$; $l = 1{,}4$; $b = 1{,}0m$; $\lambda = 0{,}1m$). The resulting stress resultants and deformations are shown below as 3D meshes.

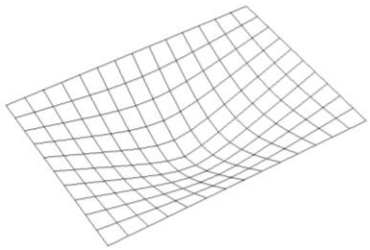

Fig.98. Displacement field (w)

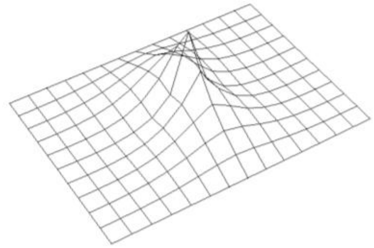

Fig.99. Bending moments in x-direction (m_{xx})

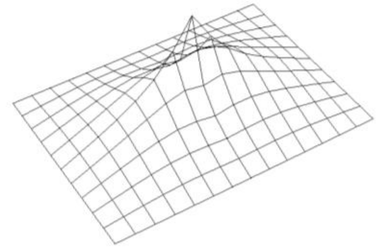

Fig.100. Bending moments in y-direction (m_{yy})

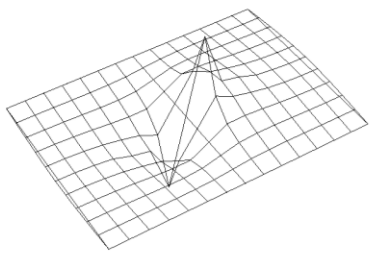

Fig.101. Shear forces in x-direction (v_x)

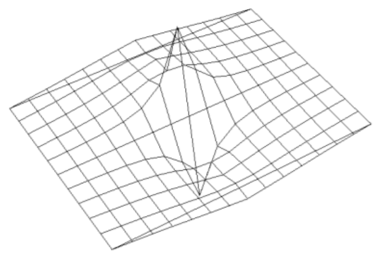

Fig.102. Shear forces in y-direction (v_y)

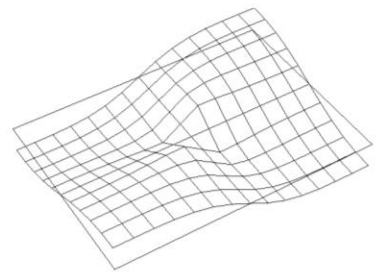

Fig.103. Torsional moments (m_{xy})

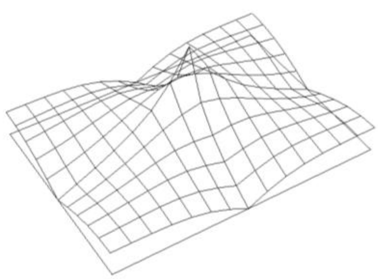

Fig.104. Minimum Principle moments (m_1)

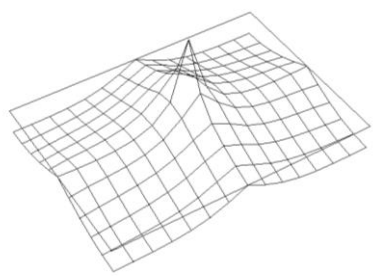

Fig.105. Maximum Principle moments (m_2)

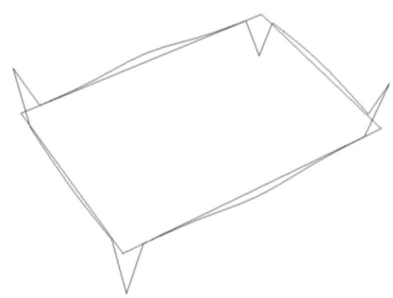

Fig.106. Concentrated shear forces (V)

3.11 Sand hill & Voronoi component

3.11.1 Introduction

The sand hill component generates parametric sand hill models for plate structures. These sand hill diagrams can be used to determine the yield lines in plates (analogous to the ridges of the sand hill models). During this research it was found that by inverting and translating these sand hill diagrams an accurate representation is obtained of the principle shear force diagrams for rectangular plates without torsional stiffness (twist-less case) along the lines of symmetry. By integrating planar sections of these diagrams along the lines of symmetry, bending moment diagrams can be obtained. Furthermore, a similarity between sand hill models and Voronoi tessellations is recognized. A Voronoi component is developed which generates Voronoi tessellation, which can be used as discrete principle shear force trajectories to obtain insight in the flow of forces and to determine the magnitude of the principle shear forces along the edges.

3.11.2 Development of the sand hill component

The sand hill component was developed by implementing two mathematical principles which determine the shape of the sand hill diagrams. These principles were defined by a series of experiments with physical sand hill models. The implementation was realized through a set of predefined components, provided by the Grasshopper application. The two principles are:

1) Sand particles flow to the nearest hole or plate edge
2) The slope is approximately 45 degrees

The sand hill component requires as input a mesh (consisting of a collection of grid points and lines, provided by the mesh component) which represents the plate surface and set of curves/lines and points which represent respectively the supported plate edges (or internal line supports) and the holes through which the sand grains can flow of the plate (analogous to the support conditions).

When these inputs are provided, the sand hill component first determines, from each grid point, the closest Euclidian distance to the provided collection of lines and points according to the first principle, by using the two “closest point on curve” and “closest point” components provided by the Grasshopper application. From the second principle it can be concluded that the height of the sand hill model in a grid is equal to the closest distance (figure 109). This knowledge is applied by translating the initial grid points over this distance in the global z-direction. As the before mentioned components also calculate the distance between the concerned grid point and the closest point, this value can be used directly to translate the initial grid point in the z direction. The result is collection of translated points which together represent the shape of the sand hill diagram. When a mesh of sufficient density is used, the shape of the sand hill becomes clearly visible as is illustrated in figure 110. The collection of points can also be used to generate a 3D mesh (figure 111).

3.11.3 Results

The generation procedure and the results produced by the sand hill component for a simply supported plate are shown in the figures below.

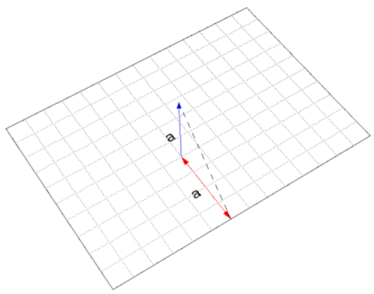

Fig.107. Generation procedure for sand hill model

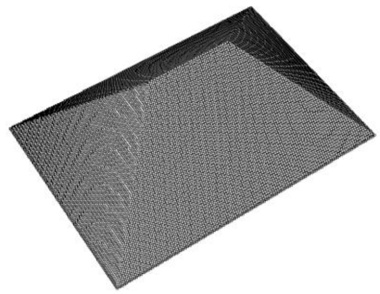

Fig.108. Sand hill model represented by dense grid

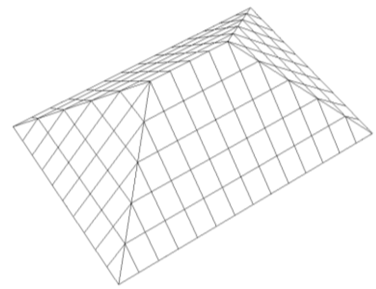

Fig.109. Sand hill model represented by 3D mesh

The influence of the support conditions for the shape of the sand hill models for a rectangular plate structure is shown in the figures below.

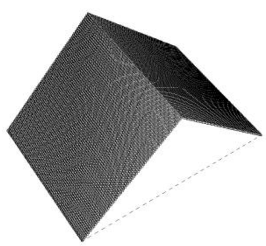

Fig.110. Parametric sand hill model: 2 edge supports

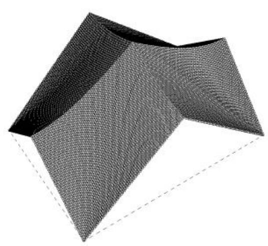

Fig.111. Parametric sand hill model: 4 corner supports

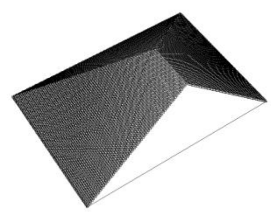

Fig.112. Parametric sand hill model: edge supports and 1 free edge

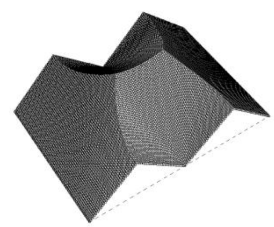

Fig.113. Parametric sand hill model: 2 edge- and 2 point supports

The output of the parametric sand hill component is validated by comparing them to physical sand hill models for a configuration of points as shown in pictures 116 and 117.

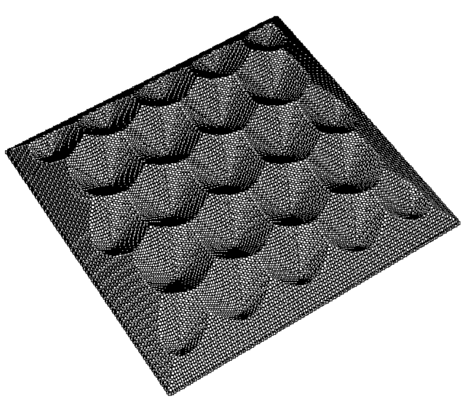

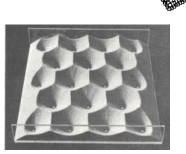

Fig.114. Parametric sand hill model: configuration of point- and line supports & physical sand hill model

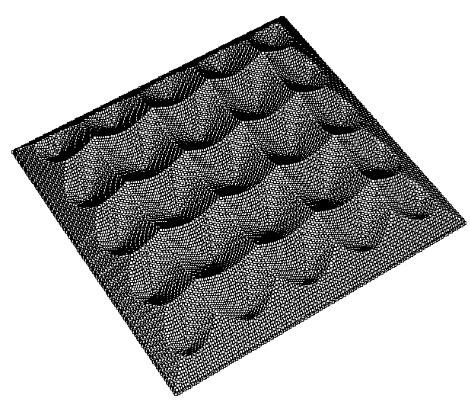

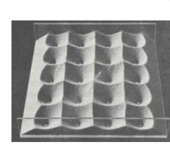

Fig.115. Parametric sand hill model: configuration of point- and line supports & physical sand hill model

3.11.4 Principle shear force diagrams and bending moment diagrams

During this research it was explored how (and to what extend) inverted and translated sand hill models can be used as a structural analysis tool to generate 3D principle shear force diagrams, determine the trajectories of the principle shear forces and to generate bending moment diagrams for simply supported plate structures (subjected to a distributed load p) by developing a series of extensions to the sand hill component which perform these operations. First, the inverted and translated sand hill diagrams were generated by performing two mathematical vector operations on the initial mesh (figure 111) of the sand hill model, which results in the 3D principle shear force diagram as shown in figure 118.

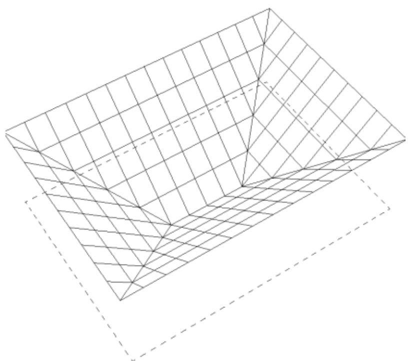

Fig.116. Mesh representation of 3D principle shear force diagram (inverted and translated sand hill model).

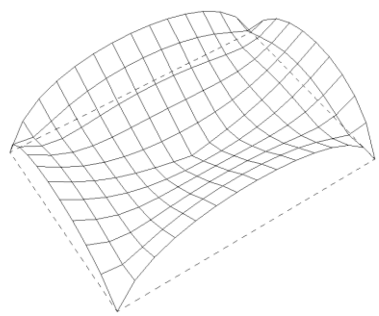

Fig.117. Principle shear force diagram for (isotropic) simply supported plate, subjected to a distributed load $p = 1$, generated by the derivative component.

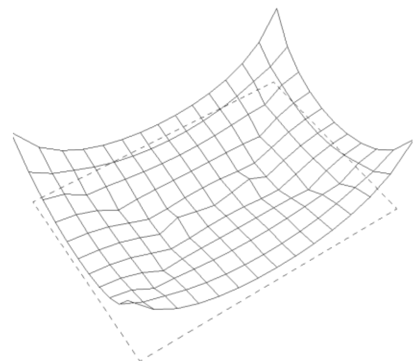

Fig.118. Differences between both principle shear force diagrams.

Similar to sand hill diagrams, the slope of these diagrams is equal to 45°. Because the first derivative of the shear force diagram is equal to the load p (see paragraph 2.2), it can be concluded that the distributed load p is equal to one. The sand hill diagram can be adapted to different magnitudes for the distributed load p by adjusting the slope α of the sand hill diagram, which can be easily achieved by calculating the height h of the diagram in the grid points by using the required slope α and the closest distance a as shown in equation (3.11).

$$h = (\tan \alpha) \cdot a \qquad ; \qquad p = \frac{h}{a} \tag{3.11}$$

The differences between both diagrams of the principle shear forces, respectively generated by the sand hill component and the derivative component are shown in figure 3.xx. These figures indicate that the sand hill component gives a reasonable representation of the magnitude of the principle shear forces along the lines of symmetry, but is less accurate towards the corners (where large deformations occur). At first, the deviations in the magnitude of the principle shear forces were devised to the effect of torsional forces on the shear force distributions on basis of equations (2.3) which indicate that the magnitude of the shear forces in the x- and y-direction are a summation of the derivatives of the bending moments m_{xx} and torsional moments m_{xy}. These torsional moments m_{xy} are zero along the lines of symmetry and reach a maximum value in the corners of the plate. Therefore, the hypothesis was stated that the principle shear force diagrams could be seen as representations of the shear force distribution within plates without torsional stiffness (twistless-case).

This hypothesis was tested by generating the corresponding bending moment diagrams for several plate sections. To achieve this, a section of the 3D principle shear force was used as 2D shear force diagram to calculate the corresponding bending moment diagram by integration (within this thesis the rectangle method is used) of a section of the principle shear force diagram along a line. This procedure is shown in figures 121 to 123.

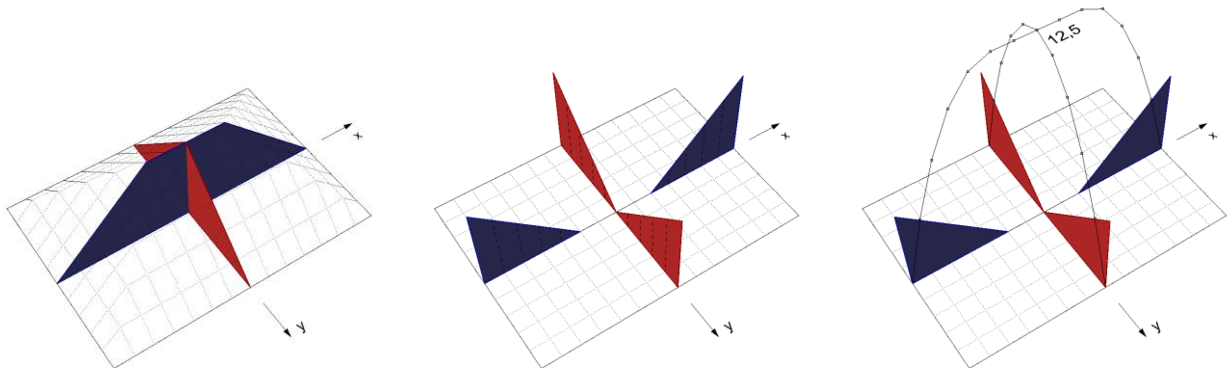

Fig.119. Sections of the sand hill model *Fig.120. Inverted and translated sections* *Fig.121. Bending moment diagram*

After comparing the obtained 2D bending moment diagrams with calculation results produced by a FEM based structural analysis program, it was validated that the bending moments give an accurate presentation of the bending moment in the x- and y-direction along the lines of symmetry for orthotropic plates without torsional stiffness. For example, the maximum value of the bending moments obtained by both calculation methods in the center of a simply supported plate subjected to a distributed load $p = 1\ kN$ is 12,5 kN (in both the x- and the y-direction). In other plate sections the deviations were too large to be considered as useful representation of the bending moment values.

3.11.5 Principle shear force trajectories and Voronoi tessellations

The analogy between sand hill diagrams and principle shear force diagrams was further explored within the scope of simply supported plates by assuming that the principle shear forces will flow to the supports analogously to the sand grains. With regard to the latter, it was again assumed that each sand grain will flow in the direction of the closest point on the plate edges, and follows a straight (planar) trajectory. These flow paths are illustrated for a grid of points in figure 124.

Furthermore, as explained in paragraph 2.8, a relation exists between sand hill models and Voronoi diagrams as they are both based on the 'closest point principle'. The predefined Voronoi-component, provided by the Grasshopper application is used to generate a Voronoi tessellation for a collection of equally spaced points on the edges of the plate. The similarity between the flow paths based on a sand hill models and Voronoi tessellations can be seen by comparing picture 124 and 125. By comparing the Voronoi tessellation to the principle shear force trajectories (generated by the rain flow component) associated with the same points it can be seen that the Voronoi tessellation can be considered as discrete principle shear force trajectories.

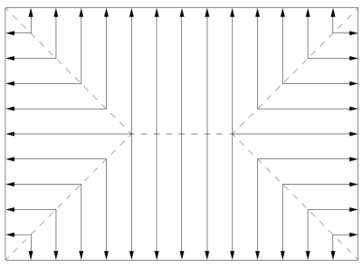

Fig.122. Flow paths sand grains

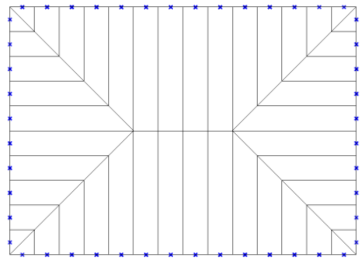

Fig.123. Voronoi tessellation

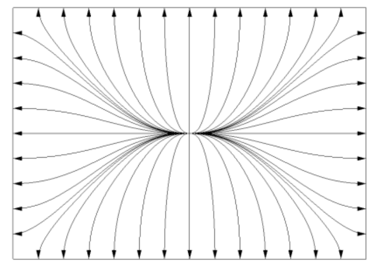

Fig.124. Principle shear force trajectories

The obtained Voronoi cells resulting from the collection of points on the plate's edge can be used directly to determine the magnitude of the shear forces along the edges of the (simply supported) plate, in the same way as before by using the rain flow trajectories (produced by the rain flow component, figure 126). The magnitude of the principle shear force in the considered points equals the surface of the Voronoi cell. Although this method gives a good indication of the discrete principle shear force diagram, it is less accurate than the results obtained from the membrane analysis (figure 128), the Voronoi component can be used to generate discrete shear force trajectories for free form plate geometries as is showed in figure 127.

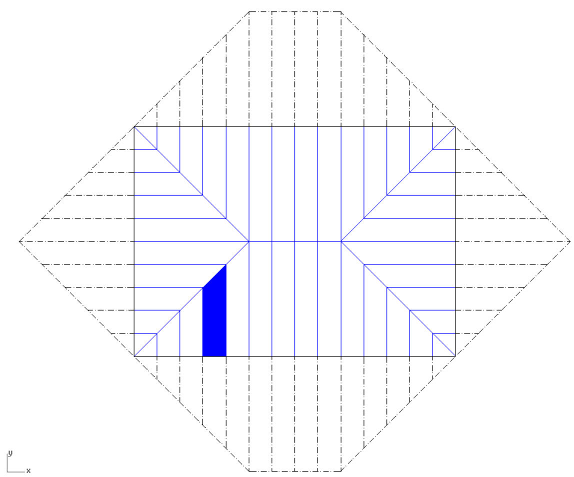

Fig.125. Discrete trajctories and magnitude of principle shear forces along the plate edges (produced by the Voronoi component)

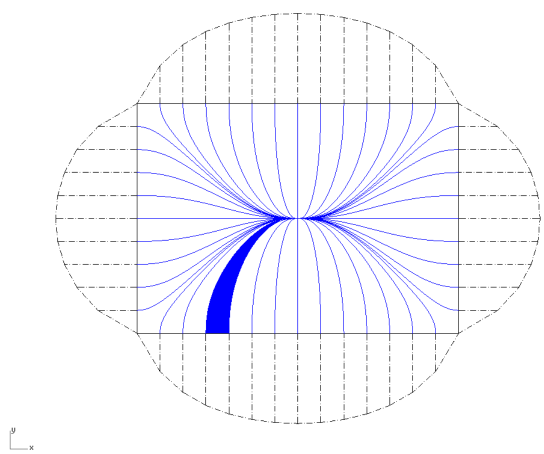

Fig.126. Trajctories and magnitude of principle shear forces along the plate edges (produced by the rain flow component)

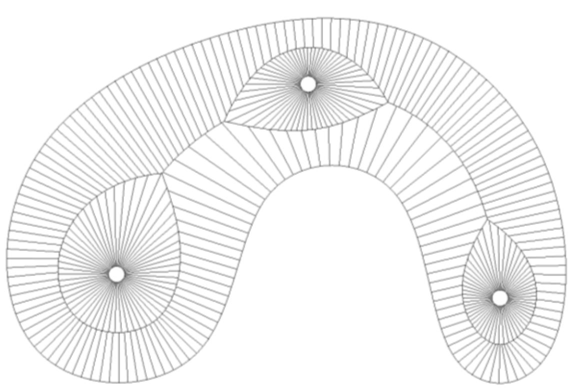

Fig.127. Discrete principle shear force trajectories (Voronoi component)

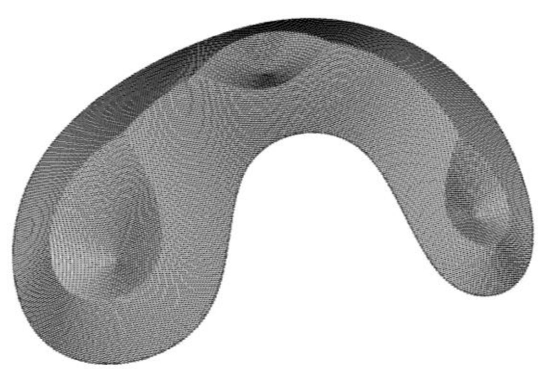

Fig.128. Sand hill model

3.12 *Conceived structure and layout of the parametric structural design tool*

In figure 5.5 the final layout of the design tool is presented as flowchart. In this diagram it can be seen which calculation results (H) can be achieved by providing a structural geometry (outlines of a plate geometry) by composing a structural analysis sequence out of a series of structural analysis components (B,C,D,E,F and G)and the mesh component (A). Furthermore, it is illustrated how the calculation results (H) can be displayed in the 3D environment of Rhinoceros by attaching one or more display components (I). It can also be noticed that the Force Density component can also be used solely as form finding tool for generating membrane/shell structures. Subsequently to this form finding process the generated geometry can be developed further in Rhinoceros.

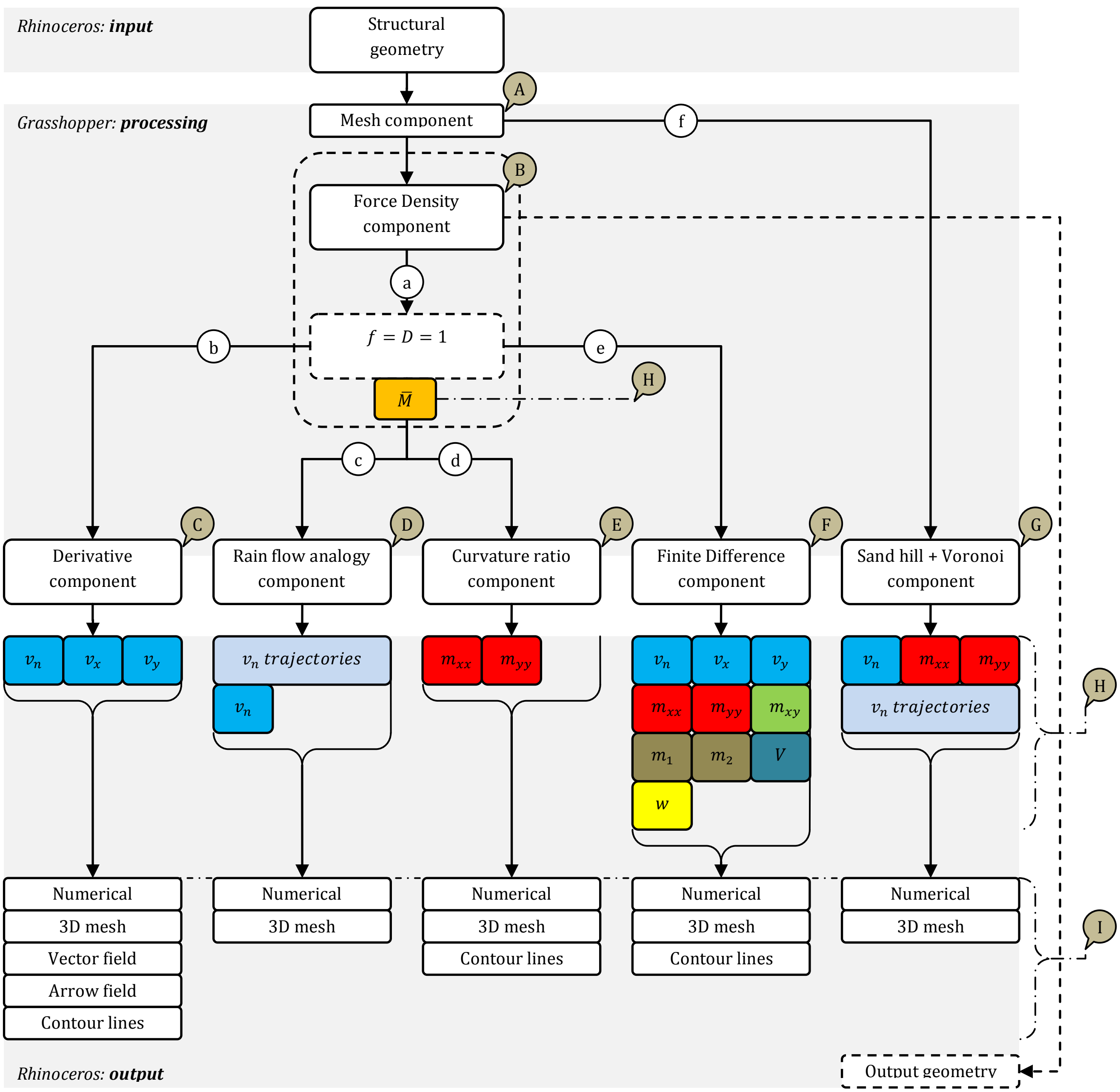

Fig.129. Flowchart of the final setup of the parametric structural design tool

4 Validation

4.1 Introduction

In this chapter the calculation results for a series of stress resultants, produced by the structural analysis sequences in combination with the display components, are both quantitatively and qualitative validated to evaluate of the performance of the developed parametric structural design tool. This relates to objective 1d, which was defined as:

"Validate the produced calculation results in a qualitative- and a quantitative manner."

The qualitative comparison evaluates the distribution of the stress resultants by comparing the contour plots produced by the parametric components to the corresponding contour plots, provided by a FEM based software package SCIA. The quantitative comparison evaluates the numerical accuracy of the produced resultants by comparing a series of analytical solutions (Czerny, 1959), related to grid points along plate sections, to the corresponding analytical results.

A thin simply supported (along its edges) rectangular plate, subjected to a distributed load p is used as case study for the validation. The geometry of the plate is shown in figure 132.

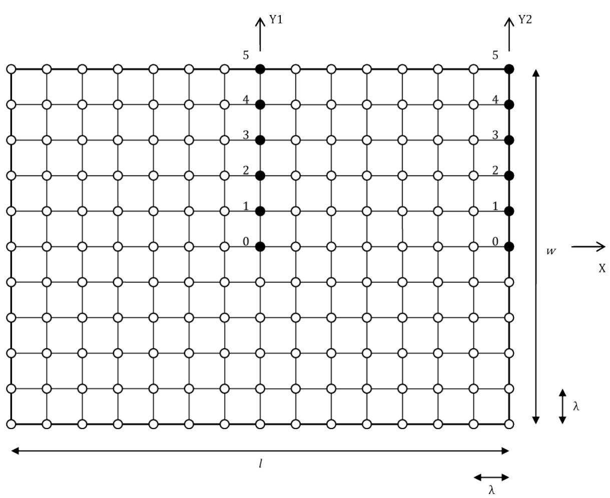

l = 1,4m
w = 1,0m
D = 1
p = 1kN/m^2
υ = 0
λ_x = 0,1m
λ_y = 0,1m

Fig.130. Sections for quantitative evaluation

The calculations performed within the parametric components and SCIA are both based on a square mesh as in indicated in figure 132. Quite a large mesh size was used for the calculation (0,1m) because this induces a fast and sufficiently accurate structural analysis and thus contributes to real time structural evaluation, which is considered as being more important than accuracy within a conceptual design process. However, it must be mentioned that it is possible to improve the accuracy of the calculation results by applying a mesh refinement, a possibility which is provided by the mesh component.

4.2 *Shear forces*

The contour plots for the (principle) shear forces v_n are shown below (figures 133 to 134). The plots were produced by respectively SCIA, the derivative component (figures 136 to 138) and the rain flow component (figure 139).

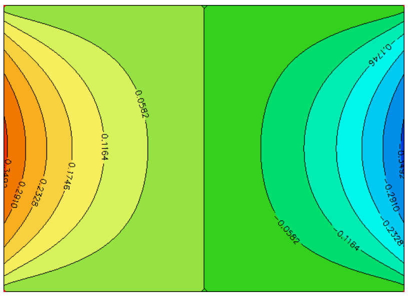

Fig.131. Derivative component (v_x)

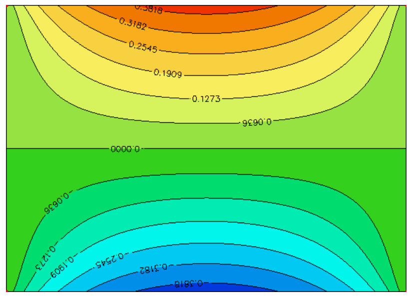

Fig.132. Finite element method (v_y)

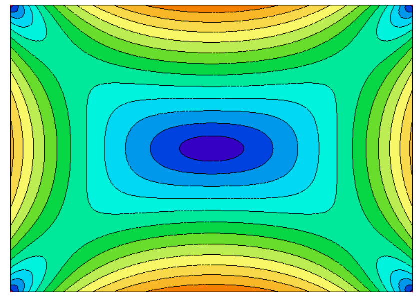

Fig.133. Finite element method (v_n)

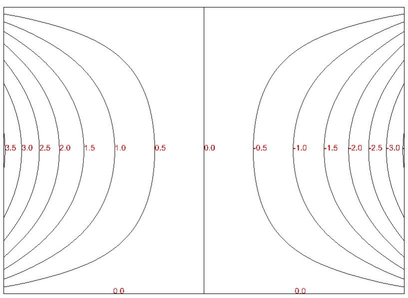

Fig.134. Derivative component (v_x)

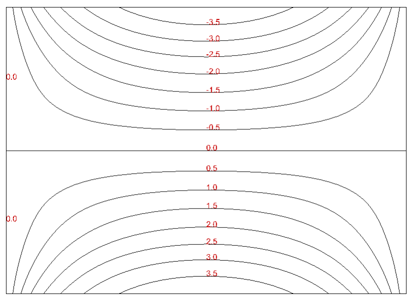

Fig.135. Finite element method (v_y)

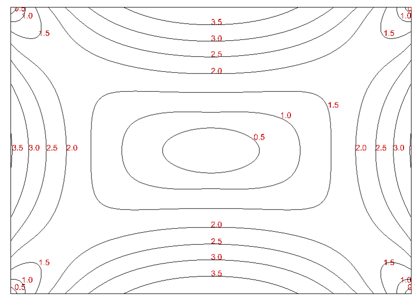

Fig.136. Derivative component (v_n)

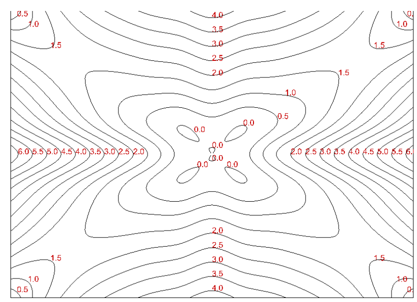

Fig.137. Rain flow component (v_n)

A clear resemblance can be noticed between the three contour plots produced by the derivative component (figures 136 to 138) and SCIA (figures 133 to 135) with respect to the shear forces in the x- and y-direction (v_x & v_y) and the principle shear forces (v_n). This is not the case for the contour plot of the principle shear forces produced by the rain flow component (figure 139). Although some similarities can be noticed with the results of SCIA, the presented distribution of shear forces deviates significantly in regions close to the lines of symmetry. With regard to this, it should be noted that the results for the principle shear forces v_n are more accurate near the edges parallel to the x-axis than for the edges parallel to the y-axis of the global coordinate system. A reason for this phenomenon could be the way in which the load accumulation (analogous to a discrete version of the rain flow analogy) is simulated within the rain flow component.

The procentual deviation between the magnitudes of the principle shear forces v_n, calculated by both the derivative component and SCIA, and anylicatal solutions (based on tables provided by Czerny) for a set of points along the Y1- and Y2-axis are peresented in figures 140 and 141.

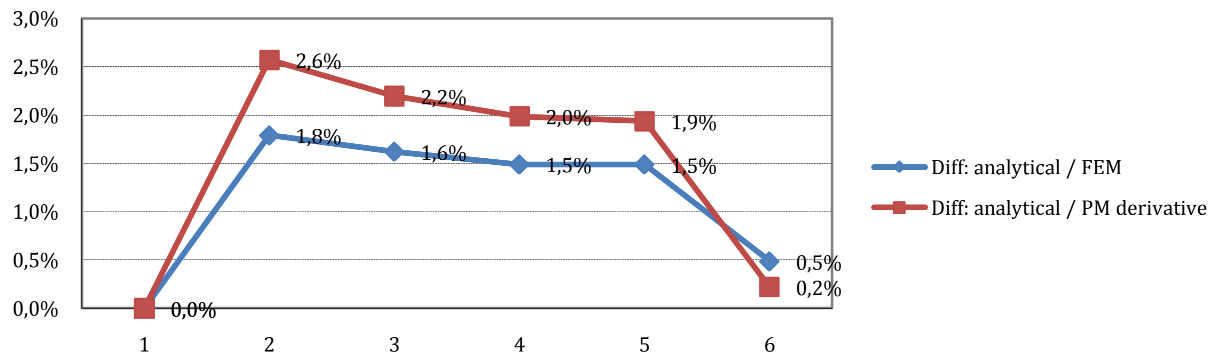

Fig.138. Procentual deviation between analytical calculation results and the corresponding solutions provided by the finite difference component and SCIA for v_n, in a series of grid points along the Y1 axis.

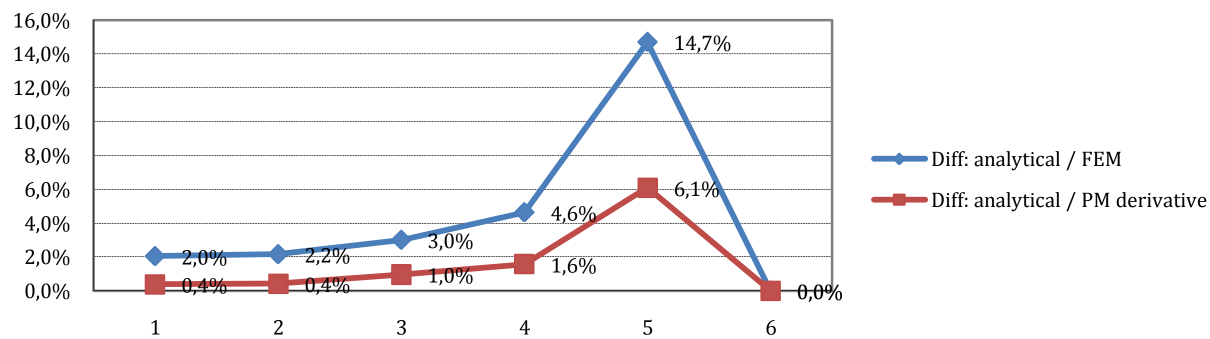

Fig.139. Procentual deviation between analytical calculation results and the corresponding solutions provided by the finite difference component and SCIA for v_n, in a series of grid points along the Y2 axis.

The average deviation between the output of the derivative component and the analytical results for v_n is 1,5% along the Y1-axis and 1,6% along the Y2-axis. The maximum deviation between the results of the derivative component and the analytical results occurs in point 5 (nearby the corner of the plate). The procentual deviation at this location is 6,1%, which is still more than twice as accurate as the result provided by SCIA (14,7%). In general, it can be said that the derivative component produces more accurate results for the principle shear forces v_n than SCIA along the Y1 axis. The opposite is true for the Y2 axis where the results produced by SCIA are more accurate.

4.3 *Bending- and torsional moments*

Below, the contour plots are shown for the bending moments in the x- and y-direction (v_n and the shear forces in the x- and y-direction (v_x & v_y), produced by respectively the finite difference component (figures 145 to 147), the curvature ratio component (figures 148 and 149) and SCIA (figures 142 to 144).

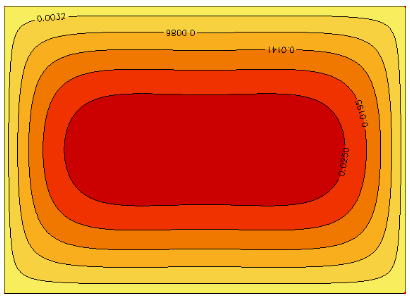

Fig.140. Finite element method (m_{xx})

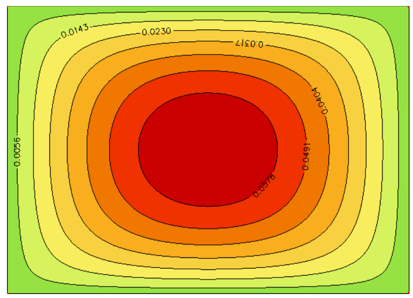

Fig.141. Finite element method (m_{yy})

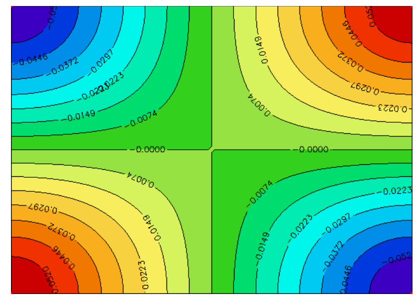

Fig.142. Finite element method (m_{xy})

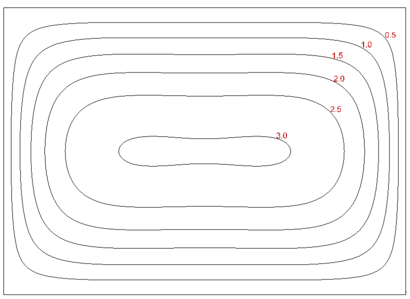

Fig.143. Finite difference component (m_{xx})

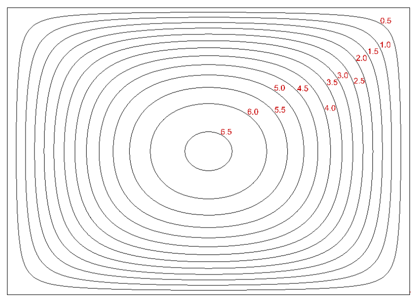

Fig.144. Finite difference component (m_{yy})

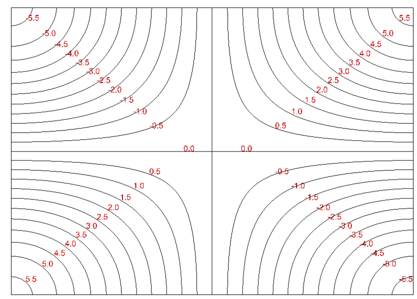

Fig.145. Finite difference component (m_{xy})

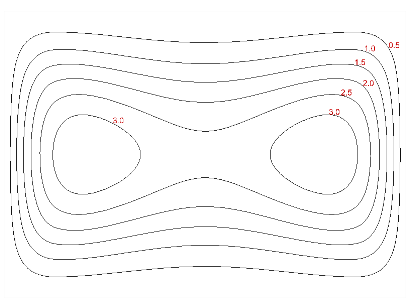

Fig.146. Curvature ratio component (m_{xx})

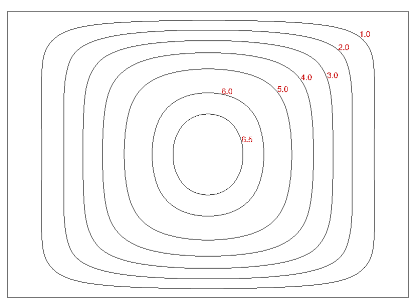

Fig.147. Curvature ratio component (m_{yy})

When comparing the contour plots for m_{xx}, m_{yy} and m_{xy}, produced by the finite difference component and SCIA, a clear resemblance can be noticed. This proves that the finite difference component presents an accurate representation of moment distribution within the plate. With respect to the results produced by the curvature ratio component for m_{xx} and m_{yy}, by comparing the contour plots with the ones provided by SCIA, both similarities and differences can be identified. In general it can be said that although the general moment distribution within the plate is represented accurately, it deviates along the lines of symmetry. The contour plot of the bending moments in the x-direction m_{xx} show two distinct local maxima located adjacent to the plate centre, where a local minimum occurs. It was found that a similar phenomenon occurs within the results produced by SCIA, although less distinct, and that the derivative component in fact exaggerates this phenomenon. A possible explanation for the deviation between the results, produced by the curvature ratio component and the analytical calculation results could be the geometrical characteristics of the NURBS surface interpolation, which is generated within the form finding component. Since the mathematical principles by which the NURBS surfaces are created have no physical meaning, this could contribute to an incorrect curvature ratio and thus incorrect bending moment values. Despite the lower accuracy compared to the finite difference component, the calculations within the curvature ratio component are performed much faster (in case of the considered rectangular plate, approximately 3 times faster).

The procentual deviation between the magnitudes of the bending moments m_{xx}, m_{yy}, calculated by the finite difference component, and anylicatal equations (based on tables provided by Czerny) for a set of points along the Y1- and Y2-axis are peresented in figures 150 and 151.

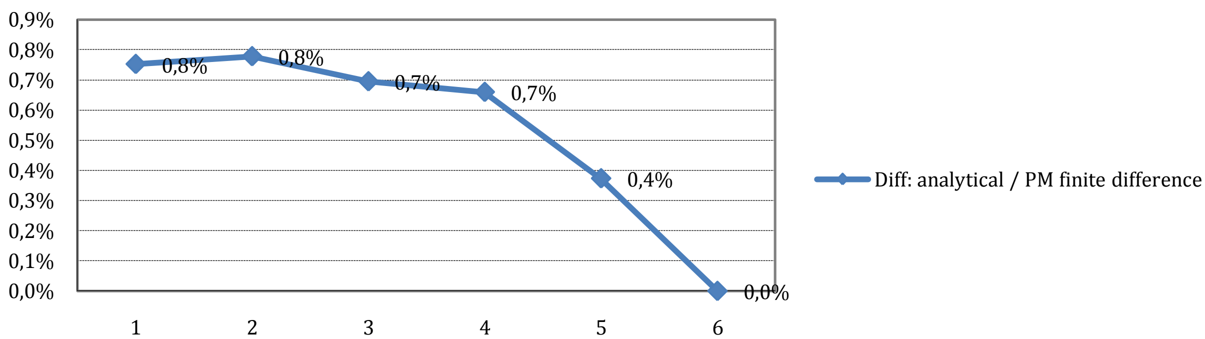

Fig.148. Procentual deviation between analytical calculation results and the corresponding solutions provided by the finite difference component for m_{xx}, in a series of grid points along the Y1 axis.

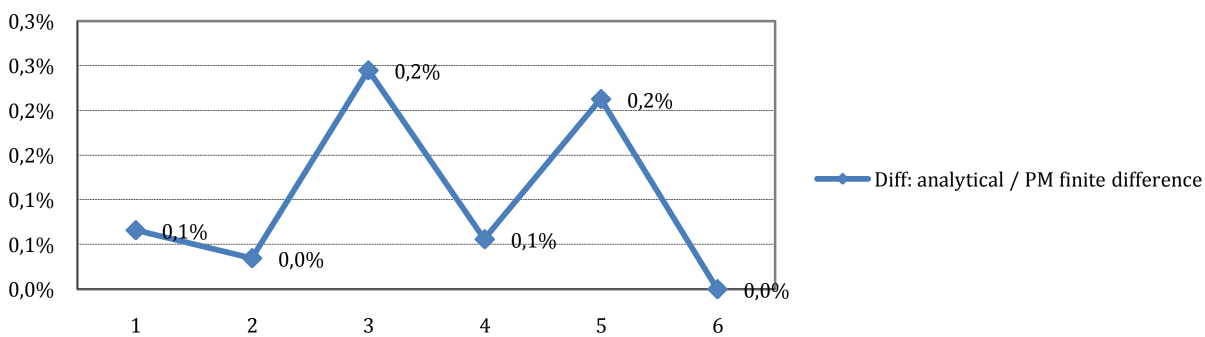

Fig.149. Procentual deviation between analytical calculation results and the corresponding solutions provided by the finite difference component for m_{yy}, in a series of grid points along the Y1 axis.

The results shown in figures 150 and 151 prove that the finite difference component provides very accurate numerical results for both the bending moments in the x- and the y-direction. The average deviation for the bending moments m_{xx} is 0,6% procent and 0,1% for m_{yy}. With respect to the bending moments in the x-direction m_{xx}, the largest deformations occur in point 2, next to the centre of the plate. The accuray increases towards the edges of the plate. With respect to the bending moments in the y-direction m_{yy}, the procentual deviations have an irregular progression and the largest deformations occur in point 3.

The procentual deviation between the magnitudes of the torsional moments m_{xy}, calculated by repsectively the finite difference component and anylicatal equations (based on tables provided by Czerny) for a set of points along the Y2-axis is presented in figure 152.

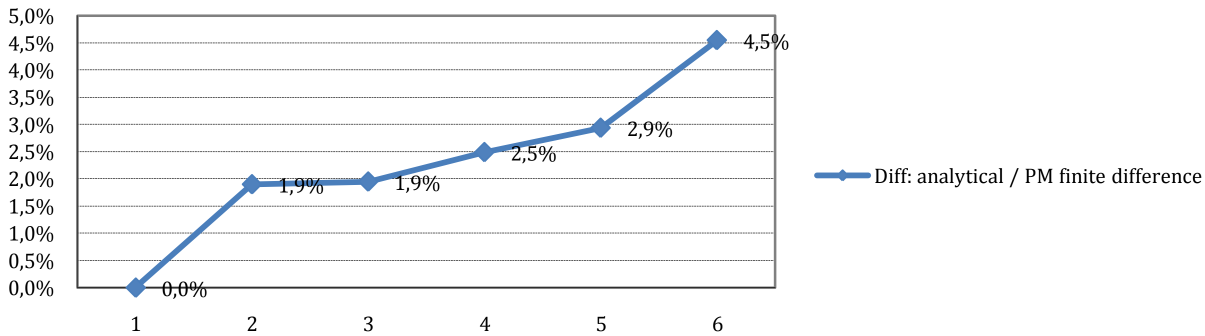

Fig.150. Procentual deviation between analytical calculation results and the corresponding solutions provided by the finite difference component for m_{xy}, in a series of grid points along the Y2 axis.

The average deviation between the output of the finite difference component and the analytical solutions is 2,3%, which indicates that the produced results are quite accurate. In figure 4.xx it can be seen that the maximum deviation of the torsional moments m_{xy} is 4,5% in the corner point of the plate.

5 Conclusions

5.1 Introduction

In this chapter it will be evaluated how (and to what extend) the main and secondary objectives have been achieved. In chapter 1 (§1.3) the main objective of this thesis, based on two related problem statements (§1.2) was stated as:

"Develop a structural design tool for architects and engineers, based on simple analytical structural analysis methods, which gives both quantitative and qualitative (real time) insight in the flow and magnitude of forces within a specific structure during a conceptual design stage."

The scope of this thesis is confined to a specific structural element: simply supported (rectangular) isotropic thin plate structures, subjected to a loads perpendicular to their plane (§ 2.4). The approach developing the structural design was to implement analytical structural analysis methods into a parametric application (Grasshopper) within a 3D modelling environment (§ 2.3).

The development of the parametric structural design tool toachieve the main objective, was guided by a set of secondary objectives. Within chapters 2,3 and 4 these objectives were achieved by respectively defining a theoretical framework, developing the parametric structural design tool and validating the produced calculation results. In the following paragraphs 5.2, 5.3 and 5.4 it will be evaluated, analogous to chapters 2,3 and 4, whether (and to what extend) the secondary objectives have been reached within this thesis. Finally, within paragraph 5.5 it will be determined whether the main objective has been reached, on basis of the secondary objectives.

5.2 Theoretical framework

The theoretical framework was defined in correspondence with secondary objective 1a:

"Define a theoretical framework, by defining which- and how- analytical and numerical structural analysis techniques can be used to provide both quantitative and qualitative insight in the relation between structural geometry and the flow- and magnitude of forces and deformations within structures and have the potential to be implemented into a (parametric) computational tool."

A theoretical framework was defined in chapter 2 by selecting several analytical and numerical structural analysis methods for obtaining both quantitative and qualitative insight in the relation between structural geometry and the flow- and magnitude of the forces and deformations within structures (§ 2.2):

8) Differential equations for thin plates (§2.2)
9) Elastic membrane analogy (§2.3)
10) Force Density method (§2.4)
11) Rain flow analogy (§2.5)
12) Curvature ratio method (§2.6)
13) Finite difference method (§2.7)
14) Sand hill analogy (§2.8)

Within paragraphs 2.2 to 2.8, the theory behind these methods is briefly explained. Within paragraph 2.9, the mentioned structural analysis methods were combined into a series of (novel) structural analysis sequences a-f which provide a contribution in determining the structural quantities as shown in figure 153.

		v_n	v_x	v_y	m_{xx}	m_{yy}	m_{xy}	m_1	m_2	$\bar{M}$	V	w	v_n $trajectories$
a)	3 + 2									√			
b)	3 + 2 + 1	√	√	√									
c)	3 + 2 + 4	√											√
d)	3 + 2 + 5				√	√							
e)	3 + 2 + 6 + 1	√	√	√	√	√	√	√	√	√	√	√	
f)	7	√											√

Fig.151. Overview of structural analysis sequences and their contribution to determining the different stress resultants (within thin plate structures)

Paragraphs 2.9.2 to 2.9.7 explain the use of the different structural analysis methods within the structural analysis sequences to calculate/determine the different quantities. In paragraph 9.8, the relations between the different structural analysis sequences a, b, c, d, e and f was explained, which resulted in a flow chart of the total theoretical framework, which is shown in figure 154.

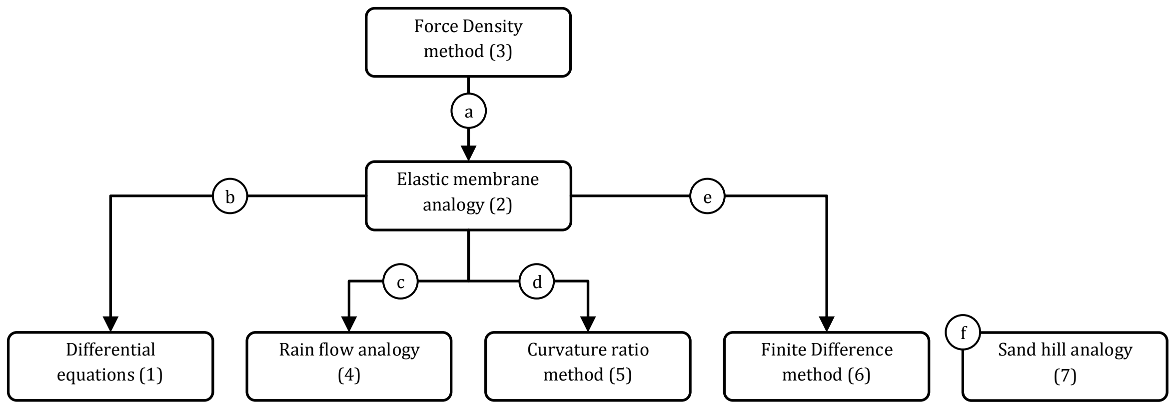

Fig.152. Flow chart of the conceived theoretical framework

5.2.1 Conclusions

The following conclusions can be drawn with respect to the structural analysis sequences within the theoretical framework:

a) The elastic membrane analogy (§ xx) can be used in combination with the Force Density method to determine the shape of sum of bending moments ($\overline{M}$) surfaces for plate structures by making the plate stiffness D equal to 1.
b) Differential equations (1) (see §2.2) can be used in combination with the sum of bending moments surface (provided by sequence a) to determine the direction and magnitude of (principle) shear forces in a grid of points.
c) The rain flow analogy (4) can be used to determine the principle shear force v_n trajectories based on the sum of bending moments surfaces (provided by sequence a), which can subsequently be used to determine the magnitude of the principle shear forces.
d) The curvature ratio method (5) is a novel structural analysis method, developed during this thesis project, which can be used to determine the bending moments m_{xx} and m_{yy} by using the ratio between the extrinsic curvatures k_{xx} and yy of a scaled version of the corresponding sum of bending moments surface (for which it must yield that: $sin\varphi \simeq \varphi$ and $cos\varphi \simeq 1$) and sum of bending moment values $\overline{M}$ for grid of points. This method cannot be used to determine the principle moments m_1 and m_2 in case the summation of bending moments consist out of two values with an opposite sign.
e) The numerical Finite Difference method (6) can be used in combination with the displacements w_m of the sum of bending moments mesh (provided by sequence a) to determine the displacement field of plates by solving a system of linear finite difference equations. This displacement field w can subsequently be used to determine the stress results m_{xx}, m_{yy} and m_{xy} by solving partial finite difference equations for a set of grid points.
f) The sand hill method (7) is conceived as a standalone structural analysis sequence, because a combination between this method and other structural analysis methods was not considered to be feasible. A mathematical relationship between sand hill models and Voronoi tessellations was noticed, which was devised to the principle of closest distance (see § xx).

In general, reflecting on the ambition to provide both quantitative and qualitative insight in the structural behaviour of thin plate structures, it can be said that the defined theoretical framework provided a good foundation for the calculation of deformations and the flow and magnitude of forces within plate structures.

5.2.2 Recommendations

With respect to the development of the different structural analysis sequences, as part of the parametric structural design tool the following recommendations are defined:

a) - Further research is needed in determining the relation with respect to the application of the membrane analogy to plates with different support conditions and other structural topologies like shear walls and subsequently shell structures.

d) - Further research is needed concerning the exact mathematical relation between the extrinsic curvature of the sum of bending moments surface and the stress resultants in plate structures. With this, especially the determining of the torsional moments is important, this is considered to be a crucial step leading to the possibility of deriving the remaining stress resultants like shear forces, principle moments and concentrated shear forces within thin plate structures on basis of the (partial) differential equations.

5.3 Parametric structural design tool

1.1.1. Functionality and usability

A set of requirements was made with respect to functionally and usability, from the perspective of the envisioned users of the structural design tool: the architect and the structural engineer. These demands were defined within paragraph 3.2, in correspondence with objective 1b:

"Define which demands, concerning functionality- and usability, have to be fulfilled by the parametric structural design tool."

The envisioned role of the parametric structural design tool, regarded from the perspective of both users (§ 3.2.1), in combination with the described character of the conceptual design stage (§ 3.2.2) has led to several demands concerning functionality (§ 3.2.3) and usability (§ 3.2.4). With respect to the functional demands, which relate directly to the structural output of the design tool, a distinction was made in demands concerning quantitative information and qualitative information, respectively shown below and in figure 155.

Quantitative information:

- Shear forces (v_n, v_x, v_y)
- Bending and torsional moments (m_{xx}, m_{yy}, m_{xy})
- Concentrated shear forces (V)
- Principle moments (m_1, m_2)
- Displacements (w)

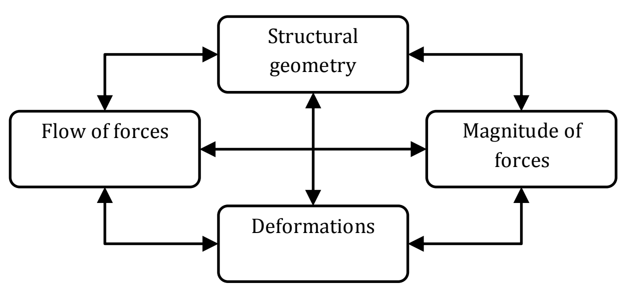

Fig.153. Qualitative information

The demands concerning usability were defined as:

- Real-time results during the (architectural) design (modelling) process.
- Ability to change the structural geometry, load cases, support conditions or material properties
- Ability to compose geometrical and analysis components into structural analysis sequences
- Ability to define which- and how calculation results are presented
- Ability to extend the functionality of the structural design tool by adding (parametric) components or procedures

1.1.2. General outline and structure of the design tool

The general outline and structure of the design tool was conceived within paragraph 3.3, by defining a software framework and the structure of the conceived structural design tool which directly relates to the theoretical framework (defined in chapter 2) (figure 154), in accordance with objective 1c:

"Define an appropriate general outline and structure for the parametric structural design tool with respect to the demands concerning functionality and usability."

In correspondence with the decision to use parametric associative design techniques for the implementation of the theoretical framework (§ 1.4), an application named Grasshopper running within the 3D modelling environment Rhinoceros was adapted as software framework. The main reason for choosing Grasshopper amongst other software applications is that this programme offers a more intuitive, and therefore a very user friendly approach to building parametric models in comparison to other parametric design applications (for example Generative Components). Scripting techniques and an external matrix class library for basic linear algebra computations named Mapack (Roeder, 2002) are used to extend the functionally of application, making it applicable for the implementation of the different structural analysis routines.

The general outline and structure of the parametric structural design tool was conceived in correspondence with the software framework and demands concerning functionality and usability (§ 2.2). The design tool was structured analogous to the flow chart of the structural analysis sequences (part of the theoretical framework, Chapter 2). Additions to this flowchart are made by defining which operations take place in the two software programs (Rhinoceros & Grasshopper), the inputs, a geometrical component for generating the calculation mesh and display components for visualizing the outputs or the structural design tool. In figure 156 a flow chart representation of the general outline and structure of the parametric structural design tool is shown.

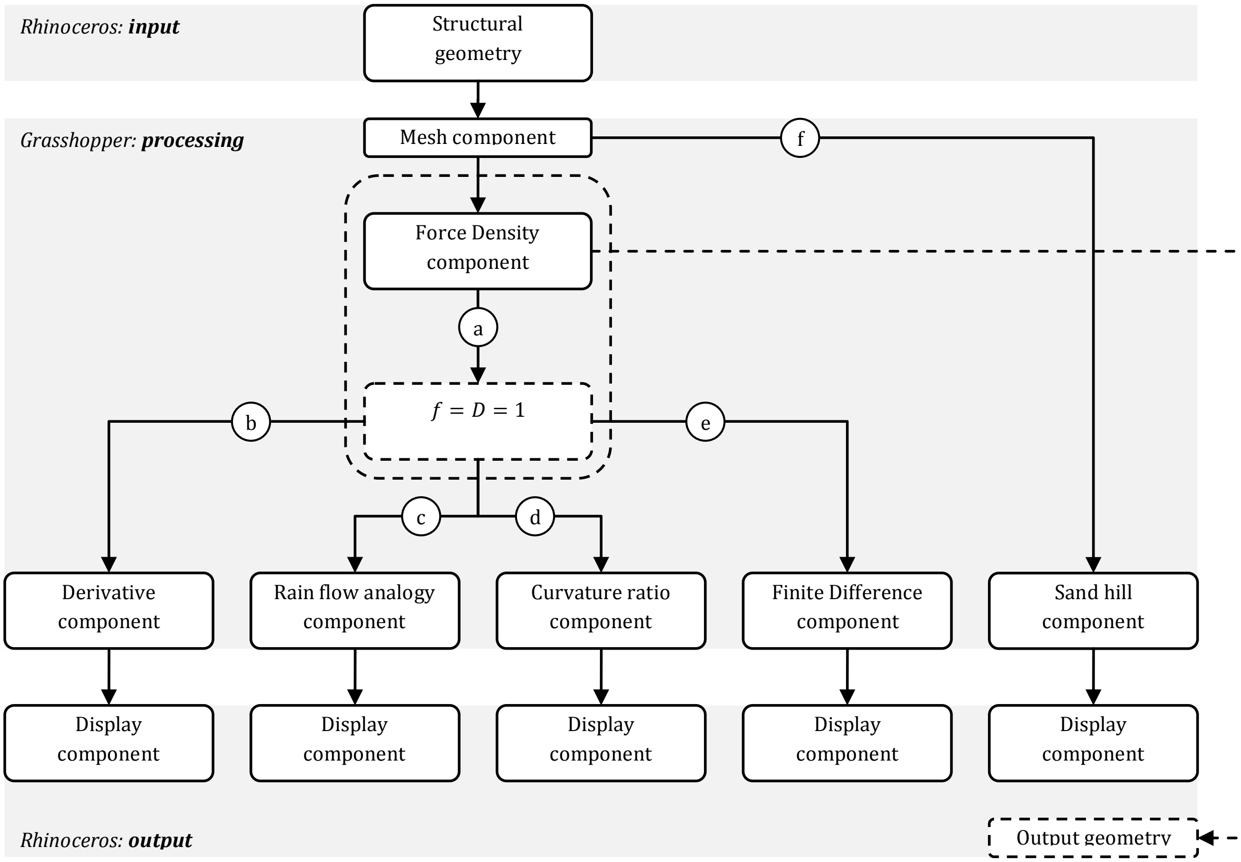

Fig.154. General outline and structure of the parametric structural design tool

1.1.3. Implementation of the theoretical framework

As described in paragraph 3.4, the theoretical framework was implemented into the conceived general structure of the design tool (§3.3.3), by describing how the different structural analysis methods were applied (by using the functionalities provided by the software framework, §3.3.2) within the structural analysis components in correspondence with objective 1d:

"Implement the theoretical framework into the defined general setup."

During the development process, it was simultaneously evaluated how each component contributes to calculating/determining the flow- and magnitude of forces and deformations within thin plate structures by presenting its output results. In figure 157 the final layout of the design tool is presented as flowchart. In this diagram it can be seen which calculation results (H) can be achieved by providing a structural geometry (outlines of a plate geometry) by composing a structural analysis sequence out of a series of structural analysis components (B,C,D,E,F and G)and the mesh component (A). Furthermore, it is illustrated how the calculation results (H) can be displayed in the 3D environment of Rhinoceros by attaching one or more display components (I). It can also be noticed that the Force Density component can also be used solely as a form finding tool for generating membrane/shell structures. Subsequently to this form finding process, the generated geometry can be developed further in Rhinoceros.

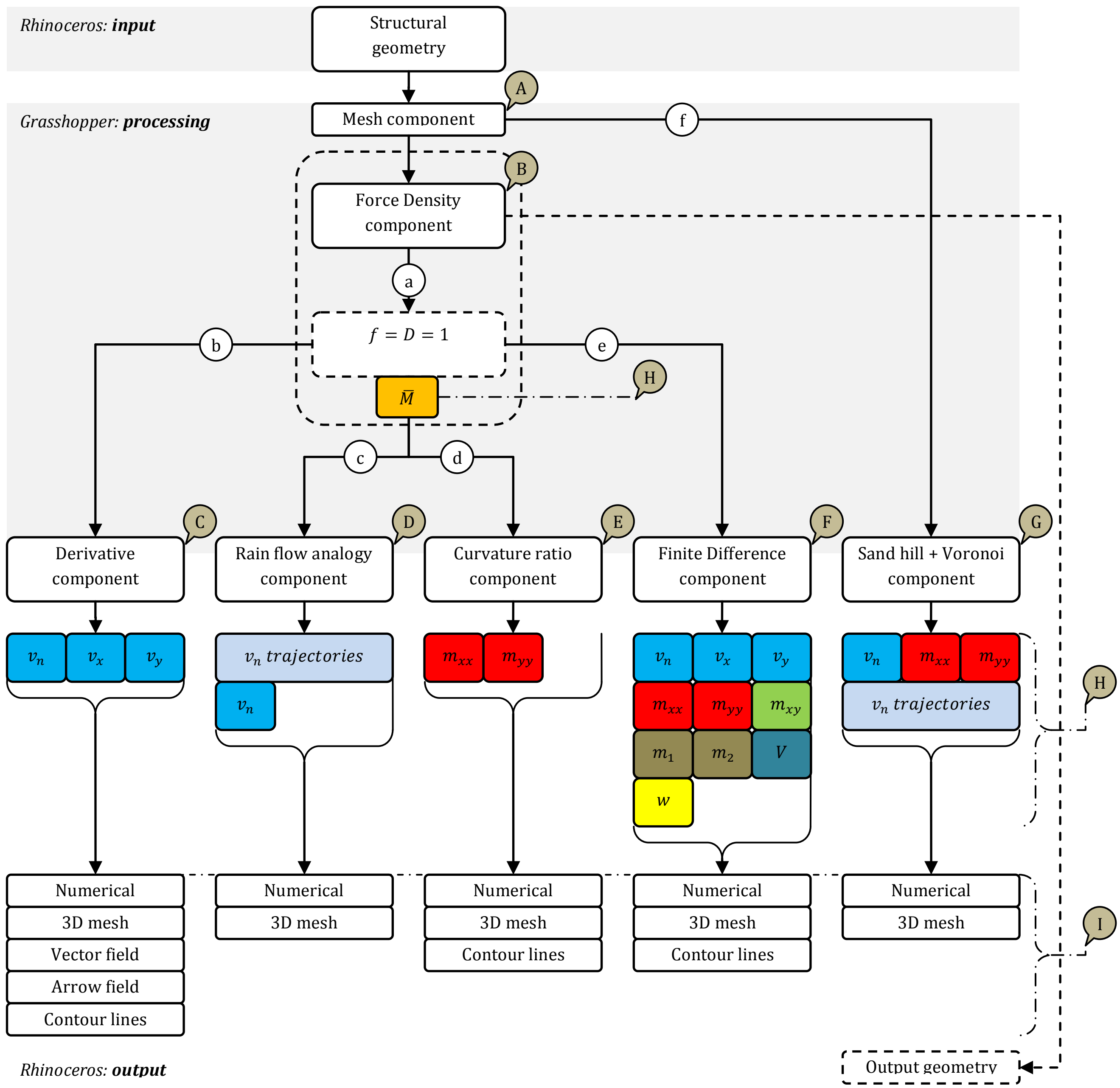

Fig.155. Flowchart of the final setup of the parametric structural design tool

5.3.1 Conclusions

The parametric application Grasshopper, running within the 3D modelling environment of Rhinoceros, was found to be an appropriate and efficient computational framework for the implementation of the theoretical framework, because:

- The Grasshopper application runs within the Rhinoceros 3D environment which means that no interfacing with an external 3D modelling program is needed for displaying the calculation results or further development of the (structural) geometry.
- The geometrical functionalities of Rhinoceros can be used in combination with mathematical expressions to establish the link between geometry and structural performance.
- Grasshopper offered an intuitive and flexible approach for developing the structural analysis components via predefined or scripting components within an attractive user interface.
- A large amount of comprehensive resources and examples were available which aided in the development of the parametric components.

With respect to the development of the different structural analysis components, as part of the parametric structural design tool the following conclusions can be drawn:

A)
- The mesh component successfully generates square mesh topologies within a collection of rectangular or free form planar boundary curves.
- The three-step-procedure for generating rectangular meshes within free form boundary curves might not be the most efficient solution. Especially with larger meshes the method becomes slow and less appropriate for a real time parametric associative structural analysis tool.

B)
- The Force Density method was successfully implemented into the form finding component. The form finding component can generate equilibrium (membrane) meshes by prescribing an initial mesh (provided by the mesh component), an optional load case (a user defined collection of vectors with a certain magnitude and direction) and a force density value.
- The output of the form finding component was compared to the output provided by an established software package named EASY (also based on the force density method), the exact similarity between the two equilibrium meshes generated on basis of the same mesh topology, boundary conditions and parameters validated the output of the parametric component.
- With respect to the work flow concerning the modelling and generation of the membranes geometry it can be concluded that the parametric form finding component offers a fast and flexible approach to exploring different geometrical alternatives induced by the possibility of altering the different parameters and boundary conditions.

C)
- Several differential equations were successfully implemented into the derivative component to calculate the direction and magnitude of (principle) shear forces based on the sum of bending moments diagram (provided by the form finding component).
- The possibility to display the principle shear forces as vector field or as 3D shear force diagram contributes to insight in their flow and magnitude. A graphical display component was successfully developed for presenting (principle) shear forces as a grid of small arrows with a certain thickness.

D) - Computational rain flow trajectories can be generated by implementing a gradient descent algorithm which iteratively performs small steps in the direction of the steepest descent.
- The accuracy of the generated trajectories is strongly dependent on the step size.

E) - The novel curvature ratio method was successfully implemented in the corresponding curvature ratio component as part of structural analysis sequence d by which 3D bending moments diagrams for $m_{xx}$and m_{yy} where fruitfully obtained.

F) - The partial differential equations were successfully implemented into the corresponding finite difference component.
- The finite difference component, when used as part of structural analysis sequence e, calculates the magnitude of all stress resultants and deformations within simply supported rectangular plate structures in a fast manner.

G) - A computational representation of the geometry of physical sand hill models was successfully achieved by implementing an algorithm, based on two principles extracted from physical experiments, into the parametric sand hill component.
- The resemblance between physical sand hill models and the geometry produced by the parametric sand hill component shows that reality is approximated accurately.
- An extension of the sand hill component was developed, which successfully extracts a 2D section out of the 3D sand hill diagram and subsequently calculates the corresponding bending moment diagrams along the lines of symmetry, belonging to plates without torsional stiffness, subjected to a distributed load.
- Voronoi tessellations were successfully generated and used to calculate the magnitude of principle shear forces along the edges of simply supported plates, subjected to a distributed load.

I) - The different display components can produce a wide range of options for visualizing the calculation results.
- Especially the (coloured) 3D mesh visualisation was found to be a very effective solution to obtaining insight in the distribution and magnitude of stress resultants and deformations.

5.3.2 Recommendations

With respect to the development of the different structural analysis components, as part of the parametric structural design tool the following recommendations are defined:

A) The functionality of the mesh component could be extended by making it possible to:

- Generate meshes within non-planar boundary curves or on basis of surface geometries
- Select different mesh options with respect to mesh topologies (e.g. triangulations)

B) - Further research is needed with respect to implementing boundary conditions within the Force Density method (B) (part of structural analysis sequence a) to generate sum of bending moments surfaces for plates with other support conditions (e.g. clamped edges or point supports) and other structural topologies like shear walls and subsequently shell structures.

D) - The speed of the rain flow algorithm could be improved by making the step size dependent on the curvature of the surface.

F) - The functionality of the component could be improved by making it possible to perform calculations for plates (or other structural topologies) with different support condition.

5.4 Validation

The calculation results, produced by three different structural analysis sequences within a parametric structural design tool, were qualitatively and quantitatively validated by respectively comparing them to the corresponding results produced by FEM based structural analysis software and the solutions of the analytical differential equations. This validation relates to objective 1e:

"Validate the produced calculation results in a qualitative- and a quantitative manner."

A thin simply supported (along its edges) rectangular plate, subjected to a distributed load p is used as case study for the validation as explained within paragraph 4.1. The validation is performed with respect to the calculation results for the (principle) shear forces (v_n, v_x and v_y), the bending moments in the x- and y-direction (m_{xx} and m_{yy}) and the torsional moments (m_{xy}).

5.4.1 Conclusions

With regard to the qualitative validation of respectively the derivative component, the rain flow component and the curvature ratio component, the following conclusions can be drawn (§ 4.2 & §4.3):

C) - The derivative component (C) (part of structural analysis sequence b) in combination with the display components (I) presents a very accurate distribution for both the shear forces in the x- and y-direction (v_x & v_y) and the principle shear forces (v_n).

D) - The rain flow component (D) (part of structural analysis sequence c) in combination with the display components (I) presents a reasonable accurate distribution for the principle shear forces (v_n).
- The presented distribution of shear forces deviates significantly in regions close to the lines of symmetry and is more accurate nearby the edges parallel to the x-axis than for the edges parallel to the y-axis of the global coordinate system.

E) - The curvature ratio component (E) (part of structural analysis sequence d) in combination with the display components (I) presents a reasonably accurate distribution for the bending moments in the x- and y-direction (m_{xx} and m_{yy}).
- The distribution of bending moments deviates mainly along the lines of symmetry.
- There are two distinct local maxima, located adjacent to the plate centre, where a local minimum occurs. It was found that a similar phenomenon occurs within the results produced by SCIA, although less distinct, and that the derivative component in fact exaggerates this

phenomenon.

- A possible explanation for the deviation between the results, produced by the curvature ratio component and the analytical calculation results could be the geometrical characteristics of the NURBS surface interpolation, which is generated within the form finding component.
- The calculation speed of the curvature ratio component is faster than the calculation speed of the finite difference component (approximately 3x).

F) - The finite difference component (E) (part of structural analysis sequence e) in combination with the display components (I) presents a very accurate distribution for the bending moments in the x- and y-direction (m_{xx} and m_{yy}) and the torsional moments (m_{xx}).

Concerning the qualitative validation of respectively the derivative component, the rain flow component and the curvature ratio component, the following conclusions can be drawn (§ 4.2 & §4.3):

C) - The average deviation between the output of the derivative component and the analytical results for the principle shear forces v_n is 1,5% along the Y1-axis and 1,6% along the Y2-axis.

- The maximum deviation between the results of the derivative component and the analytical results occurs in point 5 (nearby the corner of the plate), where the procentual deviation is 6,1%, which is more than twice as accurate as the result provided by SCIA (14,7%)
- In general, the derivative component produces more accurate results for the principle shear forces v_n than SCIA along the Y1 axis. The opposite is true for the Y2 axis where the results produced by SCIA are more accurate.

D) - The finite difference component provides very accurate numerical results for both the bending moments in the x- and the y-direction (m_{xx} and m_{yy}).

- The average deviation for the bending moments m_{xx} is 0,6% procent and 0,1% for m_{yy}.
- With respect to the bending moments in the x-direction m_{xx}, the largest deformations occur in point 2, next to the midst of the plate, and the accuray increases towards the edges of the plate.
- With respect to the bending moments in the y-direction m_{yy}, the procentual deviations have an irregular progression and the largest deformations occur in point 3.

5.5 Final conclusion

Reflecting on the main objective for this thesis it can be said that it was successfully achieved within this thesis project: a parametric structural design tool for architects and structural engineers was developed by implementing a series of (mainly) analytical structural analysis methods into corresponding structural analysis components. The different structural analysis components can be used to obtain (specific) qualitative and quantitative (real time) insight in the magnitude (and trajectories) of forces and deformations within thin plate structures within a conceptual design stage.

Bibliography

Beranek, W. (1976). *Berekening van platen.* Delft: Delft University of Technology.

Blauwendraad, J. (2006). *Plate Analysis, Theory and Application Volume 1, Theory.* Delft: Faculty of Civil Engineering and Geosciences.

Blauwendraad, J. (2006). *Plate Analysis, Theory and Application Volume 2, Numerical Methods.* Delft: Faculty of Civil Engineering and Geosciences.

Borgart, A., Hoogenboom, P., & De Leeuw, M. (2005). The relationship of form and force in (irregular) curved surfaces. *Proceedings of the 5th International Conference on Compuation of Shell and Spatial Structures.* Salzburg: IASS.

Breider, J. (2008). *Structural Components.* Delft: TU Delft University of Technology, Faculty of Civil Engineering and Geosciences (Structural Design Lab).

Coenders, J. (2006). Aproximating intelligent structures: Embedded design intelligence in systems for the early phases of design. *IASS-APCS 2006 Symposium: New Olympics – New Shell and Spatial Structures.* Beijing: IASS.

Czerny, F. (1959). *TAFELN FÜR HYDROSTATISCH BELASTETE RECHTECKPLATTEN.* Ernst.

Euler, L. (1767). Recherches sur la courbure des surfaces. *Memoires de l'academie des sciences de Berlin 16* , 119-143 .

Hanselaar, H. (2003). *Snowplace.* Delft.

Prandtl, L. (1903). Zur Torsion von prismatischen Staeben. In *Phys. Z. 4* (pp. 758-759).

Press, W., & William, H. (2007). *Numerical Recipes. The Art of Scientific Computing, 3rd Edition.* Cambridge University Press.

Roeder, L. (2002). *Mapack for .net.* Retrieved June 21, 2010, from http://www.aisto.com/roeder/dotnet

Schek, H. (1973). The force density method for form finding and computation of general networks.

Veenendaal. (2008). *Evolutionary Optimization of Fabric Formed Structural Elements.* Delft: TU Delft University of Technology, Faculty of Civil Engineering and Geosciences (Structural Design Lab).

Weisstein, E. (n.d.). *Principal Curvatures*. Retrieved June 21, 2010, from Wolfram Mathworld: http://mathworld.wolfram.com/PrincipalCurvatures.html

Weisstein, E. (2007). *Streamline*. Retrieved June 21, 2010, from Wolfram Research: http://scienceworld.wolfram.com/physics/Streamline.html

Weisstein, E. (n.d.). *Vector Field*. Retrieved June 21, 2010, from Wolfram Mathworld: http://mathworld.wolfram.com/VectorField.html

Weisstein, E. (n.d.). *Voronoi Diagram*. Retrieved June 21, 2010, from Wolfram Mathworld: http://mathworld.wolfram.com/VoronoiDiagram.html

List of symbols

List of symbols used within this thesis:

l	*Length*
b	*Width*
h	*Height*
t	*Thickness*
α, β, γ	*Angles*
n	*Number*
x, y, z	*Length coordinates*
z	*Leverage arm*
R	*Radius*
u	*Displacements*
w	*Deformations*
w_m	*Deformation of membrane surface*
Δw	*Sum of curvatures of displacement field*
κ_{xx}	*Extrinsic curvature in the x-direction of the global coordinate system*
κ_{yy}	*Extrinsic curvature in the y-direction of the global coordinate system*
$\bar{\kappa}$	*Sum of curvatures*
k_1	*Curvature of sum of bending moments surface*
k_1	*Curvature of sum of bending moments surface*
$\bar{K}$	*Sum of curvatures of sum of bending moments surface*
φ	*Angle*
ϕ	*Rotation*
ε	*Strains*
σ	*Normal tension*
τ	*Shear tension*
F	*External force*
p	*Distributed load per surface area*
q	*Distributed load along a line*
$\bar{M}$	*Sum of bending moments*
m_{xx}	*Bending moment in the x-direction of the global coordinate system*
m_{yy}	*Bending moment in the y-direction of the global coordinate system*
m_{xy}	*Torsional moment*
R	*Reaction force*
E	*Modulus of elasticity*
υ	*Poisson's ratio*

Appendix I

Several physical models were produced during this thesis by using rapid prototyping techniques in combination with the parametric form finding component in collaboration with Arnoud Herder. Several results are shown in the pictures below.

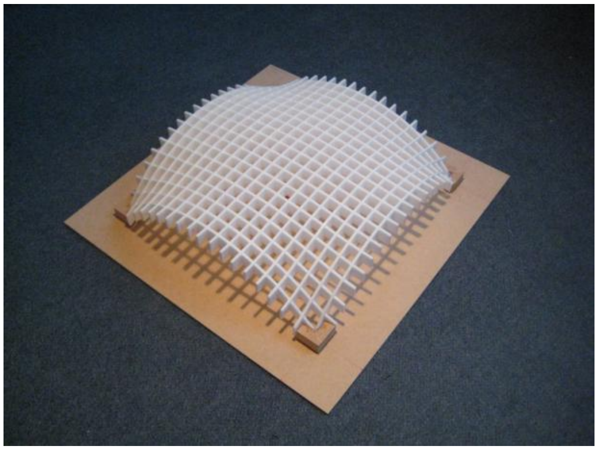

Fig.156. Grid shell structure on a square ground plan

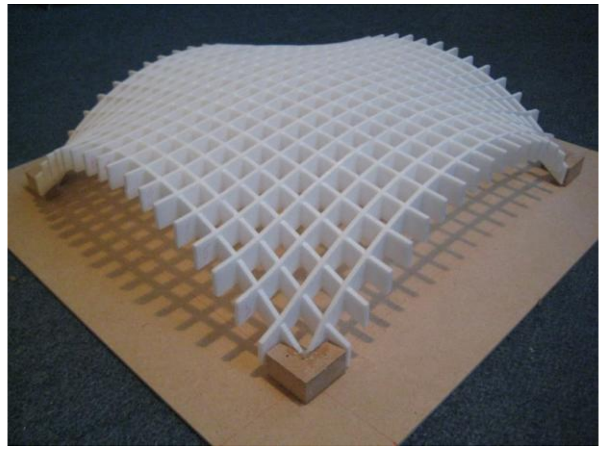

Fig.157. Grid shell structure on a square ground plan (close up)

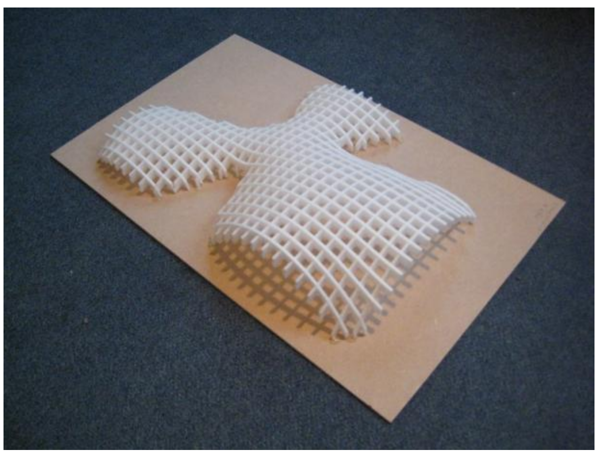

Fig.158. Grid shell structure on a free form ground plan

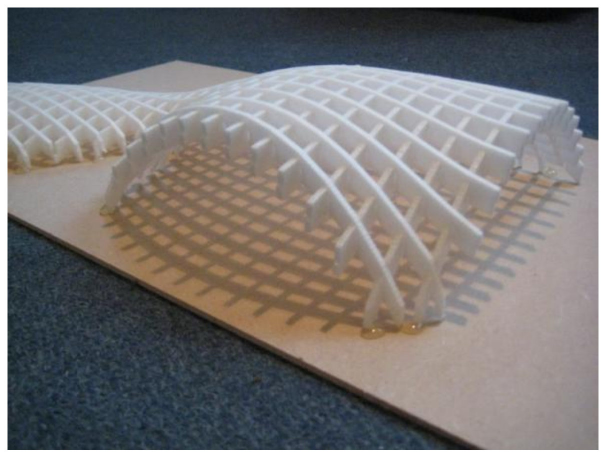

Fig.159. Grid shell structure on a square free form base (close up)

Fig.160. Grid shell structure on a square ground plan (laminated)

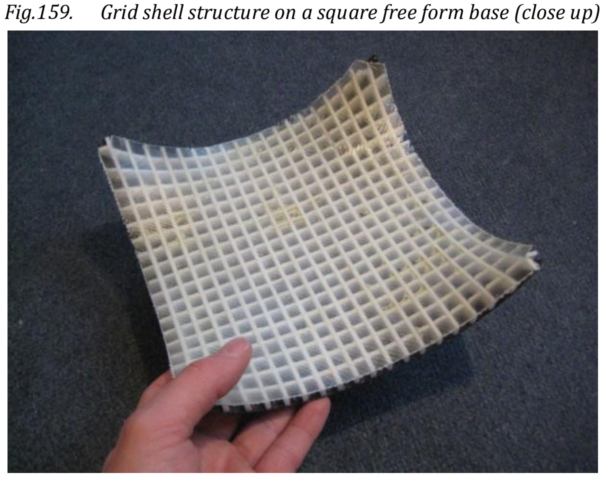

Fig.161. Close up of the laminated grid shell structure